Université de Liège

Faculté des Sciences **Département d'Astrophysique, Géophysique et Océanographie**

Time Delays in Gravitationally Lensed Quasars

THÈSE

présentée pour l'obtention du diplôme de

Docteur en Sciences

par

Eva Eulaers

Soutenue publiquement le 12 décembre 2012 devant le Jury composé de :

Président :	Dr. Marc-Antoine Dupret
Directeur de thèse :	Pr. Pierre Magain
Examinateurs :	Dr. Frédéric Courbin
	Dr. Damien Hutsemékers
	Dr. Dominique Sluse
	Pr. Hans Van Winckel

Institut d'Astrophysique et de Géophysique de l'Université de Liège

Mis en page avec la classe thloria.

To my dearest Christophe

&

to Elise,
our star.

Acknowledgements

This research was partially supported by ESA and the Belgian Federal Science Policy (BELSPO) in the framework of the PRODEX Experiment Arrangement C-90312.

Part of this work is based on observations made with the 1.2-m Flemish-Belgian Mercator Telescope. Mercator is operated on the island of La Palma by the Flemish Community, at the Spanish Observatorio del Roque de los Muchachos of the Instituto de Astrofísica de Canarias

Contents

Abstract

Starting with a concise introduction on gravitational lensing, time delays between lensed quasars and its importance as a cosmological probe to estimate the Hubble constant, we present our contribution to this domain. In a first part, we explain the details of the Numerical Model Fit, a method to estimate time delays between two or more lensed quasar images. We apply this technique to the light curves of 11 lensed quasars with known time delays in order to analyse these published delays in a more homogeneous way. Some results can be confirmed, but others prove to be unreliable.

The second part is devoted to the most recent results of our contribution to the COSMOGRAIL collaboration. We briefly summarize the data reduction and analysis tools before the presentation of the photometry and time delay analysis of 6 lensed quasars. On top of the confirmation of time delays in two objects, SDSS J1206+4332 and SDSS J1650+4251, we are the first to measure the time delay in three doubly lensed quasar systems: HS 2209+1914, SDSS J0903+5028, and SDSS J1155+6346. The time delay analysis of the well-known quadruply lensed quasar PG 1115+080 reveals interesting elements, and asks for further investigation of longer light curves.

Résumé

Après une courte introduction sur les lentilles gravitationnelles, les délais temporels entre les images de quasars et leur importance comme méthode pour estimer la constante de Hubble, nous présentons notre contribution à ce domaine. Dans une première partie, nous expliquons les détails de notre méthode qui, en utilisant un ajustement d'un modèle numérique, mesure le délai temporel entre deux ou plusieurs images d'un quasar ayant subi l'effet de lentille gravitationnelle. Nous appliquons ensuite cette technique à des courbes de lumière de 11 mirages gravitationnels ayant un délai temporel connu, afin d'analyser ces délais de façon plus homogène. Certains résultats sont confirmés, mais d'autres se révèlent être douteux.

La deuxième partie est consacrée aux résultats les plus récents de notre contribution à la collaboration COSMOGRAIL. Nous résumons brièvement les méthodes de réduction et d'analyse des données puis nous présentons la photométrie et l'analyse des délais temporels de 6 mirages gravitationnels. En plus de la confirmation des délais temporels dans deux objets, SDSS J1206+4332 et SDSS J1650+4251, nous sommes les premiers à mesurer le délai temporel dans trois mirages gravitationnels à deux images: HS 2209+1914, SDSS J0903+5028 et SDSS J1155+6346. Enfin, l'analyse des délais temporels dans la lentille quadruple bien connue PG 1115+080 révèle des éléments intéressants et demande une étude approfondie de plus longues courbes de lumière.

Part I

Time Delays in Gravitational Lenses

1

Introduction on Gravitational Lensing and Time Delays

1.1 Historical Background

We refer to Schneider et al. (1992) for a more detailed history of the field of gravitational lensing.

As early as 1704, Sir Isaac Newton asked the question of the existence of the phenomenon of gravitational lensing in his book *Opticks* : "Do not Bodies act upon Light at a distance and by their action bend its Rays; and is not this action strongest at the least distance?" In a letter to Henry Cavendish in 1783, John Michell suggested the existence of a black hole: "All light emitted from such a body would be made to return towards it, by its own proper gravity" (Michell 1784). One year later, Cavendish calculated the deflection of light by a body, using the corpuscular theory of light and Newton's law of gravitation, but did not publish his results. Independently of Michell, Pierre Simon Laplace came up with the same idea. They both anticipated the possible existence of black holes. In 1801, the astronomer Johann von Soldner calculated the orbit of a body with constant velocity v, which passes near a spherical mass M with impact parameter r. His work, in which he insisted that the deflection could not be observed, was published in 1804 (von Soldner 1804). If we consider only very small deviations, the deflection angle α is given by

$$\alpha \simeq \frac{2GM}{v^2 r}$$

This is the Newtonian value for the deflection angle of light if we set $v = c$. Probably being unaware of the work of his predecessors, Einstein obtained the same value for the deflection angle of light in 1911, assuming that the spatial metric is Euclidean. One year later, he discussed the possibility of testing his ideas through astronomical observations with a friend and astronomer Erwin Freundlich, but they believed that a lens effect would be unobservable. Only in the framework of the full equations of General Relativity published in 1915 did Einstein obtain twice the Newtonian value of the deflection angle of light

$$\alpha = \frac{4GM}{c^2 r}$$

This value could be confirmed by Sir Arthur Eddington and his team through measurements during a Solar eclipse in 1919.

In his book *Space, Time and Gravitation* published in 1920 (Eddington 1920), Sir Arthur Eddington was also the first one to point out the possible formation of multiple images if two stars are sufficiently well aligned, but he was convinced that this was unobservable. Four years later, in 1924, Orest Chwolson remarked that in case of perfect alignment of the background and the foreground star, a ring-shaped image centred on the foreground star should result. This phenomenon is known today under the name of

an Einstein Ring. But he did not want to pronounce himself on the existence of what he called "fictitious double stars" (Chwolson 1924).

On a suggestion by a Czech engineer Rudi Mandl, Einstein published a paper in 1936 on the major characteristics of gravitational lensing, including the possible amplification, but he did not believe that there was a great chance of observing this phenomenon (Einstein 1936). In spite of Einstein's scepticism this little note aroused the interest and reaction of three colleagues. Henry Norris Russell published an article in the popular magazine *Scientific American*, in which he described the effects of gravitational lensing that could be seen on an imaginary planet around the companion star of Sirius: multiple images, arcs, and amplification effects (Russell 1937). In 1937, Gavil Tikhov referred to the work of Orest Chwolson and calculated the amplification in the case of lensing by a star (Tikhov 1938). The same year, Fritz Zwicky published two articles, which both have proven to be prescient. In the first one (Zwicky 1937a), Zwicky showed that "extragalactic nebulae" - now called galaxies - are more efficient lenses than stars. He described the possible astrophysical applications of the observations of gravitational lensing: the theory of general relativity could be tested, nebulae could be detected at higher distances and their mass could be derived. In the second paper (Zwicky 1937b), he was the first to realize the very high probability of observing multiple images due to gravitational lensing.

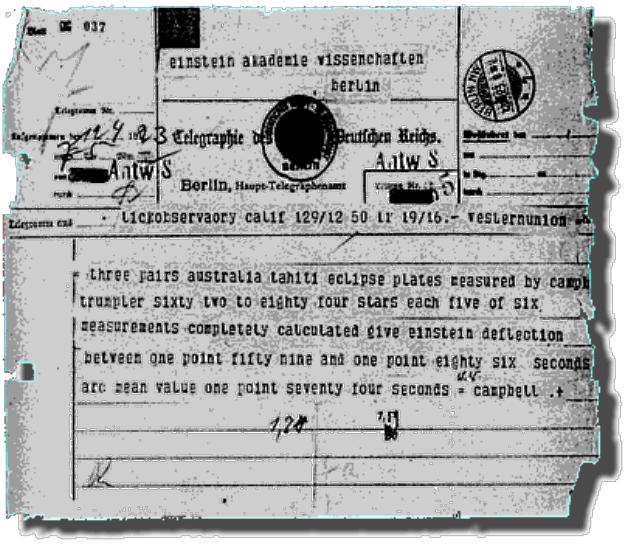
einstein akademie wissenschaften
berlin
Telegraphie des Deutschen Reichs.
Antw S
Berlin, Haupt-Telegraphenamt
Antw S
Lick observatory calif 129/12 50 lt 19/16.- westernunion
three pairs australia tahiti eclipse plates measured by campb
trumpler sixty two to eighty four stars each five of six
measurements completely calculated give einstein deflection
between one point fifty nine and one point eighty six seconds
arc mean value one point seventy four seconds - campbell .+

Figure 1.1: Telegram from Sir Arthur Eddington to Albert Einstein announcing their measurements confirming General Relativity.

In 1963, the first quasar, a "quasi-stellar" compact, very luminous and distant source, was identified by Maarten Schmidt (Schmidt 1963). In the same period, Yu Klimov, Sidney Liebes and Sjur Refsdal independently revived interest in the theory of gravitational lensing. Liebes discussed the probability of detecting the gravitational lens effect (Liebes 1964), focusing on stellar lenses, whereas Klimov considered lensing by galaxies (Klimov 1963). Sjur Refsdal described the properties of a point-mass gravitational lens (Refsdal 1964b), considered the time delay for the two images, and argued that geometrical optics could be used for gravitational lensing. In a second paper he showed that the Hubble parameter and the mass of the galaxy can be expressed as a function of the time delay, the redshifts of the lens and the source, and the angular separation of the lensed images (Refsdal 1964a). He already recognized the potential importance of quasars in gravitational lenses.

Throughout the seventies, theoretical work continued (Sanitt 1971; Bourassa et al. 1973), but without any systematic observational search. In 1979 the dream of some astronomers, who had not always received the respect of their fellows, finally became true: Dennis Walsh, Bob Carswell and Ray Weymann found two quasar images with the same colour, redshift and spectra, separated by only 6.1 arcseconds. As the title of their article indicates (Walsh et al. 1979), they asked the question of 0957+561 being the first gravitational lens candidate. The story of this discovery is told in Walsh (1989). Gravitational lensing had become reality instead of just theory. A second candidate was discovered one year later: the "triple" quasar PG 1115+080 (Weymann et al. 1980), of which four images could be resolved one year later using speckle interferometry. In 1983, the first international conference entirely devoted to "Quasars and Gravitational Lensing" was held at the University of Liège. Nowadays, more than 30 years after the discovery of the first lensed quasar, it has become a very wide field of theoretical and observational research with thousands of publications.

1.2 The Gravitational Lensing Effect

Excellent introductions into the basic theory of gravitational lensing can be found in Refsdal & Surdej (1994) and Claeskens (1998).

1.2.1 Working hypotheses

- Geometrical optics approximation: in nearly all cases of practical importance for lens theory, geometrical optics suffices. Astrophysical sources are usually too large for the corrections from the wave properties of light to be important.

- Homogeneous and isotropic Universe: We accept the homogeneous and isotropic Friedmann - Lemaître - Robertson - Walker model of the Universe. Although this standard choice might seem to be in contradiction with the phenomenon of gravitational lensing, caused by inhomogeneities, it has worked so far. For a comparison between homogeneous and non-homogeneous models, we refer to Claeskens (1998) and Schneider et al. (1992).

- Weak gravitational fields: although gravitational lensing effects in some close binaries consisting of neutron stars and black holes might need another description, we consider the deflection of light in a weak gravitational field. The deflection angle is always very small ($< 1'$), so that its value in radian can be equalled to that of its tangent or sine.

- Thin and transparent lens approximation: the size of the lens is very small in comparison to the distances source - lens and lens - observer involved, so it is justified to consider that the deviation of light takes place in the deflector plane. As long as we do not take the phenomenon of extinction into account, we can consider a lensing galaxy as a transparent lens.

1.2.2 Deflection angle

Within the framework of these hypotheses, Einstein's theory of General Relativity predicts the deflection angle $\hat{\alpha}$ of a light ray passing near a compact mass M at a distance r:

$$\hat{\alpha}(r) = 4\frac{GM}{c^2 r} \tag{1.1}$$

where G stands for the constant of gravitation ($G \simeq 6.67\ 10^{-11}$ m^3.kg^{-1}.s^{-2}) and c for the velocity of light ($c \simeq 3\ 10^8$ m.s^{-1}). If the Schwarzschild radius R_{sc} associated with the mass M is given by

$$R_{sc} = 2\frac{GM}{c^2}$$

then we can rewrite the deflection angle $\hat{\alpha}$ as

$$\hat{\alpha}(r) = \frac{2R_{sc}}{r} \tag{1.2}$$

with $\hat{\alpha}(r) << 1$.

For an extended lens we just have to sum up the contributions from the different mass elements constituting the lens:

$$\vec{\hat{\alpha}}(\vec{\zeta}) = \sum_i \frac{4Gm_i}{c^2}\frac{\vec{\zeta} - \vec{\zeta}_i}{|\vec{\zeta} - \vec{\zeta}_i|^2} \tag{1.3}$$

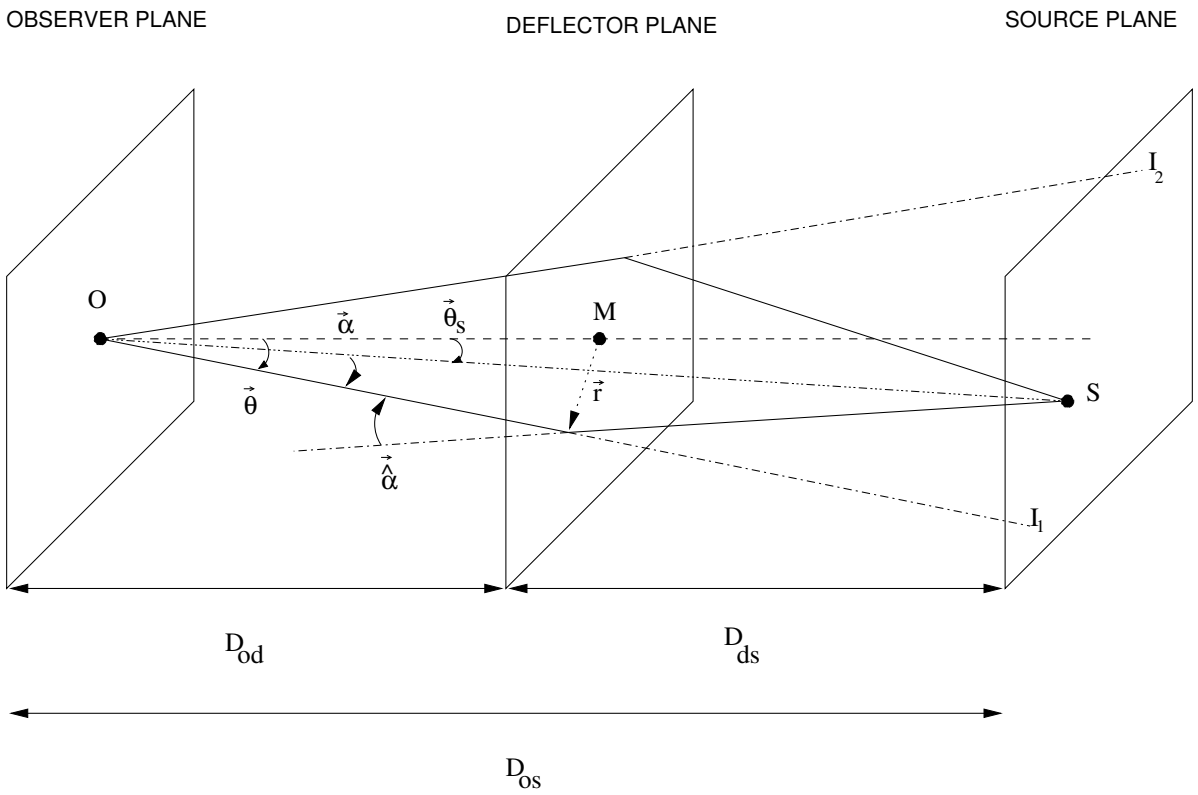

Figure 1.2: Geometrical representation of a gravitational lensing situation

where $\vec{\zeta} = (\xi, \eta)$ describes the position of the light ray in the lens plane, and $\vec{\zeta_i}$ that of the mass m_i. We now replace the sum in (1.3) by an integral by defining $dm = \sum(\vec{\zeta})d\xi d\eta$ with $\sum(\vec{\zeta})$ the surface mass density of the lens at position $\vec{\zeta}$:

$$\vec{\hat{\alpha}}(\vec{\zeta}) = \frac{4G}{c^2} \int\int \sum(\vec{\zeta'}) \frac{(\vec{\zeta} - \vec{\zeta'})}{|\vec{\zeta} - \vec{\zeta'}|^2} d\xi' d\eta'. \tag{1.4}$$

1.2.3 Lens equation

As can be seen on Figure 1.2, the true position angle of the source with respect to the lens is defined by the angle $\vec{\theta_s}$; $\vec{\alpha}$ is the deflection angle and D_{od}, D_{ds} and D_{os} indicate respectively the observer-deflector, deflector-source and observer-source angular size distances. Simple geometric relations lead to the *lens equation*:

$$\vec{\theta_s} = \vec{\theta} - \vec{\alpha}(\vec{\theta}). \tag{1.5}$$

Considering only small deflection angles, we can say that $\vec{\theta} = \frac{\vec{r}}{D_{od}}$ and put $\vec{\alpha}(\vec{\theta}) = -\frac{D_{ds}}{D_{os}}\vec{\hat{\alpha}}(\vec{r})$:

$$\vec{\theta_s} = \vec{\theta} + \frac{D_{ds}}{D_{os}}\vec{\hat{\alpha}}(\vec{r}). \tag{1.6}$$

It is very important to realize that a given image position always corresponds to a specific source position, but that in order to find all the image positions for a given source, it is necessary to invert the lens equation (1.6) or (1.5), which may lead to analytical solutions in the case of spherically symmetric lenses.

Since the deflection angle is not constant over the source structure, the resulting lensed images are often distorted.

A more formal approach, using Fermat's principle and General Relativity, leads to the same equation. More details on this reasoning can be found in Claeskens (1998).

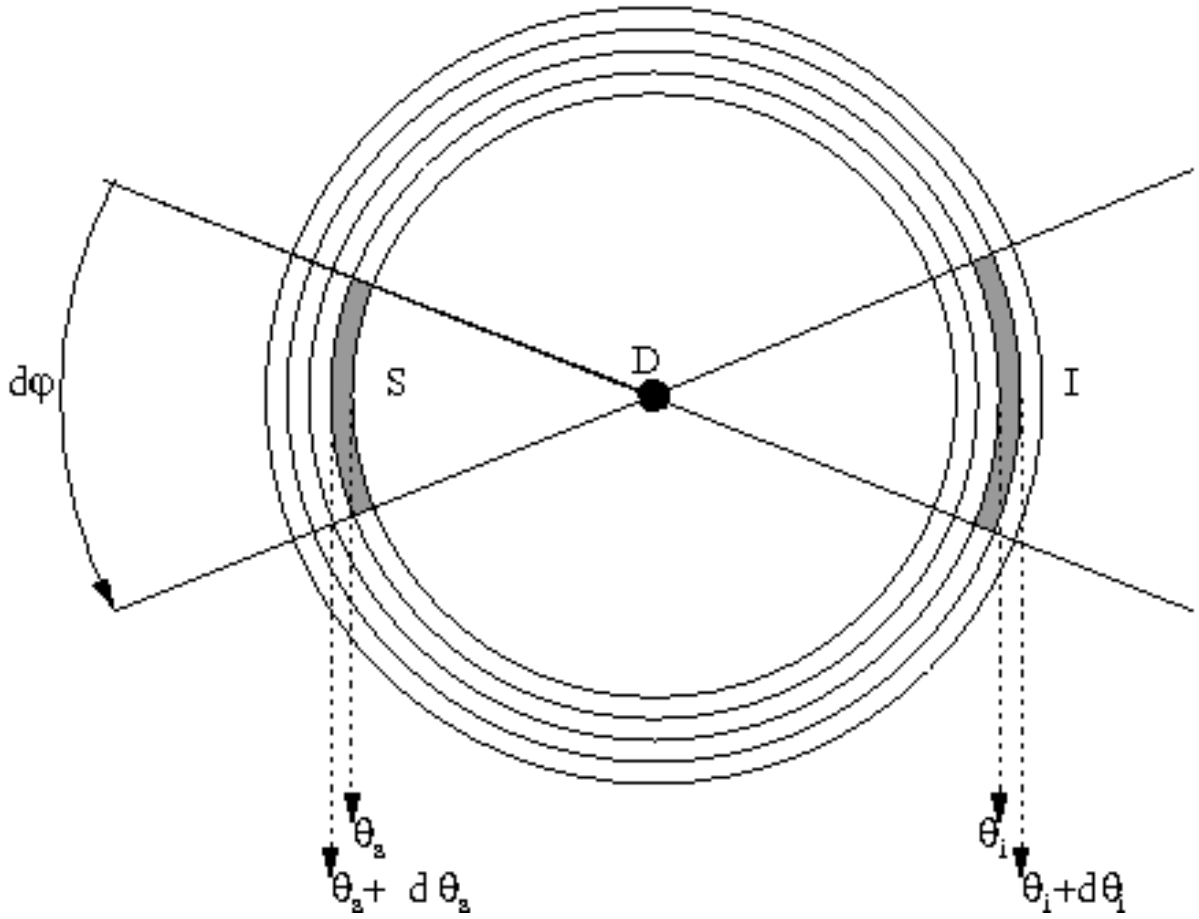

Figure 1.3: Magnification in axially symmetric lenses

1.2.4 Magnification and amplification

Gravitational lensing may not only create multiple images of a source, it can also amplify the source. Since the surface brightness of an image is identical to that of the source in the absence of a lens (Etherington 1933), the flux amplification μ_i is given directly by the ratio between the solid angle $d\omega_i$ covered by the lensed image and that of the real source $d\omega_s$:

$$\mu_i = \frac{d\omega_i}{d\omega_s}. \tag{1.7}$$

This ratio is thus given by the inverse of the determinant of the Jacobian matrix of the lens equation, if this equation is considered as a change of variables from the image plane to the source plane.

If we consider an axially symmetric lens, we can reduce the problem to a one-dimensional (see Figure 1.3). So equation (1.7) can be simplified to

$$\mu_i = \frac{\theta_i d\theta_i d\varphi}{\theta_s d\theta_s d\varphi} = \frac{\theta_i d\theta_i}{\theta_s d\theta_s}. \tag{1.8}$$

1.2.5 Einstein ring

In the case of perfect alignment between a source S, an axially symmetric deflector D and an observer, the lensed image of the source will be a ring, called the Einstein Ring, because the whole configuration is rotationally symmetric around the line-of-sight. In order to obtain the angular radius of this ring, let us express the condition for a light ray to reach the observer (see Figure 1.4):

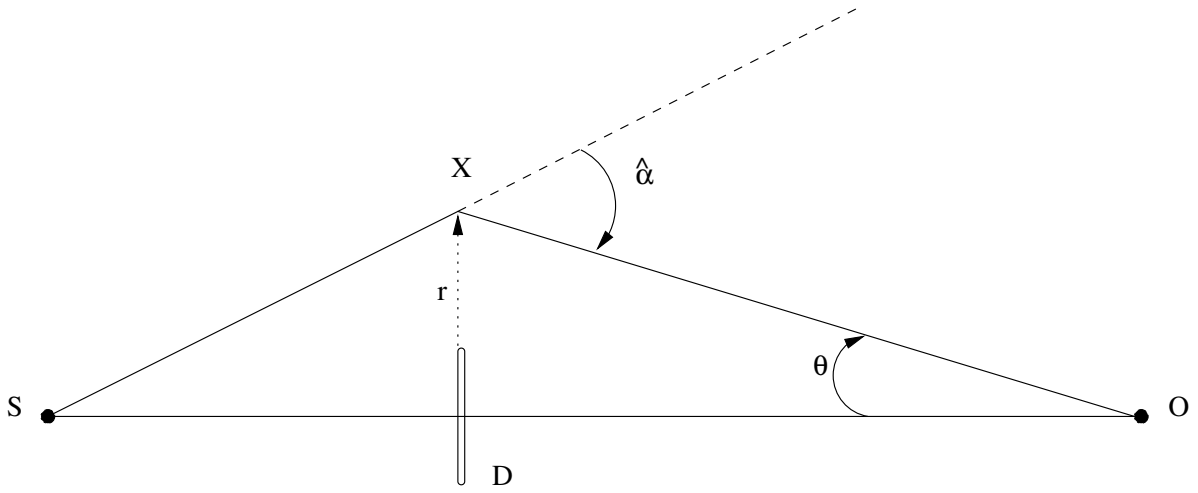

Figure 1.4: Condition for an observer to see a deviated light ray assuming perfect alignment and axial symmetry.

$$\frac{\theta}{D_{ds}} \simeq \frac{\hat{\alpha}}{D_{os}} \tag{1.9}$$

which results from the application of the sine rule. The angle θ can be expressed as:

$$\theta \simeq \frac{r}{D_{od}}. \tag{1.10}$$

Combining expressions (1.1), (1.9) and (1.10) gives us the angular radius θ_E of the Einstein Ring:

$$\theta_E = \sqrt{\frac{4GMD_{ds}}{c^2 D_{od} D_{os}}} \tag{1.11}$$

with M being the mass within the radius $D_{od}\theta_E$.

Even if the source, the deflector and the observer are not perfectly aligned, or when there is no axial symmetry, this value has its importance, for the maximal image separation is always close to $2\theta_E$.

1.2.6 The point-mass lens model

It is useful to have a close look at the properties of the point-mass lens, or Schwarzschild lens, even if this model is an idealization. Because of the symmetry of the model, exact solutions can be found for the lens equation. Combining equations (1.1), (1.6) and (1.11) allows to rewrite the lens equation as follows:

$$\theta^2 - \theta_s\theta - \theta_E^2 = 0. \tag{1.12}$$

The two solutions of this equation are

$$\theta_{1,2} = \frac{1}{2}\theta_s \pm \sqrt{(\frac{1}{2}\theta_s)^2 + \theta_E^2}. \tag{1.13}$$

When $\theta_s = 0$, which expresses perfect alignment, the image positions are $\theta_{1,2} = \pm\theta_E$. As the magnification is given by the ratio of the solid angles, the magnification of the ring is the ratio of the surface of the ring to the surface of the source (see Figure 1.5):

$$\mu_E = \frac{2\pi\theta_E d\theta_s}{\pi d\theta_s^2} = \frac{2\theta_E}{d\theta_s} \tag{1.14}$$

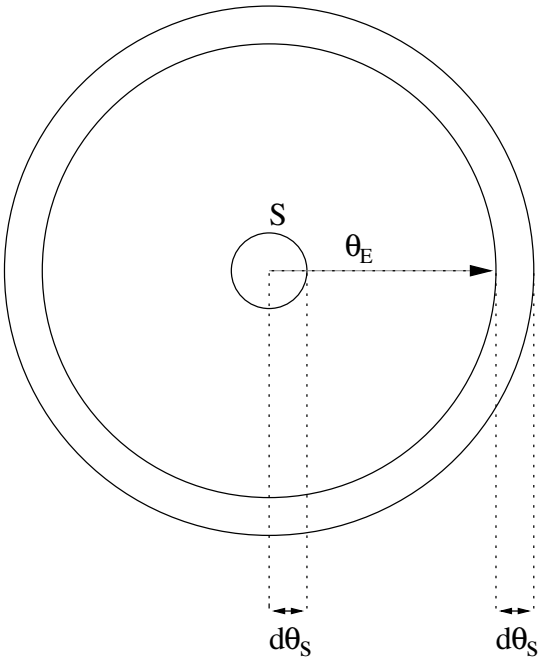

Figure 1.5: Magnification in case of perfect alignment and a point-mass lens.

with $d\theta_s$ the true angular radius of the source.

The angular separation between the two lensed images $\Delta\theta$, of which the positions are given by (1.13), is

$$\Delta\theta = \sqrt{\theta_s^2 + 4\theta_E^2}. \tag{1.15}$$

Using equations (1.8) and (1.15) allows us to express the magnification of the lensed images as

$$\mu_{1,2} = \frac{1}{4}\left(\frac{\Delta\theta}{\theta_s} + \frac{\theta_s}{\Delta\theta} \pm 2\right). \tag{1.16}$$

Knowing that usually $\mu_1 > 0$ and $\mu_2 < 0$ the total magnification is given by

$$\mu_T = \mu_1 - \mu_2 = \frac{1}{2}\left(\frac{\Delta\theta}{\theta_s} + \frac{\theta_s}{\Delta\theta}\right). \tag{1.17}$$

When the source, the lens and the observer are significantly misaligned, θ_s becomes much larger than the radius of the Einstein ring θ_E and equation (1.13) leads to $\theta_1 \simeq \theta_s$ and $\theta_2 \simeq 0$, meaning that the second image comes very close to the position of the deflector. At the same time, equation (1.16) teaches us that this second image becomes very faint, $\mu_2 \simeq 0$, and that the first image approaches its true luminosity, $\mu_1 \simeq 1$.

By convention, lensing becomes significant when $\mu_T \geq 1.34$, this value being the result of equation (1.17) for $\theta_s \leq \theta_E$, so when the source lies inside the imaginary Einstein ring.

1.2.7 The SIS lens model

The Singular Isothermal Sphere lens model provides us with a good first approximation of lensing properties of a real galaxy, even if the deflection angle for light rays passing close to its centre is too large. One can show that for this model, the mass M of the galaxy is proportional to the impact parameter $\vec{r}$ of a source light ray. As a consequence, equation (1.1) tells us that the deflection angle $\hat{\alpha}$ is a constant, which is

$$\hat{\alpha}(r) = \hat{\alpha}_0 = \frac{4\pi\sigma^2}{c^2}, \tag{1.18}$$

as it has been derived from galaxy modelling with σ^2 the one-dimensional velocity dispersion of the galaxy, which is a measurable quantity proportional to $\frac{GM}{r}$ via the Virial theorem. Defining $\alpha_0 = \hat{\alpha}_0 \left(\frac{D_{ds}}{D_{os}}\right)$ we can easily derive the solutions for the lens equation (1.5) for $|\theta_s| \leq \alpha_0$:

$$\theta_{1,2} = \theta_s \pm \alpha_0. \tag{1.19}$$

When $\theta_s = 0$, which expresses perfect alignment, the angular radius of the Einstein ring is $\theta_E = \alpha_0$. Its thickness is twice as large as the one for a Point Mass lens model, so its magnification is

$$\theta_E = \frac{4\theta_E}{d\theta_s}. \tag{1.20}$$

Combining equations (1.8) and (1.19) gives us the magnification of the two images:

$$\mu_{1,2} = \frac{\theta_E}{\theta_s} \pm 1. \tag{1.21}$$

so the total magnification is

$$\mu_T = 2\frac{\theta_E}{\theta_s}. \tag{1.22}$$

1.3 Fields of Gravitational Lensing

We present a short overview of the different fields of gravitational lens studies.

1.3.1 Strong lensing

We speak of *strong lensing* when the surface mass density of the lens is higher than the critical threshold to produce multiple images (see Figure 1.6). Strong lenses are mostly early-type elliptical galaxies, or clusters of galaxies. We can observe multiple distorted images, arcs, or a complete Einstein ring. Strong lenses allow us to study the mass distribution of the lens and determine the part of dark matter if we assume the Hubble constant H_0 is known. The other way around, we can estimate H_0 if we model the lensing mass distribution. Recently, Courbin et al. (2012) reported the first case of quasars acting as a lens.

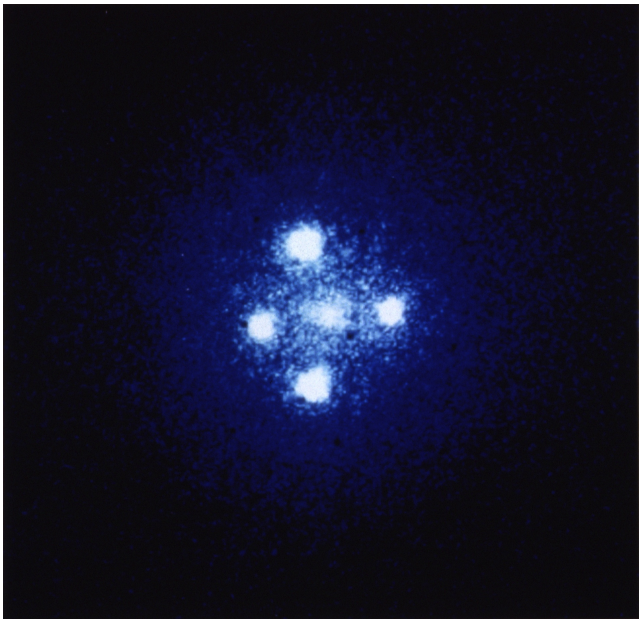

Figure 1.6: The quadruply imaged quasar Q2237+0305, also called the Einstein Cross, as seen by the Faint Object Camera on board the Hubble Space Telescope.

1.3.2 Weak lensing

Weak lensing is the statistical study of minor image distortions of a high number of background objects. These shape distortions are most prominent when the lens is a cluster of galaxies, but have

also been studied in the case of galaxy-galaxy lensing. From the measurement of the average ellipticities of lensed background objects we can reconstruct the mass distribution of the (cluster) lens and its dark matter distribution, and we can search for clusters of galaxies.

1.3.3 Microlensing

When the lens is of a stellar mass, we speak of *microlensing*. As the image separation between lensed images is too small, we can only observe a time-dependent magnification of the background object due to the relative motion of source, lens, and the observer. There are two types of microlensing:

- Galactic microlensing: the lens is a star in our Milky Way. Several surveys look for massive compact halo objects, but the technique also allows to detect extrasolar planets.
- Quasar microlensing: due to the relative motion of the quasar, lensing galaxy and observer, the stars in the lensing galaxy produce flux variability that is uncorrelated in the different images. Microlensing in lensed quasars can be studied on its own, but is a source of noise in time delay studies.

1.3.4 Surveys

The majority of the strong lenses have been discovered through systematic searches for gravitationally lensed systems. The first systematic optical survey was the ESO/Liège survey. In a selected sample of highly luminous quasars, they discovered five lensed quasar systems: UM 673 or Q0142-100 (Surdej et al. 1987), H1413+117, also called the 'Cloverleaf' (Magain et al. 1988), Q1208+1011 (Magain et al. 1992), LBQS 1009-0252 (Surdej et al. 1993), and Q1017-207 (Claeskens et al. 1996).

The Jodrell-Bank Very Large Array Astrometric Survey (JVAS; Patnaik et al. (1992)) and the Cosmic Lens All-Sky Survey (CLASS; Browne et al. (2003), Myers et al. (2003)) scanned bright radio sources for multiple components, and discovered 22 lenses (e.g. York et al. (2005)). Other lens searches are part of wider astronomical surveys. Many lenses were for example discovered in the SDSS (Sloan Digital Sky Survey) (e.g. Kayo et al. (2010)) and the Cosmos survey (Faure et al. 2008).

1.4 Time Delays

When a distant quasar shows intrinsic variations, they may appear at different moments in the multiple images. This time difference is called the time delay between two images of a lensed quasar. It is directly related to the Hubble parameter H_0, as was first pointed out by Refsdal (1964a).

1.4.1 Theoretical link between time delays and the Hubble constant H_0

There are at least three ways to derive the relation between the time delay Δt and H_0. One of them is based on Fermat's principle and has been developed by Schneider (1985). Cooke & Kantowski (1975) showed that there are two contributions to the time delay: one is due to the difference in geometrical path length between two light rays from a distant source, and the other is due to the difference in the gravitational potential through which they travel.

We explain here the so-called wavefront method for the case of an axially symmetric lens, as can be found in Refsdal & Surdej (1994). We refer to Figure 1.7 for a schematic representation of the lensing situation. For an observer at point O, at a certain distance x from the symmetry point E, the distance between two wavefronts gives the time delay between these two images since all the points on the same

wavefront have identical propagation times. Under the hypothesis of small angles, we can write the following relations:

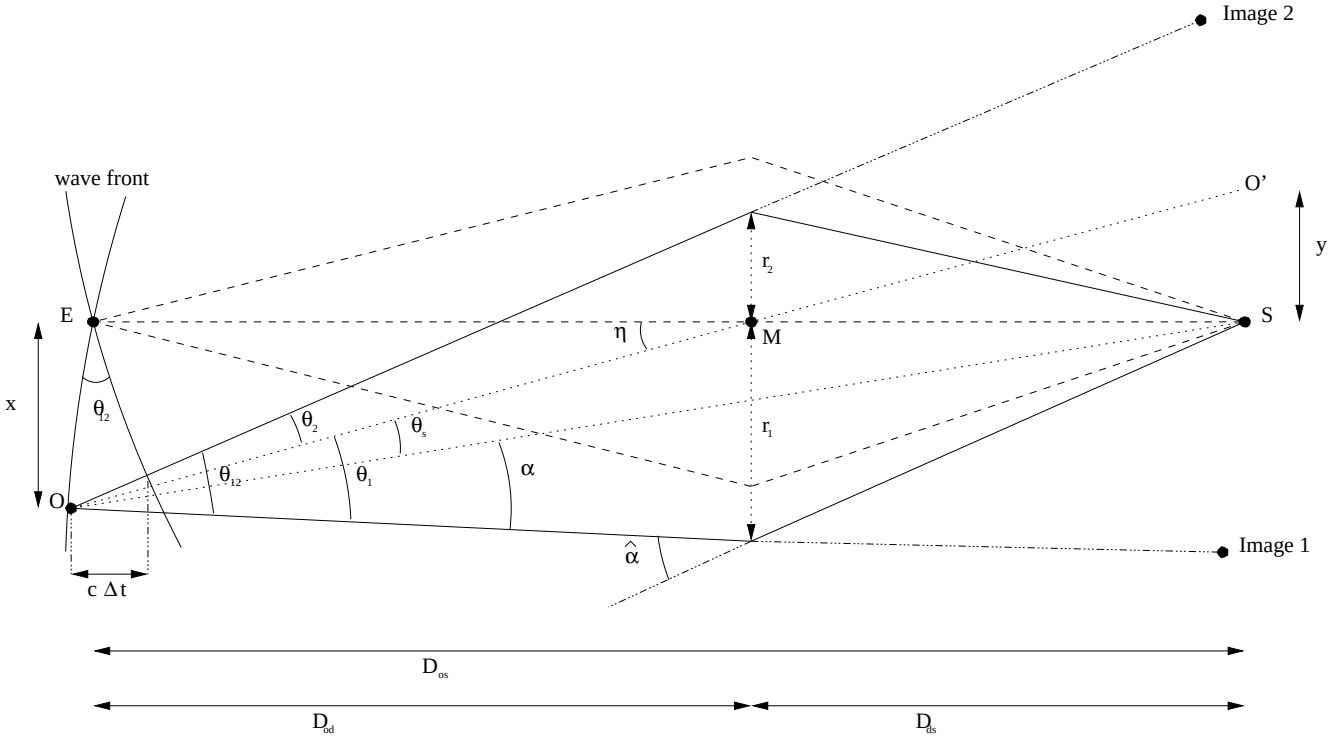

Figure 1.7: Schematic representation of the wavefront method for the determination of the time delay in the case of two light rays coming from a lensed source.

$$\begin{aligned}
\theta_s &= \frac{y}{D_{os}} \quad \text{(triangle OSO')} \\
&= \frac{\eta D_{ds}}{D_{os}} \quad \text{(triangle MSO')} \\
&= \frac{x D_{ds}}{D_{od} D_{os}} \text{ (triangle MEO)} \\
&= x \frac{D_{os} - D_{od}}{D_{od} D_{os}} \\
&= x \left(\frac{1}{D_{od}} - \frac{1}{D_{os}} \right)
\end{aligned} \tag{1.23}$$

We also have

$$c\Delta t = x\theta_{12}. \tag{1.24}$$

Starting from equations (1.13) and (1.19), it is easy to verify that

$$\theta_s = (\theta_1 + \theta_2) \frac{(2 - \epsilon)}{2} \tag{1.25}$$

is correct with $\epsilon = 0$ for a Point Mass and $\epsilon = 1$ for a SIS lens model, θ_2 being negative and assuming that the impact parameter for the first image is larger than the one for the second image.

Combining equations (1.23), (1.24) and (1.25) with the Hubble law for small redshifts,

$$D_{od} = cz_d H_0^{-1} \tag{1.26}$$

$$D_{os} = cz_s H_0^{-1} \tag{1.27}$$

leads us to

$$\begin{aligned}(\theta_1 + \theta_2)\frac{(2-\epsilon)}{2} &= \frac{\Delta t}{H_0^{-1}\theta_{12}}\left(\frac{1}{z_d} - \frac{1}{z_s}\right) \\ &= \frac{\Delta t}{H_0^{-1}\theta_{12}}\left(\frac{z_s - z_d}{z_s z_d}\right)\end{aligned} \tag{1.28}$$

from which we derive the expression linking the time delay to the Hubble parameter H_0:

$$H_0 = \frac{z_d z_s \theta_{12}(\theta_1 + \theta_2)(2-\epsilon)}{2\Delta t(z_s - z_d)}. \tag{1.29}$$

On top of a time delay measurement for a multiply imaged quasar, we need to know the image separations θ_{12}, θ_1 and θ_2 as well as the redshift of the lensing galaxy z_d and of the quasar itself z_s. The factor ϵ indicates the dependency on the lens mass distribution.

We note that the local Hubble law is of course not valid in quasar lensing, where redshifts are not small anymore, but it serves here for didactic purposes. In reality, the link between angular distances and redshifts, and thus H_0, is a lot more complicated and depends on cosmological parameters. For an illustration of this dependence, we refer to Figure 4.11 in Schneider (2006).

1.4.2 Practical problems

As it is correctly noted by Hirv et al. (2011), the determination of the time delay between two lensed images seems to be a very simple problem in its formulation. However, previous controversies on time delays (e.g. on QSO 0957+561 see Press et al. (1992a), Press et al. (1992b), Pelt et al. (1996), Kundic et al. (1997b)) have proven that the reality is far from trivial. Both physical and observational causes explain this difficulty:

- The angular separation between lensed images is often very small, typically 1-2", with the fainter lensing galaxy still lying in between these images;
- The intrinsic photometric variations of the quasar do not always show sufficient changes in shape and amplitude;
- Microlensing variability interferes with the overall quasar variability;
- Most quasars cannot be observed year round due to their position in the sky, and to meteorological conditions;
- Expensive telescope time compromise a regular sampling of the observations over a long enough time span.

On top of these limitations, the data analysis of quasar light curves has been far from homogeneous, as pointed out by Eulaers & Magain (2011), using very different ways to treat photometric error bars, to determine time delays, and to express final error bars on time delays.

Once the time delay between lensed quasar images is known, the second major obstacle towards an estimate of the Hubble constant, is the mass model for the lens. The well-known degeneracy between the spatial distribution of the lensing mass, and the Hubble constant is commonly designated as the "mass-sheet degeneracy": the steeper the lensing galaxy, the higher must be H_0 for a given set of image positions and time delays. This degeneracy as well as others are well explained in Saha (2000) and Saha & Williams (2006).

Method	H_0 (km s^{-1} Mpc^{-1})	Reference
Lensing	$68 \pm 6 \pm 8$	Oguri (2007)
	71^{+6}_{-8}	Coles (2008)
Cepheids + SNIa	$73 \pm 4 \pm 5$	Riess et al. (2005)
	$62.3 \pm 1.3 \pm 5.0$	Sandage et al. (2006)
HST Key Project	72 ± 8	Freedman et al. (2001)
+ Spitzer	74.3 ± 2.1	Freedman et al. (2012)
CMB WMAP3	73 ± 3	Spergel et al. (2007)
CMB WMAP5	$71.9^{+2.6}_{-2.7}$	Hinshaw et al. (2009)
CMB WMAP7	71.0 ± 2.5	Jarosik et al. (2011)
Sunyaev-Zel'dovich	66^{+11+9}_{-10-8}	Jones et al. (2005)

Table 1.1: Overview of recent Hubble constant estimates. If mentioned, the second set of error bars are systematics.

1.4.3 Comparison with other cosmological probes

The value of the Hubble constant has long been the topic of intense debates between scientists claiming a value around 50 km s^{-1} Mpc^{-1} and others in favour of a value as high as 100 km s^{-1} Mpc^{-1}. Several methods to estimate the Hubble constant exist, of which the method based on the Cepheid candles is probably the most well-known. Other techniques use supernovae type Ia measurements, the analysis of Cosmic Microwave Background anisotropies, or the Sunyaev-Zel'dovich effect in galaxy clusters.

The first attempts to estimate the Hubble constant through gravitational lenses were all based on individual lens systems and favoured low values for H_0 (Courbin et al. 1997; Kundic et al. 1997b; Fassnacht & Cohen 1998; Burud 2001), not compatible with estimates from Cepheids. In recent years however, the situation has changed. Estimates based on lensing include several systems simultaneously, and are now compatible within their error bars with H_0 values derived from different methods. Table 1.1 gives an overview of actual values.

Even if gravitational lensing might not yield the same accuracy on the Hubble constant as the one achieved by the HST Key Project using Cepheids or the analysis of fluctuations in the Cosmic Microwave Background, the method presents the huge advantage of measuring H_0 on cosmic scales without a distance ladder involved, and is now recognized as a complementary tool to determine cosmological parameters (Linder 2011; Suyu et al. 2012).

2

The Numerical Model Fit

In this chapter we explain in detail the Numerical Model Fit (NMF): our numerical method to determine time delays between the images of lensed quasars. It is originally based on Burud et al. (2001), but has been largely revised and improved. Our version is described and applied in Eulaers & Magain (2011).

2.1 Basic Method

2.1.1 The idea

The basic idea can be summarized as follows: for a series of given time delays, the method minimizes the difference between the data and a numerical model light curve with equally spaced sampling points while adjusting two parameters: the difference in magnitude between the light curves and a slope that models slow linear microlensing variations. The model is smoothed on the scale of the typical sampling of the observations, and this smoothing term is weighted by a Lagrange multiplier. The best time delay is the one that minimizes the reduced χ^2_{red} between the model and the data points.

2.1.2 In practice

Let us describe this idea in detail for the light curves of two images of a lensed quasar. Data are represented by $d_1(t_i)$ and $d_2(t_i)$ with their measurement errors $\sigma_1(t_i)$ and $\sigma_2(t_i)$. These light curves are supposed to be nearly identical except for the time delay Δt and a shift in magnitude Δm. In order to model slow microlensing in one of the images due to individual stars in the lensing galaxy, we introduce a linear slope α between the two light curves. The model curve $g(t_j)$ consists of equally spaced sampling points, for which the spacing should be adapted to the mean observation frequency. The total number of sampling points in the model M is the first power of $2 \geqslant N_{max}$, with N_{max} being the maximal number of sampling points of the model curve $g(t_j)$ falling into the time interval where data for both curves are available after having shifted them for the time delay to be tested.

This model light curve is then χ^2 minimized to the data for a given time delay while adjusting the linear slope α and the magnitude difference Δm between the two light curves, but this is done only for the number N_A (N_B) of data points from light curve A (B) that lie in the common time interval between the two light curves after having shifted them by this given time delay Δt. As the observation dates and the regularly spaced time of the model curve do not match, the model curve is interpolated linearly between the two closest sampling points.

As we assume that the mean observation frequency is high enough to obtain a continuous light curve, we can smooth the model curve on the same time scale by introducing the convolution of the model curve

with a gaussian r of which the Full Width at Half Maximum (FWHM) is this time scale. The smoothing term is multiplied by a Lagrange parameter λ.

The total function to minimize is the following:

$$\begin{aligned} S &= \sum_{i=1}^{N_A} \left(\frac{d_1(t_i) - g(t_j)}{\sigma_1(t_i)} \right)^2 \\ &+ \sum_{i=1}^{N_B} \left(\frac{d_2(t_i - \Delta t) - (\Delta m + \alpha(t_i - \Delta t)) - g(t_j)}{\sigma_2(t_i)} \right)^2 \\ &+ \lambda \sum_{j=1}^{N_{max}} \Big(g(t_j) - (r * g)(t_j) \Big)^2 \end{aligned} \tag{2.1}$$

where $g(t_j)$ is the result of a linear weighted interpolation between the two nearest sample points of the model curve:

$$g(t_j) = (1 - a_j) g_{1j} + a_j g_{2j} \tag{2.2}$$

with g_{1j} and g_{2j} being these nearest sample points for the data $d(t_i)$, with $a_j = 0$ (resp. $a_j = 1$) if $d(t_i)$ falls exactly on g_{1j} (resp. g_{2j}) or otherwise with a_j expressing the fraction of the distance between the data $d(t_i)$ and these two sample points.

In order to accelerate minimization, the convolution $(r * g)(t_j)$ in equation 2.1 is done on the entire model curve $g(t_j)$ containing M sampling points, but when minimizing the function, we only take into account the sampling points of the model that fall in the time interval where data are available, hence the sum on N_{max} in equation 2.1.

The final reduced χ-square χ^2_{red} of the tested time delay is

$$\begin{aligned} \chi^2_{red} = \frac{1}{N_A + N_B} \Bigg(& \sum_{i=1}^{N_A} \left(\frac{d_1(t_i) - g(t_j)}{\sigma_1(t_i)} \right)^2 \\ & + \sum_{i=1}^{N_B} \left(\frac{d_2(t_i - \Delta t) - (\Delta m + \alpha(t_i - \Delta t)) - g(t_j)}{\sigma_2(t_i)} \right)^2 \Bigg). \end{aligned} \tag{2.3}$$

Note that a non-reduced χ^2 depends on the numbers N_A and N_B of points falling in the common time interval between both light curves, and these numbers depend on Δt. Using the non-reduced χ^2 would introduce a bias towards higher time delays (i.e. smaller $N_A + N_B$).

Calculating this χ^2_{red} for a series of possible time delays allows to choose the best time delay, i.e. the one with the lowest χ^2_{red}.

A simplified imaginary example in Figures 2.1, 2.2 and 2.3 illustrates the method.

2.1.3 Advantages and improvements

The advantages of this method are manifold. First, none of the light curves is taken as a reference curve, they are all treated on an equal basis. Furthermore, as the model is purely numerical, no assumption is made on the quasar's intrinsic light curve, except that it is sufficiently smooth. Finally, a model light curve is obtained for the intrinsic variations of the quasar, which is also the case for the polynomial fit method described by Kochanek et al. (2006), but not for the Minimum Dispersion Method developed by

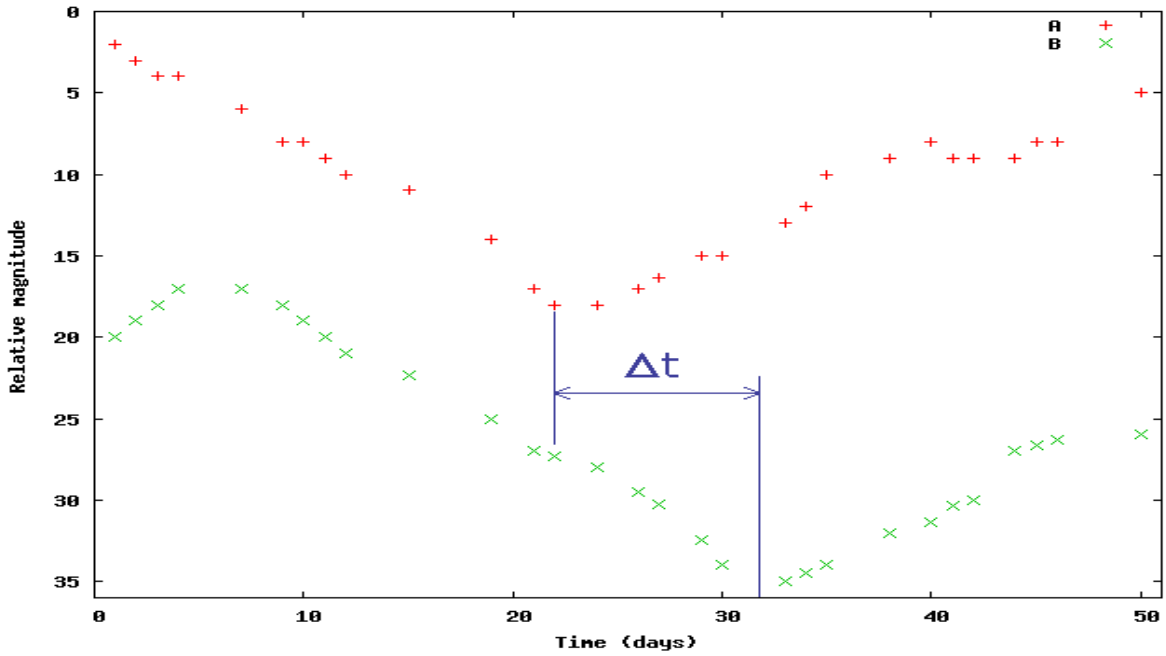

Figure 2.1: Two imaginary data curves A and B with error-free data points taken during 29 nights spread over a period of 50 days. A clear feature in the variation of the light curve allows to determine the time delay.

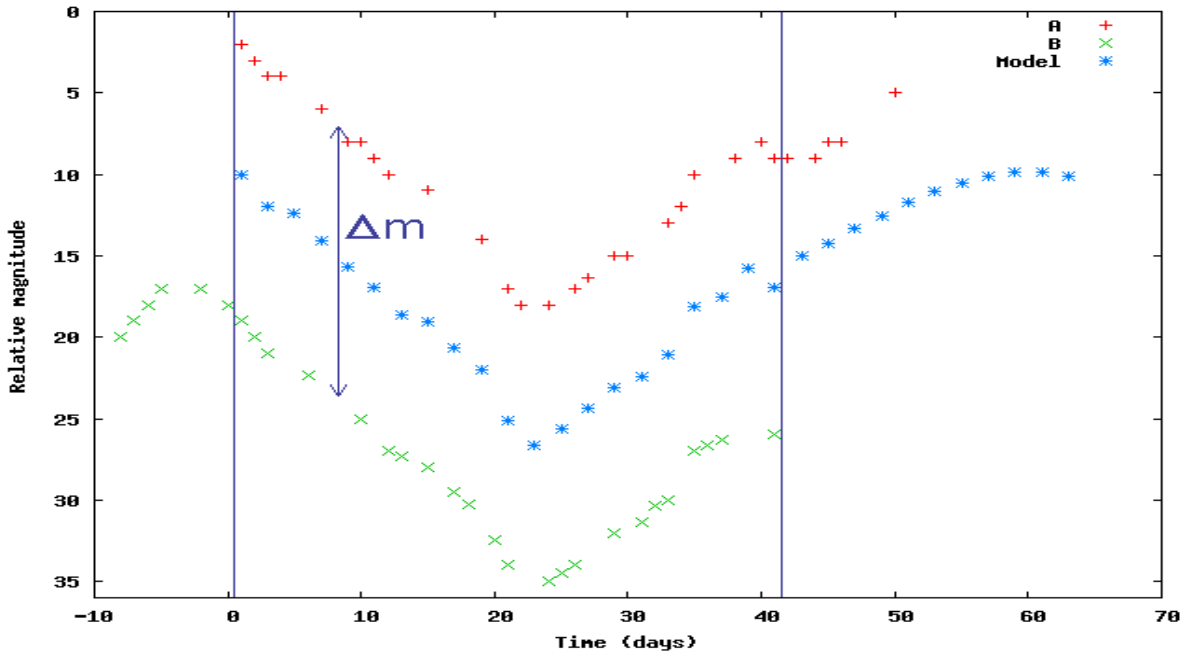

Figure 2.2: The B curve has been shifted by $\Delta t = 9$ days. For this delay, $N_B = 23$ data points from the B curve and $N_A = 24$ data points from the A curve fall into the common time interval that is indicated by the vertical bars. The spacing of the model curve has been chosen to be one point every second day, as is suggested by the mean observation frequency. In this case the model consists of $N_{max} = 21$ sampling points within the common time interval, so the first power of $2 \geqslant N_{max}$ is $M = 32$. The difference in magnitude between both curves is $\Delta m = 17$ in this example, and the linear slope α has been put to 0 for clarity.

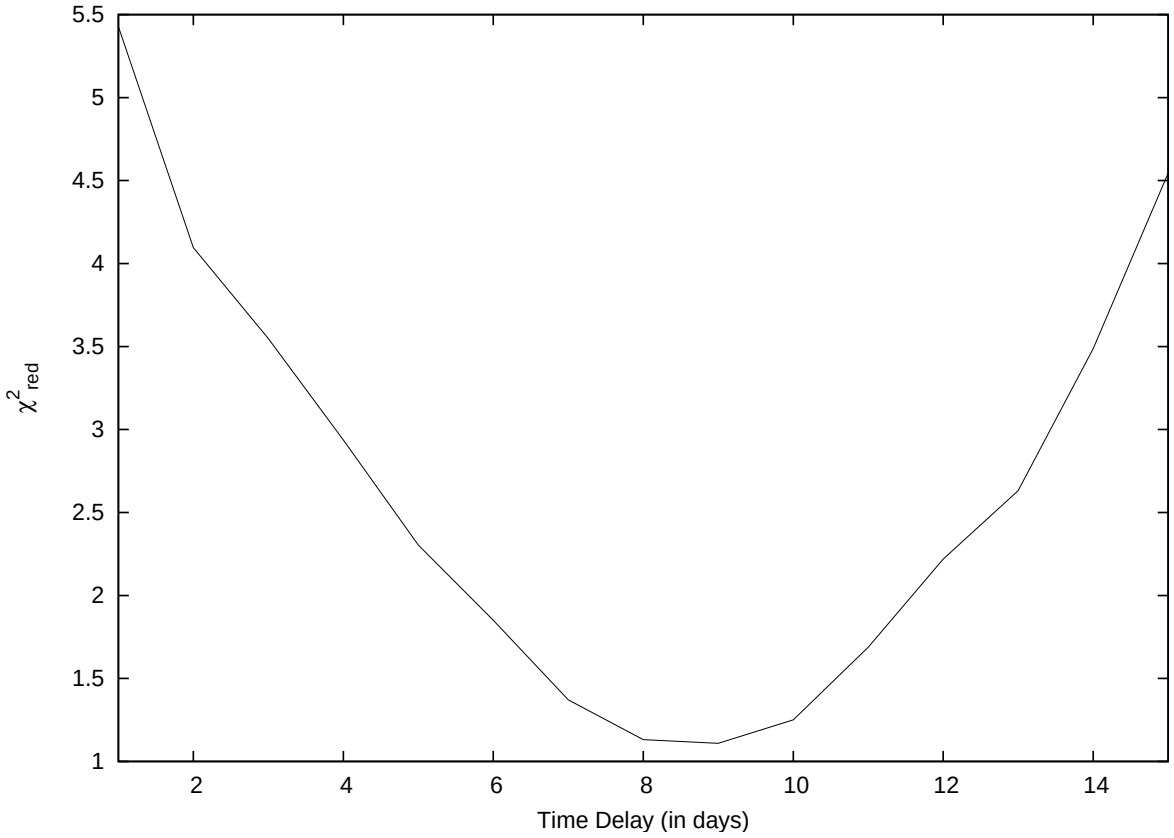

Figure 2.3: Repeating the minimization process for a range of time delays easily shows for which time delay the reduced χ^2_{red} between the model and the data points is minimized: the time delay $\Delta t = 9$ days.

Pelt et al. (1996). This is important for the calculation of the error bars, as will be explained in Section 2.4.

Burud et al. (2001) pointed out that every observation gets the same weight in the way we calculate the χ^2_{red}. But in reality, too many observations at the same time do not really improve the light curve. A regular sampling is a lot more important. Therefore, Burud et al. (2001) suggest that we introduce a weight for each point of the light curve. This weight should be higher if there are fewer data around the point and lower if else. Even if we totally agree with the idea, tests have shown that this weight only influences the time delay if the weight is high enough. We therefore decided to leave it out, the more because it introduces another parameter that can be chosen freely.

Out of the various adaptations we have applied to the original method, two have proven to be major improvements. First of all, the use of the reduced χ^2_{red} is of the utmost importance to avoid a bias towards higher time delays. Secondly, the introduction of the new variable N_{max} into the minimization process has been necessary to correct the weight of the smoothing term, which in some particular situations, when the model had to be nearly doubled in length to reach a power of 2, could dominate too much the minimization process. Examples will be presented in the following chapter.

2.2 Iterative Version

The iterative version of this method was already described in Burud et al. (2001). We have developed a more automatized version while adding some changes.

The basic version of the method as described above in 2.1.2 models microlensing with the linear slope parameter α. As we use light curves that span several years of observations, it is unlikely that this slope remains the same over this period. The iterative version of the method provides us with a possible solution.

First, the light curve is separated into the different observation seasons. For a given time delay, the basic version is used on every season separately, resulting in a slope parameter α per season. Then the light curve of every season is corrected by this individual α and all the seasonal light curves are put together again. One could also correct every season for the obtained flux ratio Δm, but as there are big gaps in the light curve due to the limited observability anyway, we can do without. The new light curve has now been corrected for microlensing, and we can run the basic version of the program on this corrected light curve so that one obtains a time delay measurement. This procedure is repeated for a series of input delays, and the results usually converge towards the same time delay.

2.3 Three and Four Curves Version

2.3.1 The idea

The idea of this version is the same as for the basic version. The difference lies in the fact that this version minimizes a more complicated function including three or four light curves simultaneously. Instead of having one single parameter for the flux ratio, and one for the slope, we now handle twice two or three parameters, as will be explained in the next paragraph.

2.3.2 In practice

Even if the principle of the method is s straightforward as for the basic version, its implementation is a lot more complicated in practice. Let us explain the case of four light curves A, B, C and D of a quadruply imaged quasar. Data are represented by $d_A(t_i)$, $d_B(t_i)$, $d_C(t_i)$ and $d_D(t_i)$ with their respective measurement

errors $\sigma_A(t_i)$, $\sigma_B(t_i)$, $\sigma_C(t_i)$ and $\sigma_D(t_i)$. Supposing that A is the leading image, we define the time delays Δ_{AB}, Δ_{AC} and Δ_{AD} and impose as a condition that

- $\Delta_{BC} = \Delta_{AC}$ - Δ_{AB}
- $\Delta_{BD} = \Delta_{AD}$ - Δ_{AB}
- $\Delta_{CD} = \Delta_{AD}$ - Δ_{AC}

The flux ratios between the four light curves and the slope parameters are Δm_{AB}, Δm_{AC}, Δm_{AD}, α_{AB}, α_{AC} and α_{AD}. Coherence is imposed through

- $\Delta m_{BC} = \Delta m_{AC}$ - Δm_{AB}
- $\Delta m_{BD} = \Delta m_{AD}$ - Δm_{AB}
- $\Delta m_{CD} = \Delta m_{AD}$ - Δm_{AC}

and

- $\alpha_{BC} = \frac{\alpha_{AC}-\alpha_{AB}}{1+\alpha_{AC}\alpha_{AB}}$
- $\alpha_{BD} = \frac{\alpha_{AD}-\alpha_{AB}}{1+\alpha_{AD}\alpha_{AB}}$
- $\alpha_{CD} = \frac{\alpha_{AD}-\alpha_{AC}}{1+\alpha_{AD}\alpha_{AC}}$.

However, the second term in the denominator of these fractions is negligibly small, and will not be taken into account.

The model light curve still consists of M equally spaced grid points, with M being a power of 2. In order not to lose too many observation points, we do not only consider the data lying in the common time interval between the four light curves, but also those that are in the common time interval between at least two out of the four light curves. We therefore introduce the number $N_{X_{XY}}$ of data of X lying in the common time interval between the light curves X and Y after shifting for the delay Δt_{XY}. Figure 2.4 and Table 2.1 show with the help of a simplified artificial light curve that these numbers can be different for all the pairs of light curves.

	AB	AC	AD	BC	BD	CD
$N_{X_{XY}}$	28	27	24	28	26	28
$N_{Y_{XY}}$	26	25	23	27	25	25

Table 2.1: Results of counting the number of data points in Figure 2.4 lying in the common time interval between the pairs of light curves.

The total function to minimize, which respects all the conditions, is

$$\begin{aligned} S &= \chi^2_{AB} + \chi^2_{AC} + \chi^2_{AD} + \chi^2_{BC} + \chi^2_{BD} + \chi^2_{CD} \\ &+ \lambda \sum_{j \geq N_{min}}^{j \leq N_{max}} \Big(g(t_j) - (r * g)(t_j) \Big)^2 \end{aligned} \tag{2.4}$$

where $g(t_j)$ is the result of a linear weighted interpolation between the two nearest sample points of the model curve as previously explained in equation (2.2), and where N_{min} and N_{max} are determined for every

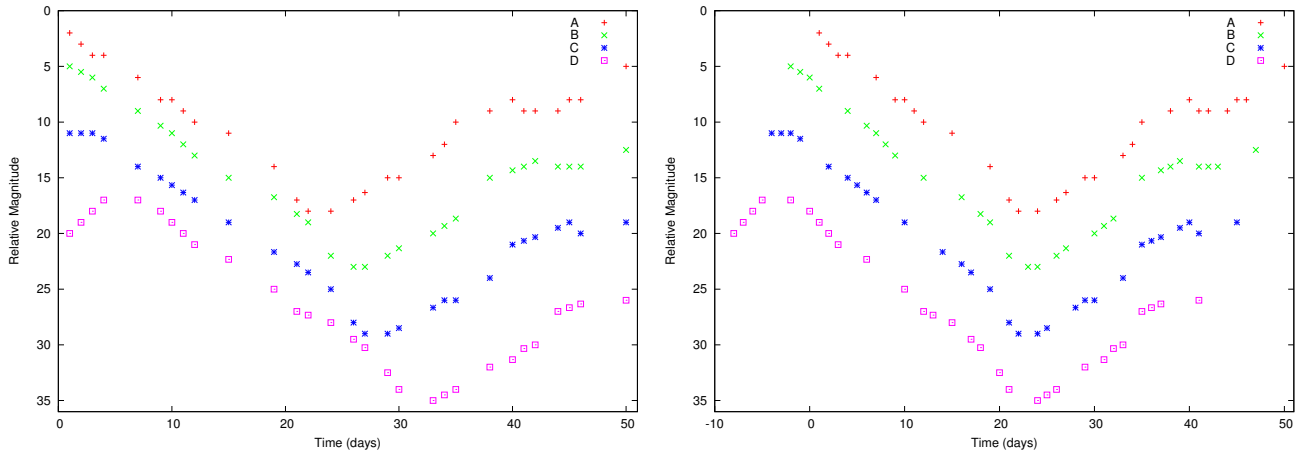

(a) (b)

Figure 2.4: (a) Four artificial light curves as they could be observed: four data points, one for each light curve, are taken at every night of observation, 29 nights spread over a period of 50 days. (b) After shifting each of the light curves for the delay to be tested, the correct one in this case, we can count the number of data points that lie in the overlapping time interval between every pair of two curves: see Table 2.1. The used time delays here are $\Delta t_{AB} = 3$, $\Delta t_{AC} = 5$, $\Delta t_{AD} = 9$.

combination of tested delays: they are the first and last sampling points from the model curve that fall into the time interval where data are available for at least two out of the four curves, and with

$$\chi^2_{AB} = \sum_{i=1}^{N_{A_{AB}}} \left(\frac{d_A(t_i) - g(t_j)}{\sigma_A(t_i)} \right)^2 + \sum_{i=1}^{N_{B_{AB}}} \left(\frac{d_B(t_i - \Delta t_{AB}) - (\Delta m_{AB} + \alpha_{AB}(t_i - \Delta t_{AB})) - g(t_j)}{\sigma_B(t_i)} \right)^2$$

$$\chi^2_{AC} = \sum_{i=1}^{N_{A_{AC}}} \left(\frac{d_A(t_i) - g(t_j)}{\sigma_A(t_i)} \right)^2 + \sum_{i=1}^{N_{C_{AC}}} \left(\frac{d_C(t_i - \Delta t_{AC}) - (\Delta m_{AC} + \alpha_{AC}(t_i - \Delta t_{AC})) - g(t_j)}{\sigma_C(t_i)} \right)^2$$

$$\chi^2_{AD} = \sum_{i=1}^{N_{A_{AD}}} \left(\frac{d_A(t_i) - g(t_j)}{\sigma_A(t_i)} \right)^2 + \sum_{i=1}^{N_{D_{AD}}} \left(\frac{d_D(t_i - \Delta t_{AD}) - (\Delta m_{AD} + \alpha_{AD}(t_i - \Delta t_{AD})) - g(t_j)}{\sigma_D(t_i)} \right)^2$$

$$\chi^2_{BC} = \sum_{i=1}^{N_{B_{BC}}} \left(\frac{d_B(t_i - \Delta t_{AB}) - (\Delta m_{AB} + \alpha_{AB}(t_i - \Delta t_{AB})) - g(t_j)}{\sigma_B(t_i)} \right)^2 + \sum_{i=1}^{N_{C_{BC}}} \left(\frac{d_C(t_i - \Delta t_{AC}) - (\Delta m_{AC} + \alpha_{AC}(t_i - \Delta t_{AC})) - g(t_j)}{\sigma_C(t_i)} \right)^2$$

$$\chi^2_{BD} = \sum_{i=1}^{N_{B_{BD}}} \left(\frac{d_B(t_i - \Delta t_{AB}) - (\Delta m_{AB} + \alpha_{AB}(t_i - \Delta t_{AB})) - g(t_j)}{\sigma_B(t_i)} \right)^2 + \sum_{i=1}^{N_{D_{BD}}} \left(\frac{d_D(t_i - \Delta t_{AD}) - (\Delta m_{AD} + \alpha_{AD}(t_i - \Delta t_{AD})) - g(t_j)}{\sigma_D(t_i)} \right)^2$$

$$\chi^2_{CD} = \sum_{i=1}^{N_{C_{CD}}} \left(\frac{d_C(t_i - \Delta t_{AC}) - (\Delta m_{AC} + \alpha_{AC}(t_i - \Delta t_{AC})) - g(t_j)}{\sigma_C(t_i)} \right)^2 + \sum_{i=1}^{N_{D_{CD}}} \left(\frac{d_D(t_i - \Delta t_{AD}) - (\Delta m_{AD} + \alpha_{AD}(t_i - \Delta t_{AD})) - g(t_j)}{\sigma_D(t_i)} \right)^2 .$$

Theoretically, the best combination of the three time delays Δ_{AB}, Δ_{AC} and Δ_{AD} is the one that minimizes the total sum of reduced χ^2s:

$$\chi^2_{red_{TOT}} = \frac{1}{N_{A_{AB}} + N_{B_{AB}}}\chi^2_{AB} + \frac{1}{N_{A_{AC}} + N_{C_{AC}}}\chi^2_{AC} + \frac{1}{N_{A_{AD}} + N_{D_{AD}}}\chi^2_{AD} + \frac{1}{N_{B_{BC}} + N_{C_{BC}}}\chi^2_{BC} + \frac{1}{N_{B_{BD}} + N_{D_{BD}}}\chi^2_{BD} + \frac{1}{N_{C_{CD}} + N_{D_{CD}}}\chi^2_{CD}. \quad (2.5)$$

2.3.3 Advantages and improvements

The most obvious advantage of this version is the fact that the model light curve is a lot better constrained, as it should fit the three or four light curves simultaneously. At the same time, all the delays are forced to be consistent with each other, which is not the case if one applies the basic version to all the pairs of light curves of a multiply imaged quasar.

It is evident that computation time is a lot higher, as the program tests all the possible combinations of the series of time delays for each of the two or three basic time delays Δ_{AB}, Δ_{AC} and Δ_{AD} in the case of four curves. These series of delays can overlap if the order is not known.

In order to speed up computation time for the four curves version, we have developed a variant of the method, in which we do not test all combinations of the three basic time delays anymore, but explore 'cubes' of a certain size we can choose and around a given delay. This allows us to have a first idea of the values for the three basic delays before testing in more detail.

2.4 Robustness and Errors

2.4.1 Tests on the robustness of a time delay

The final time delay should ideally be independent of the parameters intervening in the method. In order to verify this, we recalculate time delays for a series of parameter values that are adapted to the data, and we look at the stability of the results. This is done for three parameters that determine the model light curve: the spacing of the model curve g's sampling points, the FWHM of the smoothing gaussian r and the Lagrange parameter λ in equation 2.1.

In a second step we want to test the influence of each individual point of the light curve on the time delay. This is done with a classical jackknife test: recalculating N times the time delay while leaving out one data point at the time, with N being the number of data points in one light curve. This can of course be repeated on the light curve with $N-1$ or $N-x$ data points after having eliminated 1 or x data points. Time delays should not change drastically due to the removal of a single point from the light curve. If they do, we should investigate the reason for this, as for example a point with a very small error bar deviating from the general tendency.

2.4.2 Calculating error bars

Errors are calculated through Monte Carlo simulations. The model curve with equally spaced sampling points is re-interpolated on the observation dates in order to create a model that corresponds to the data. Normally distributed random errors with the appropriate standard deviation are then added to this model light curve and the time delay is redetermined. It is important to note that errors are not added to the data as they already contain the observed error, so adding a new error contribution would bias the results. On the other hand, the model is assumed to better represent the real light curve of the quasar.

This procedure is repeated at least 1000 times, preferably on different combinations of smoothing parameters. The mean value of the time delay distribution that we obtain is considered to be the final time delay and its dispersion gives the one sigma error bar. When we have a markedly asymmetrical distribution, we take its mode as the final time delay and use the 68% confidence intervals to obtain error bars. In this thesis, all quoted uncertainties are one sigma error bars except if mentioned otherwise explicitly.

3

Time Delays for 11 Gravitationally Lensed Quasars Revisited

We present our re-analysis of previously published time delays for 11 lensed quasars. We apply our Numerical Model Fit (NMF) to all of these objects, and use a second, completely independent, method derived from the minimum dispersion (MD) by Pelt et al. (1996), as a comparison. Our results were published in Eulaers & Magain (2011).

3.1 JVAS B0218+357

JVAS B0218+357 was first identified as a doubly imaged gravitational lens by Patnaik et al. (1993). It is variable in radio wavelengths and presents the smallest Einstein ring known so far.

We have used the data set published by Cohen et al. (2000), consisting of 51 flux density measurements at 8.4 and at 15 GHz.

The authors obtained a time delay $\Delta t_{AB} = 10.1^{+1.5}_{-1.6}$ days, where A is the leading image, thus confirming independently two values published earlier by Biggs et al. (1999) and Corbett et al. (1996) of $\Delta t_{AB} = 10.5 \pm 0.4$ days and $\Delta t_{AB} = 12 \pm 3$ days, respectively.

After transforming the flux densities onto a logarithmic scale as shown in Fig. 3.1, we applied the NMF method to the 8.4 GHz and 15 GHz light curves. Using the entire light curve did not give a clear and unique solution. The jackknife test shows that certain data points can change the value of the time delay. After eliminating three of these points, the 9th, 12th and 35th, from the 8.4GHz light curve, and choosing appropriate smoothing parameters, we obtain a time delay $\Delta t_{AB} = 9.8^{+4.2}_{-0.8}$ days at 68% confidence level. The larger error bars for higher values of the time delay are due to a secondary peak in the histogram (see Fig. 3.2) around $\Delta t_{AB} \sim 14$ days.

Taking into account all points of the 15 GHz light curve provided a comparable value of the time delay of $\Delta t_{AB} = 11.1^{+4.0}_{-1.1}$, even though we noted that the importance of the secondary peak around $\Delta t_{AB} \sim 14$ days was significantly lower after we had eliminated outlying points in both the A and B curve, in the same way as for the 8.4 GHz curve. This suggests that the secondary peak around $\Delta t_{AB} \sim 14$ days is probably caused by artefacts in the data, hence we can confirm with confidence the previously published results: combining the values based on the 8.4 GHz and 15 GHz light curves gives a time delay of $\Delta t_{AB} = 9.9^{+4.0}_{-0.9}$ days.

The MD method confirms the strong influence of these deviating points: the secondary peak around $\Delta t_{AB} \sim 14$ days even completely disappears when they are removed from both the 8.4 GHz and the 15 GHz light curves. The 8.4 GHz curve gives a time delay of $\Delta t_{AB} = 12.6 \pm 2.9$ days, and the 15 GHz data lead to $\Delta t_{AB} = 11.0 \pm 3.5$ days, which gives a combined result of $\Delta t_{AB} = 11.8 \pm 2.3$ days, all in agreement with the above-mentioned values.

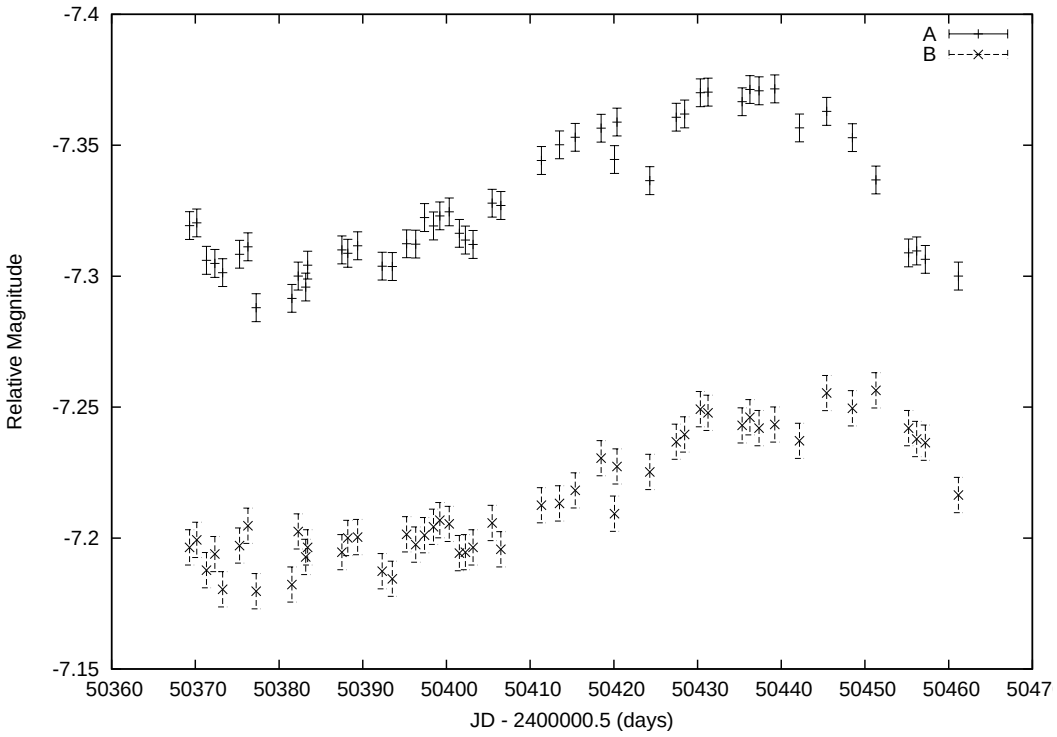

(a) 8.4 GHz

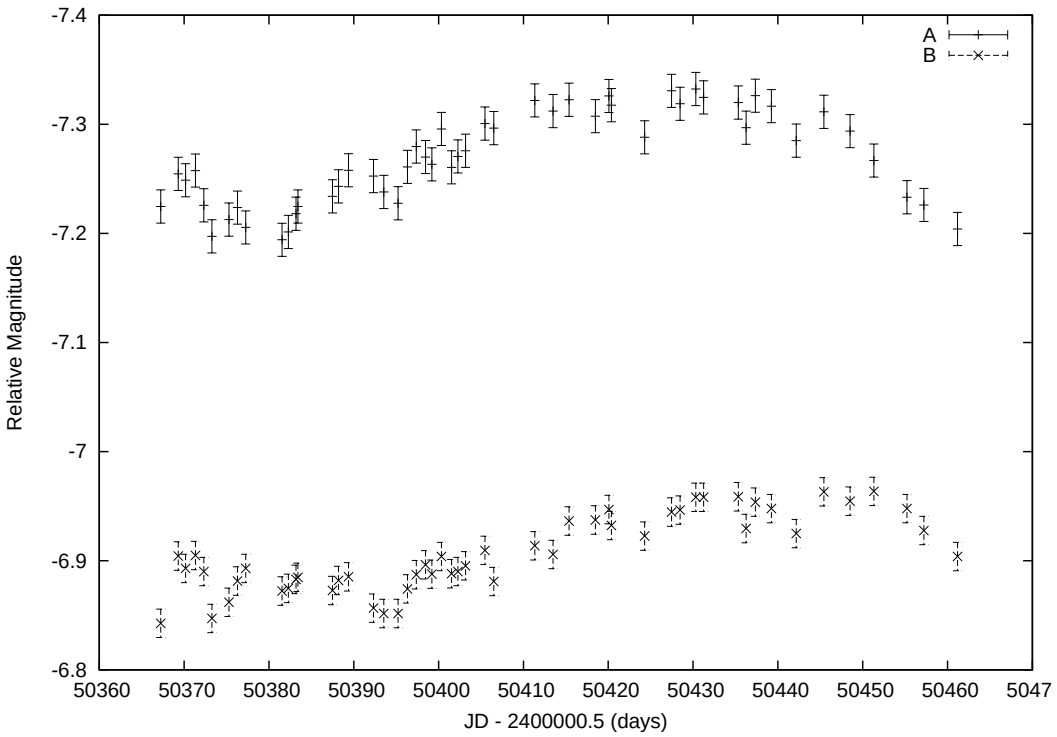

(b) 15 GHz

Figure 3.1: Light curves at 8.4 GHz and 15 GHz for JVAS B0218+357 after transforming the flux density measurements into magnitudes.The B curve has been shifted by 1 magnitude for clarity.

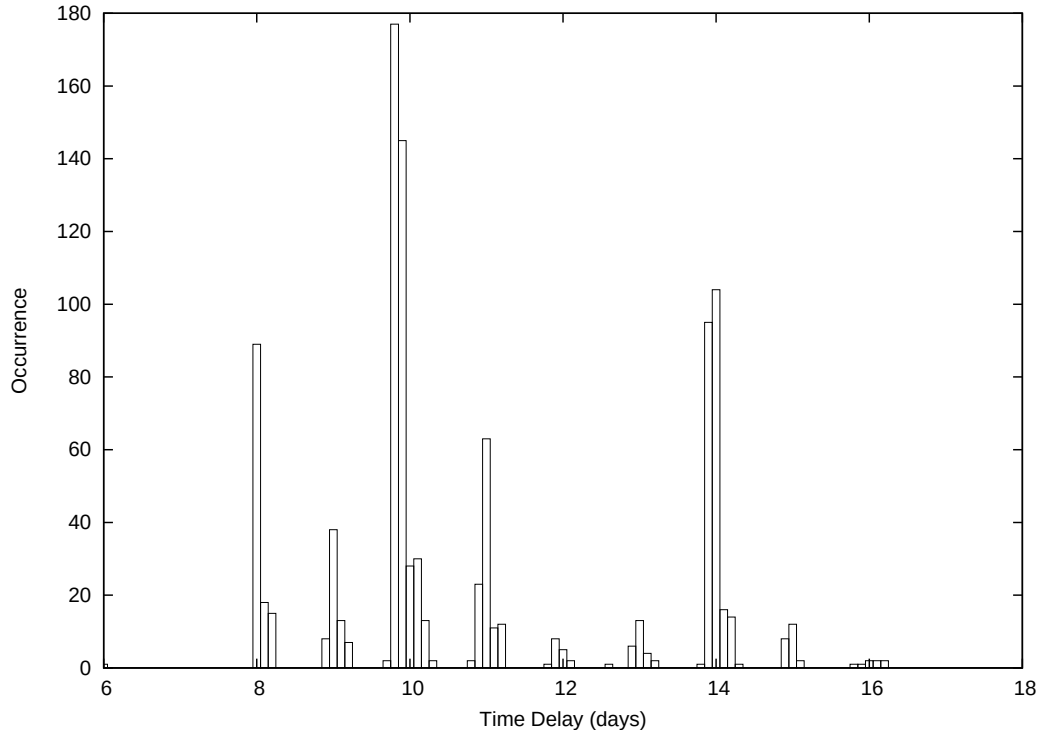

Figure 3.2: Histogram of 1000 runs of the NMF method for the 8.4 GHz data light curve of JVAS B0218+357 leaving out three deviating points. One day gaps in the histogram are artefacts due to the quasi-periodicity of the data.

Even if all of these time delay values for this object are in agreement with each other, the data do not allow a precision of the order of 5% in the delays, which would be necessary for a useful estimate of H_0.

3.2 SBS 0909+523

This object was identified as a double quasar by Kochanek et al. (1997), who at the same time suggested that it might be a lensed quasar rather than a close binary, but some doubts subsisted. Oscoz et al. (1997) confirmed the lensed nature of the object.

We used the data set published by Goicoechea et al. (2008), which contains 78 data points spread over two observing seasons.

Their analysis leads to a time delay $\Delta t_{BA} = 49 \pm 6$ days where B is the leading image, confirming the previously reported delay $\Delta t_{BA} = 45^{+11}_{-1}$ of Ullán et al. (2006).

The NMF method, when applied to the entire light curve, gives a delay $\Delta t_{BA} \sim 47$ days, as displayed in Fig. 3.3, which is within the error bars of the previously published delay. On closer inspection however, we note that this delay strongly depends on two points that are outside the general trend of the lightcurve for image B and fall right at the end of the time interval covered by the A data points for this time delay value: the 63rd and the 64th data points. Recalculating the delay while omitting these two points gives a different result of $\Delta t_{BA} \sim 40$ days or even lower values, which is not within the published ranges. The same happens if we only take into account the second observing season, which is the longer one: the delay then shortens to $\Delta t_{BA} \sim 40$ days. The parameter modelling slow linear microlensing is also significantly smaller in this case. Visually, both results, with and without the two problematic points, are acceptable. Nevertheless, although both values have proven to be independent of the two smoothing parameters, the NMF method is sensitive to the addition of normally distributed random errors with the

appropriate standard deviation at each point of the model curve. This is because the dispersion in the data points is too small compared to the published error bars. That we obtain $\chi^2_{red} \ll 1$ also highlights some possible problems in the data reduction or analysis.

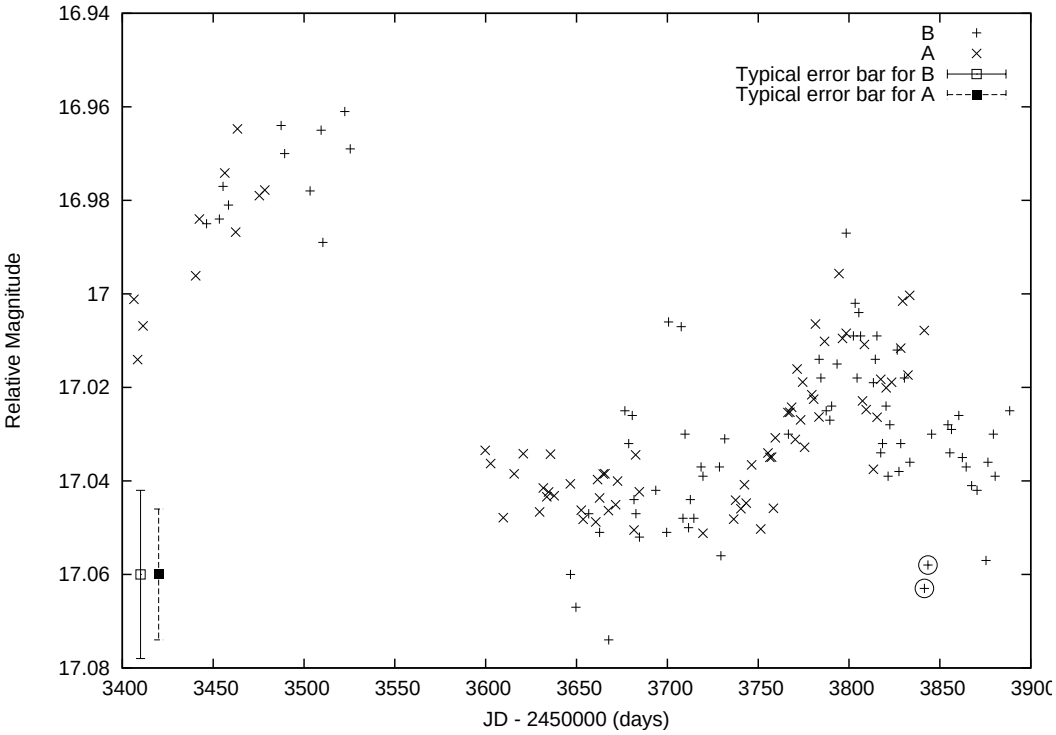

Figure 3.3: Light curves of SBS 0909+523: A is shifted by a time delay $\Delta_t = 47$ days and a difference in magnitude $\Delta m = -0.6656$. The slope parameter $\alpha = 6.0587 \cdot 10^{-5}$ corresponds to a model of slow linear microlensing. The encircled points are the 63rd and 64th observations that were omitted from later tests.

The MD method gives similar results. When using all data points, two possible delays can be seen, depending on the way microlensing is modelled: $\Delta t_{BA} \sim 49$ and $\Delta t_{BA} \sim 36$. When the two aforementioned data points are left out, we only find $\Delta t_{BA} \sim 36$, independently of how microlensing is handled.

In all cases, with or without these points, leaving more or less freedom for the microlensing parameters, the large photometric error bars result in very large error bars in the time delay when adding normally distributed random errors to the light curves, so that delays ranging from $\Delta t_{BA} \sim 27$ to $\Delta t_{BA} \sim 71$ are not excluded at a 1 σ level.

We conclude that this light curve does not allow a reliable determination of the time delay. To determine whether these two data points that do not follow the general trend are due to genuine quasar variations and thus crucial for the time delay determinations or whether in contrast, they are affected by large errors and contaminate the published results, we will need new observations and an independent light curve.

3.3 RX J0911+0551

Bade et al. (1997) identified this system as a gravitationally lensed quasar, finding evidence for three images. One year later Burud et al. (1998) reported the detection of four images and the lensing galaxy.

Data for this quadruply lensed quasar were made available by Paraficz et al. (2006), but had been previously treated and analysed by Burud (2001) and Hjorth et al. (2002), who proposed time delays of

$\Delta t_{BA} = 150 \pm 6$ days and $\Delta t_{BA} = 146 \pm 4$ days respectively, where B is the leading image of the system and A the sum of the close components A1, A2 and A3.

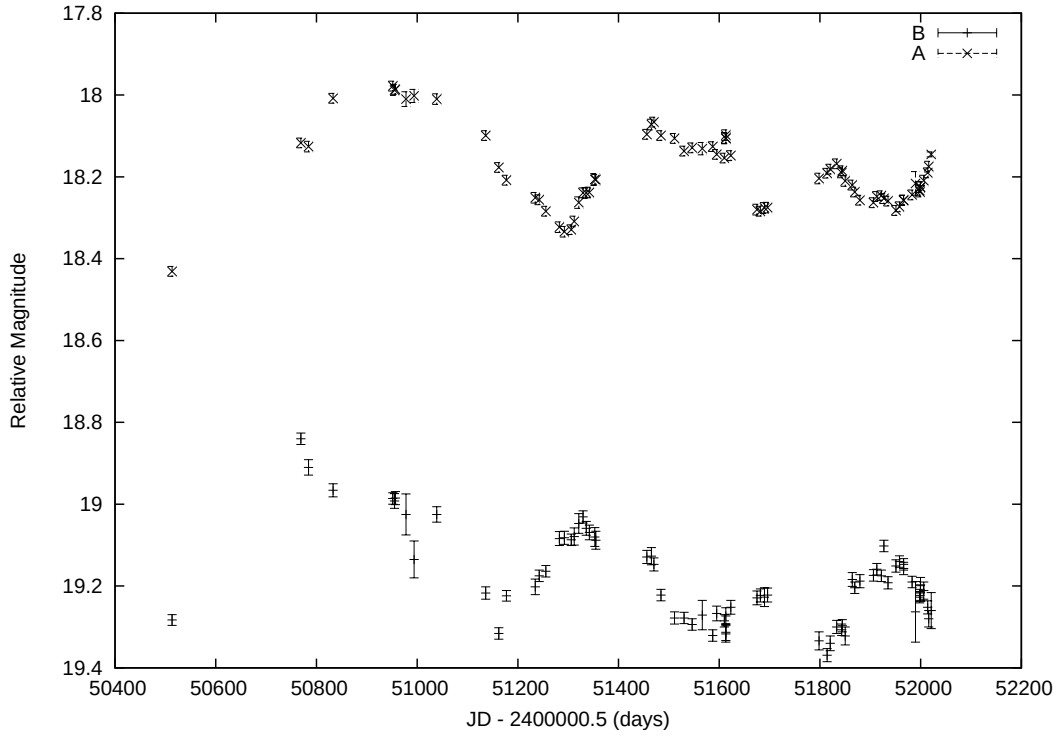

Figure 3.4: Light curves of RX J0911+0551: *A*, which is the sum of the close components A1, A2 and A3, has been shifted by one magnitude for clarity.

Using all data except the first point, which has too strong an influence on our slope parameter because of its isolation as can be seen in Fig. 3.4, we can at first sight confirm the published delays: the NMF method gives $\Delta t_{BA} = 150 \pm 2.6$ days and the MD method results in $\Delta t_{BA} = 147.4 \pm 4.6$ days. However, the histogram in Fig. 3.5 shows a secondary peak at $\Delta t_{BA} \sim 157$ days. Investigating this peak further, we come to the conclusion that some points have a very strong influence on the delay: the first observing season, and especially the first ten points of the light curve, indicate a shorter time delay. According to **?**, these points were added to supplement the regular monitoring data of the Nordic Optical Telescope. However, the first three points of the regular NOT monitoring in the B curve are similarly crucial. Omitting these three points leads to larger error bars of $\Delta t_{BA} = 151.6 \pm 7.0$ days using the NMF method. Finally, recalculating the time delay in the regular monitoring data only and without the first three points in the B curve, gives $\Delta t_{BA} = 159 \pm 2.4$ days with the NMF method. The MD method results in this case in a histogram with two gaussian peaks, one around $\Delta t_{BA} \sim 146$ days and one around $\Delta t_{BA} \sim 157$ days, implying a mean time delay of $\Delta t_{BA} = 151.4 \pm 6.7$ days. Only a new and independent light curve of similar length could tell us with more confidence which of these values is correct and which is possibly biased (e.g. by microlensing).

3.4 FBQS J0951+2635

Schechter et al. (1998) identified this system as a gravitational lens with an image separation of 1.1".

We used the data set containing 58 points published by Paraficz et al. (2006) and presented in Fig. 3.6.

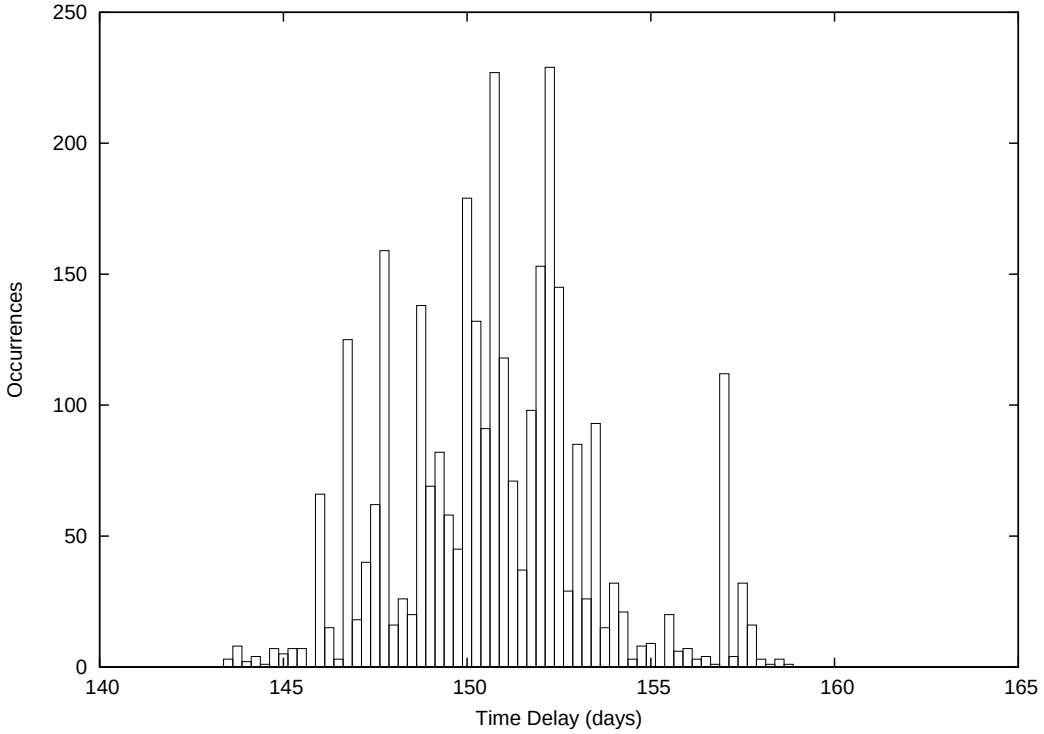

Figure 3.5: Sum of three histograms of 1000 runs each for RX J0911+05, using three different combinations of smoothing parameters.

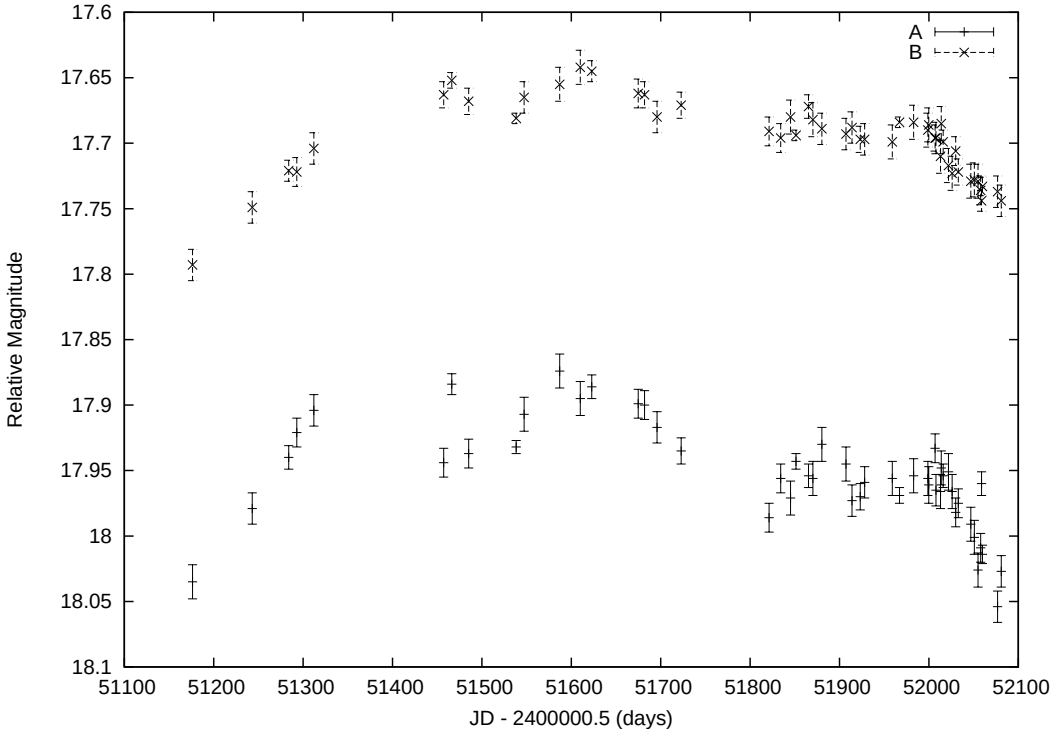

Figure 3.6: Light curves of FBQ J0951+2635. The *B* curve has been shifted by 0.8 magnitude for clarity.

Jakobsson et al. (2005) published a time delay $\Delta t_{AB} = 16 \pm 2$ days, a result that is only based on the last 38 points of the light curve when the system had been observed more intensively. They found various possible time delays according to the method, the smoothing, and the data points included, so we performed the same tests.

We can confirm that the time delay is very sensitive to the choice of smoothing parameters in the NMF method, especially when using the entire light curve, but is still more sensitive to the data points used: leaving out a single point completely changes the time delay. We calculated time delays in the light curve using between 55 and 58 data points and we found delays ranging from $\Delta t_{AB} = 14.2 \pm 4.5$ days to $\Delta t_{AB} = 26.3 \pm 4.7$ days. Taking into account three possible smoothing combinations and four sets of data (leaving out one more data point in each set) leads to a combined histogram of 12000 Monte Carlo simulations, as shown in Fig. 3.7. It is clear that a mean value with error bars $\Delta t_{AB} = 20.1 \pm 7.2$ days is not of any scientific use: the error bars are too large relative to the time delay. Moreover, the histogram is quite different from a normal distribution. There is no significant concentration of the results, which would allow the determination of a meaningful mode, independently of the chosen binning. One can see that different time delays are possible and can be divided in two groups: shorter values of ~ 10.5, ~ 15, and ~ 18.5 days, and longer values of ~ 26.5 and 30.5 days.

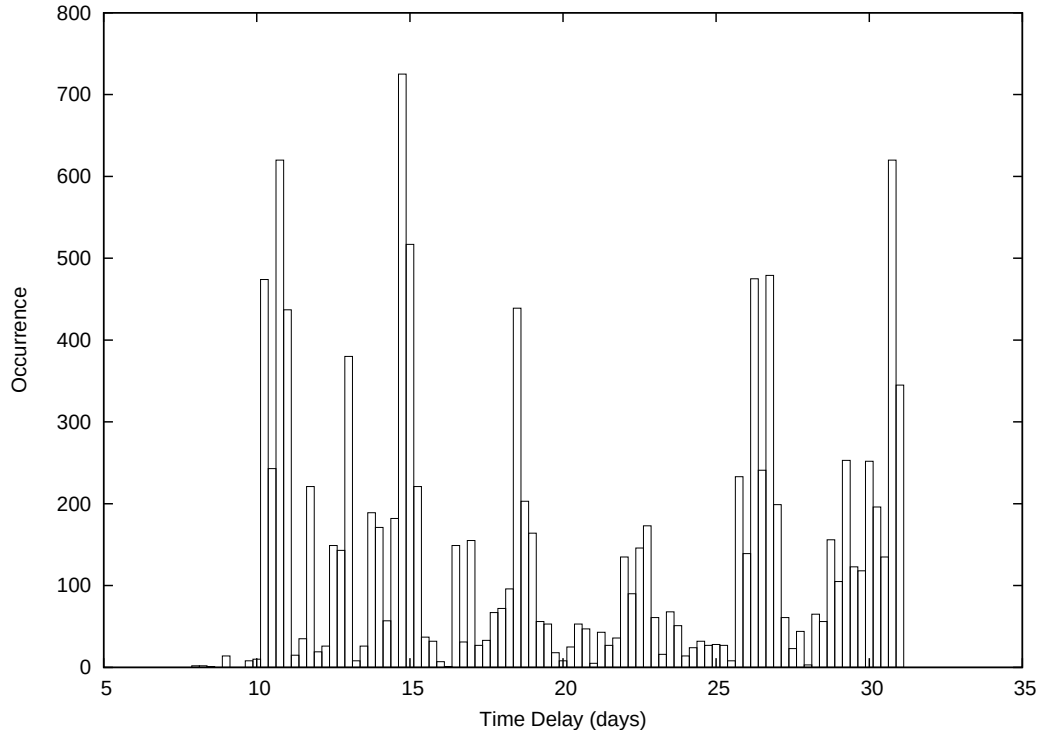

Figure 3.7: Sum of twelve histograms of 1000 runs each for FBQ J0951+2635, using three different combinations of smoothing parameters for four sets of data consisting of 58, 57, 56, and 55 data points.

When using only the third observing season, which is more finely sampled, a relatively stable time delay $\Delta t_{AB} = 18.8 \pm 4.5$ is measured, but once a single point is left out (for example the 19th point of this third season, a point that deviates from the general trend in spite of a small error bar), the result completely changes towards longer values ($\Delta t_{AB} = 25.0 \pm 4.9$ days) and becomes sensitive to smoothing. As the measured time delay should not depend on the presence or absence of a single point, we can only conclude that this light curve, even if it consists of three observing seasons, does not allow a precise determination of this delay.

The MD method entirely confirms the large uncertainty in this time delay: using all data points we

find a time delay of $\Delta t_{AB} = 21.5 \pm 6.8$ days, whereas the third season only leads to $\Delta t_{AB} = 19.6 \pm 7.6$ days, with peaks in the histogram around $\Delta t_{AB} \sim 12$ and $\Delta t_{AB} \sim 28$ days.

According to Schechter et al. (1998) and Jakobsson et al. (2005), there are spectroscopic indications of possible microlensing, so this might explain the difficulty in constraining the time delay for this system. Longer and more finely sampled light curves might help us to disentangle both effects. However, at the present stage, we can conclude that this system is probably not suitable for a time delay analysis.

3.5 HE 1104-1805

Wisotzki et al. (1993) reported the discovery of this bright double quasar, and suggested that it was a gravitationally lensed quasar rather than a binary, and that it was affected by microlensing. The first attempts to determine the time delay of the system were based on only 19 data points and lead to a very high value of $\Delta t_{BA} \sim 300$ days (Wisotzki et al. 1998; Gil-Merino et al. 2002; Pelt et al. 2002). Schechter et al. (2003) published longer light curves but did not succeed in pinning down the time delay. Some months later, two independent groups, Wyrzykowski et al. (2003) and Ofek & Maoz (2003), published nearly at the same time new time delays for the system of half the previous value.

We used the data published by Poindexter et al. (2007), which combine their own SMARTS R-band data with Wise R-band data from Ofek & Maoz (2003) and OGLE V-band data from Wyrzykowski et al. (2003). The three data sets are shown in Figure 3.8. Table 3.1 lists the four time delay values published for HE 1104-1805, where B is the leading quasar image.

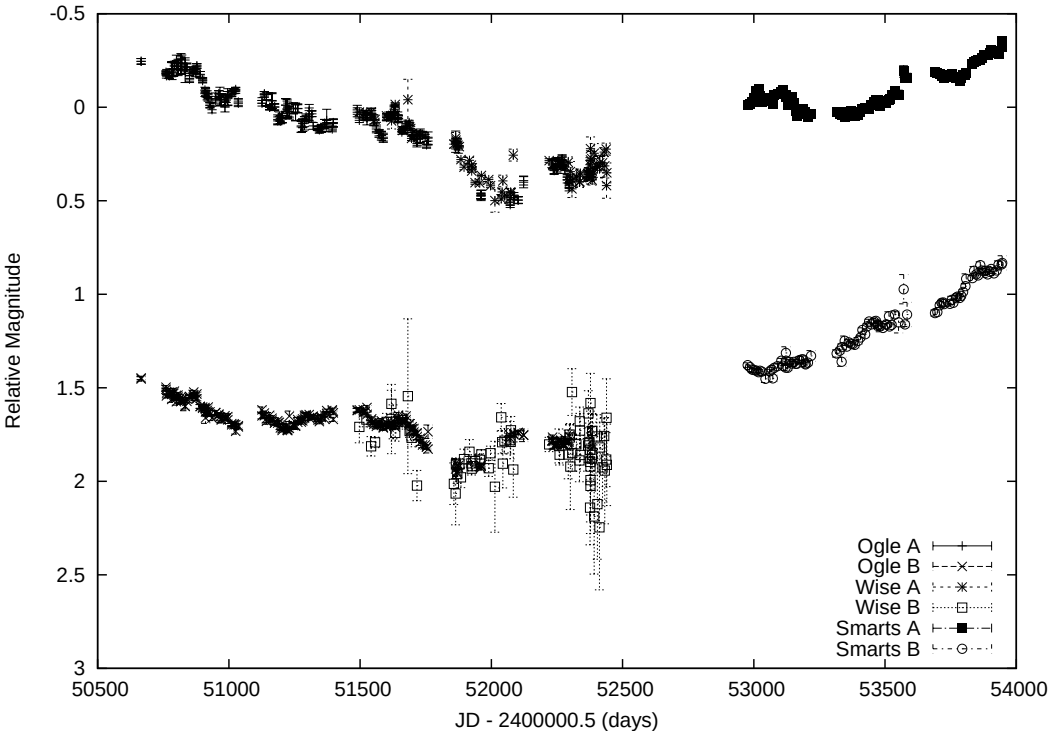

Figure 3.8: Light curves of HE 1104-1805, combining the OGLE V-band data, the Wise R-band data and the SMARTS R-band data.

We performed tests with both methods on different combinations of the data using all telescopes or only one or two of them. Unfortunately, the results seem to be sensitive to this choice, as they are to the way in which microlensing is treated: both the OGLE and Wise data sets were analysed to find a

Time Delay (days)	Reference
$\Delta t_{BA} = 161 \pm 7$	Ofek & Maoz (2003)
$\Delta t_{BA} = 157 \pm 10$	Wyrzykowski et al. (2003)
$\Delta t_{BA} = 152^{+2.8}_{-3.0}$	Poindexter et al. (2007)
$\Delta t_{BA} = 162.2^{6.3}_{-5.9}$	Morgan et al. (2008a)

Table 3.1: Published time delays for HE 1104-1805.

time delay $\Delta t_{BA} \sim 157$ days, whereas SMARTS data converge to a higher value of $\Delta t_{BA} \sim 161$ days or more as is shown in Fig. 3.9. In addition, Poindexter et al. (2007)'s smaller value is recovered with the MD method when including OGLE and Wise data but only for some ways of modelling microlensing. We therefore conclude that we can neither make a decisive choice between the published values, nor improve their error bars, which are large enough to overlap.

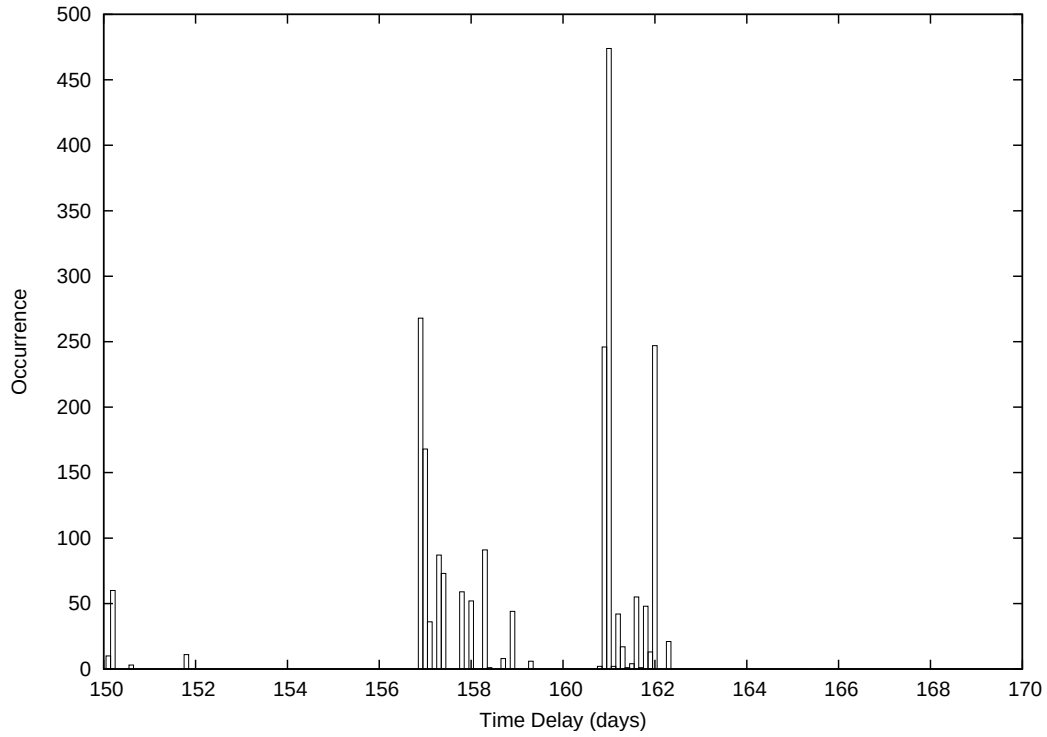

Figure 3.9: Sum of three histograms for HE1104-1805, using three different combinations of smoothing parameters combining only OGLE and SMARTS data. OGLE data point to a time delay $\Delta t_{BA} \sim 157$ days, whereas SMARTS data converge to a longer value of $\Delta t_{BA} \sim 161$ days.

3.6 PG 1115+080

This system was the second example to be identified as a gravitational lens. It has been studied for more than 30 years now, and we refer to Section 3.6 in the next part of this work for a short overview of the literature.

We used the data taken by Schechter et al. (1997). They published a time delay $\Delta t_{CB} = 23.7 \pm 3.4$ days between the leading curve C and curve B and estimated the delay between C and the sum of $A1$

and $A2$ at $\Delta t_{CA} \sim 9.4$ days. Barkana (1997) used the same data, which are shown in Fig. 3.10, but a different method to determine the delays. His value of $\Delta t_{CB} = 25.0^{+3.3}_{-3.8}$ is compatible with Schechter's one. Morgan et al. (2008b) published new optical light curves for this quadruply imaged quasar in order to study microlensing in the system. Unfortunately, these light curves cannot be used to determine a time delay independently because of the clear lack of features in the variability of the quasar and the inconsistency of the individual error bars relative to the dispersion in the data.

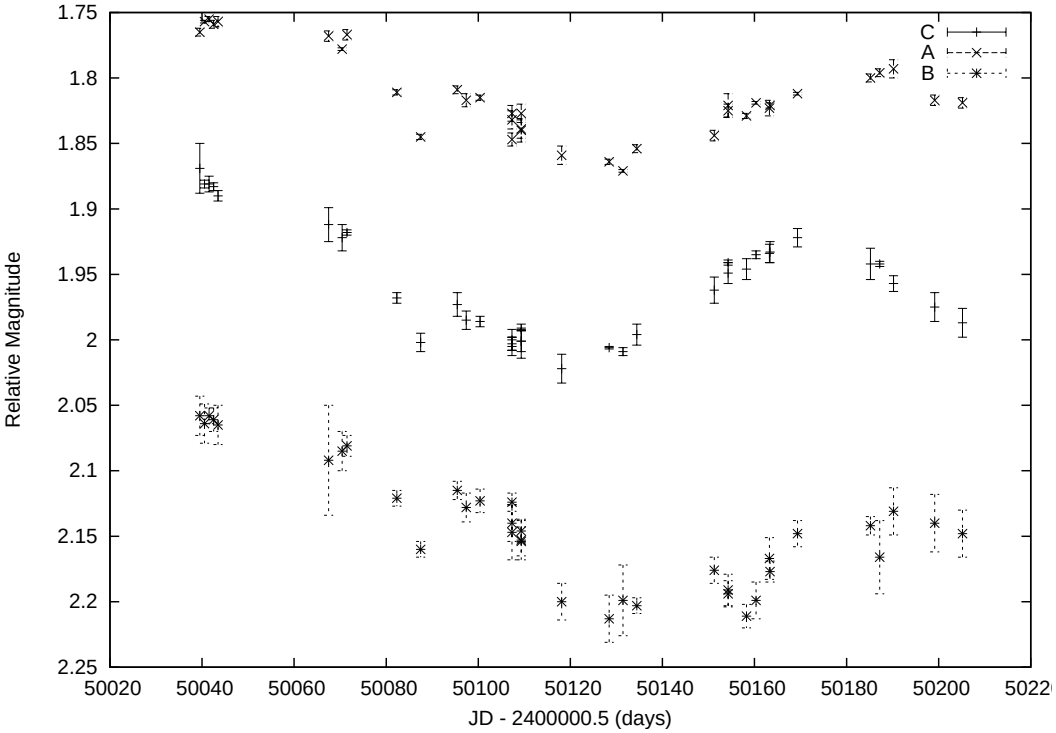

Figure 3.10: Light curves of PG 1115+080, where the A curve is the sum of the $A1$ and $A2$ component. The A and the B curve have both been shifted by 1.9 and -0.3 magnitude, respectively.

A first series of tests on Schechter's data with the NMF method led to time delays of $\Delta t_{CA} \sim 15$ days and $\Delta t_{CB} \sim 20.8$ days with a minor secondary peak around $\Delta t_{CB} \sim 23.8$. We then corrected the published data for the existing photometric correlation between the quasar images and the two stars used as photometric references, as mentioned by Barkana (1997). This caused the shorter time delay to shift either towards $\Delta t_{CA} \sim 11$ days or $\Delta t_{CA} \sim 16$ days, and transformed the longer delay into two nearly equally possible results of $\Delta t_{CB} \sim 20.8$ days or $\Delta t_{CB} \sim 23.8$, as indicated by the two main peaks in the histogram in Fig. 3.11. Adding observational errors to the model light curves and taking into account four different ways of smoothing results in $\Delta t_{CA} = 11.7 \pm 2.2$ (see Fig. 3.12) and $\Delta t_{CB} = 23.8^{+2.8}_{-3.0}$ (see Fig. 3.11).

The MD method confirms a delay of $\Delta t_{CB} \sim 20.0$ days, but finds a second solution around $\Delta t_{CB} \sim 12.0$ days, which results in $\Delta t_{CB} = 17.9 \pm 6.9$. The value for Δt_{CA} is also shorter than the one obtained with the other methods namely $\Delta t_{CA} = 7.6 \pm 3.9$ days and has larger error bars. Unfortunately, the length and quality of this light curve do not allow one to choose between the possible time delays that differ according to the method used, but are generally lower than published values.

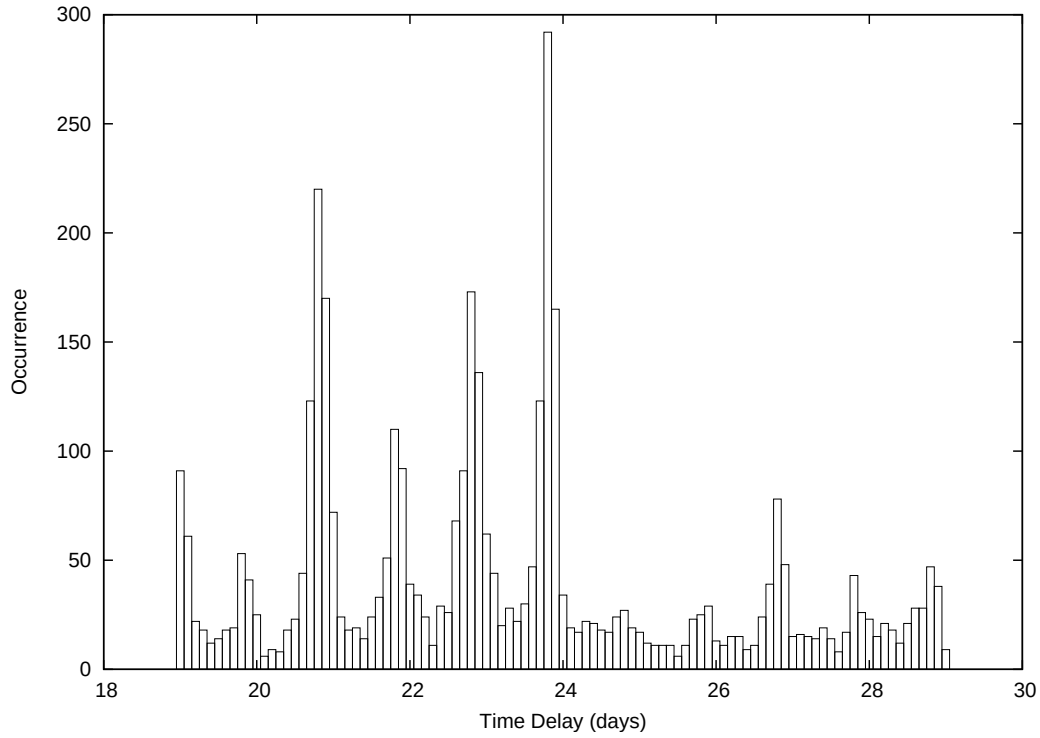

Figure 3.11: Sum of four histograms of 1000 runs each for Δt_{CB} in PG1115+080, using four different combinations of smoothing parameters.

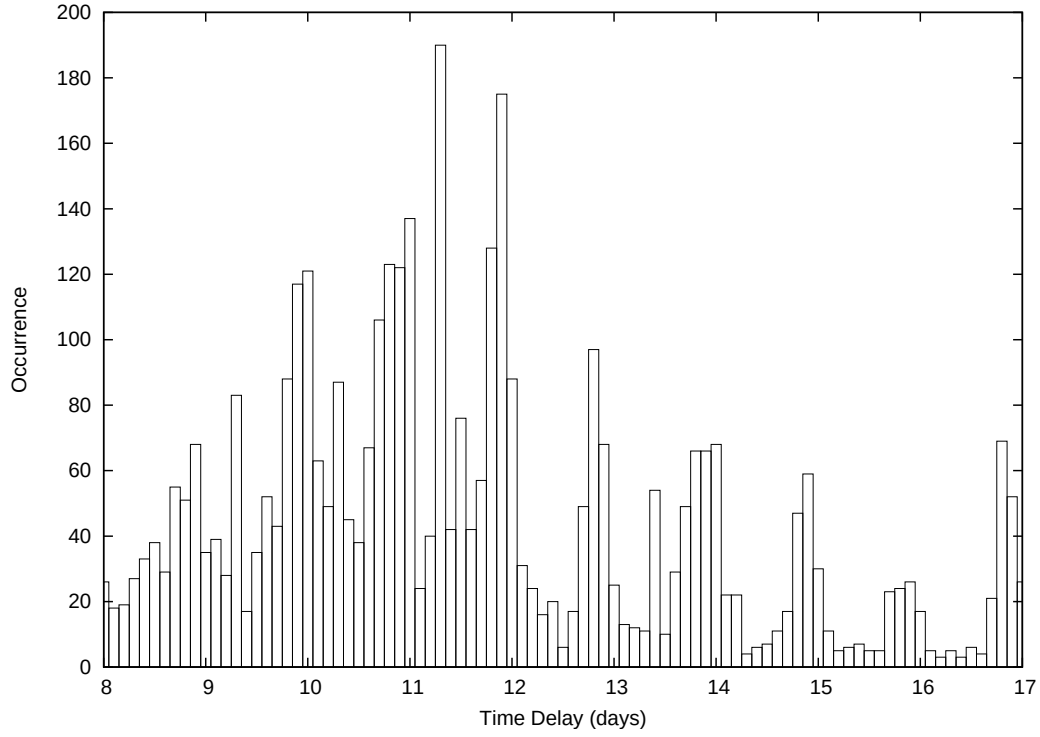

Figure 3.12: Sum of four histograms of 1000 runs each for Δt_{CA} in PG1115+080, using four different combinations of smoothing parameters.

3.7 JVAS B1422+231

This quadruply lensed quasar was first detected by Patnaik et al. (1992) in radio wavelengths. Lawrence et al. (1992) and Remy et al. (1993) detected the infrared and optical counterparts respectively and confirmed the lensing hypothesis.

For this quadruply lensed quasar, we used the data published by Patnaik & Narasimha (2001), consisting of flux density measurements at two frequencies, 8.4 and 15 GHz. Their results for the time delays were based only on the 15 GHz data without image *D*, which is too faint. These data are shown in Fig. 3.13. They obtained $\Delta t_{BA} = 1.5 \pm 1.4$ days, $\Delta t_{AC} = 7.6 \pm 2.5$, and $\Delta t_{BC} = 8.2 \pm 2.0$ days when comparing the curves in pairs.

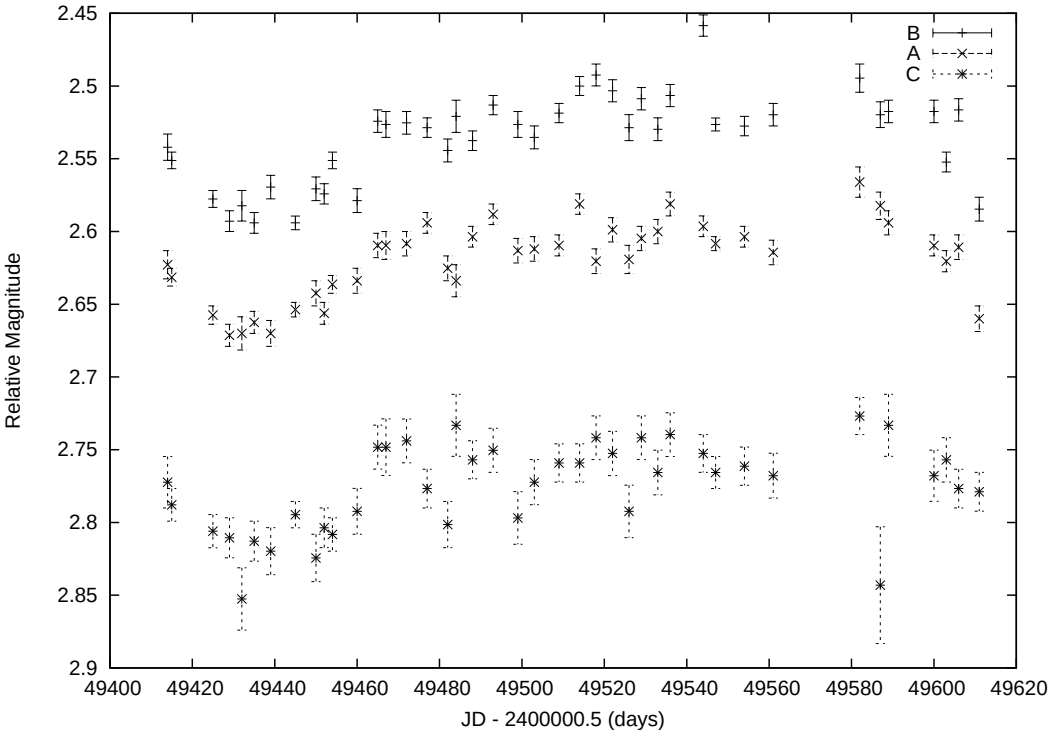

Figure 3.13: Light curves of JVAS B1422+231 for the *A*, *B*, and *C* components after transforming the flux density measurements at the 15 GHz frequency into magnitudes. The *C* curve has been shifted by half a magnitude.

The NMF method allows time delays to be tested for the three light curves simultaneously, thus imposes coherence on the results. Given the error bars in the published results, which are large compared to the time delays, we can confirm the results here, but we emphasize that they include two distinct groups of solutions between which we cannot decide based on the actual light curves: for the shortest delay, we either have $\Delta t_{BA} \sim 1.0$ day or $\Delta t_{BA} \sim 2.0$ days, as shown in Fig. 3.14. The choice between both solutions is sensitive to the smoothing parameters: the importance of the first group $\Delta t_{BA} \sim 1.0$ day is lower, and even disappears completely, with greater smoothing.

For Δt_{BC}, the situation is similar but even less clear: low smoothing parameters lead to a range of possible solutions between $\Delta t_{BC} \sim 6$ and $\Delta t_{BC} \sim 10$ days, which are all within the error bars of the published results. However, Monte Carlo simulations of reconstructed light curves with higher smoothing parameters give a time delay $\Delta t_{BC} = 10.8 \pm 1.5$ days with a secondary peak around $\Delta t_{BC} \sim 8$ days.

The MD method gives a completely different result: it converges towards time delays that invert the BAC-order into CAB but with error bars large enough not to exclude the BAC order of $\Delta t_{BA} = -1.6 \pm 2.1$

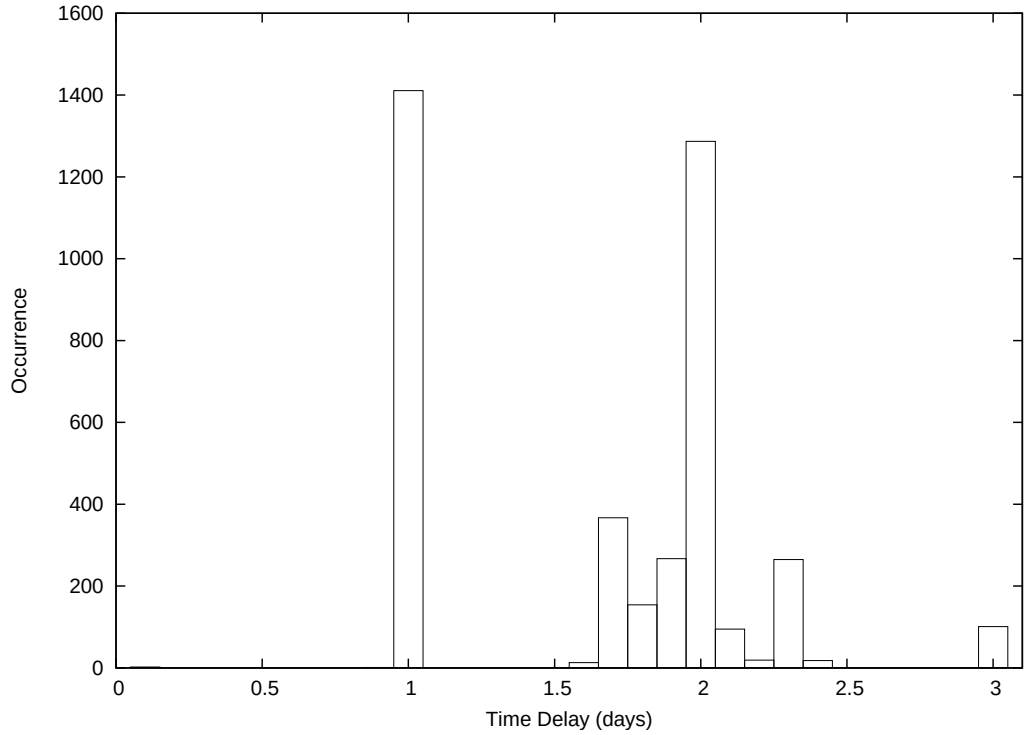

Figure 3.14: Sum of four histograms for Δt_{BA} of 1000 runs each for JVAS B1422+231, using four different combinations of smoothing parameters.

days, $\Delta t_{AC} = -0.8 \pm 2.9$, and $\Delta t_{BC} = -2.4 \pm 2.7$ days.

New observations are clearly necessary to reduce the uncertainties in both the different solutions and the error bars that are too large in comparison with the time delays to be useful to any further analysis.

3.8 SBS 1520+530

Chavushyan et al. (1997) reported the discovery of this doubly lensed quasar. One year later, Crampton et al. (1998) detected the lens galaxy between the quasar components thus confirming this system as a gravitational lens.

Two data sets exist for this doubly lensed quasar: the set made available by Burud et al. (2002b) and the one published by Gaynullina et al. (2005a). Burud et al. (2002c) were the first to publish a time delay for this system $\Delta t_{AB} = 128 \pm 3$ days, where A is the leading image, or $\Delta t_{AB} = 130 \pm 3$ days when using the iterative version of the method (Burud et al. 2001). Gaynullina et al. (2005b) used an independent data set and found four possible time delays, of which the one with the largest statistical weight, $\Delta t_{AB} = 130.5 \pm 2.9$, is perfectly consistent with the previously published time delays.

Even if the light curve based on Gaynullina et al. (2005a) data contains more than twice as many data points as Burud et al. (2002b)'s older light curve, we decided not to use it because of the lack of overlapping data between the A and the B curves of the quasar after shifting the B curve for the time delay, as can be seen in Fig. 3.15.

Applying different tests to Burud et al. (2002c)'s light curves, shown in Fig. 3.16, using the NMF method led to a time delay for which the error bars overlap with the published value: $\Delta t_{AB} = 126.9 \pm 2.3$. That the delay is slightly shorter than Burud et al. (2002c)'s value can be explained by our use of the reduced χ^2_{red} instead of the χ^2, the latter implying that longer delays are the more likely ones, as explained in the previous Chapter 2. This effect was also noted using the iterative method.

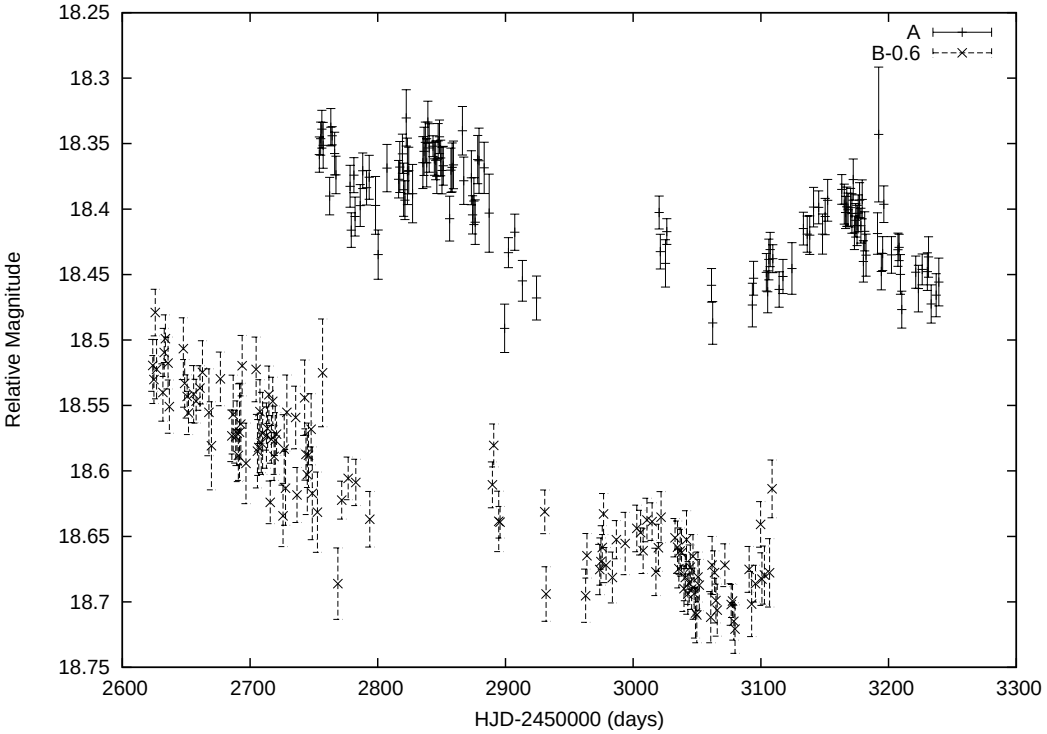

Figure 3.15: Light curves for SBS 1520+530 based on Gaynullina et al. (2005a)'s data after shifting the B curve by $\Delta t_{AB} = 130.5$ days. Hardly any data points overlap between the light curves for images A and B.

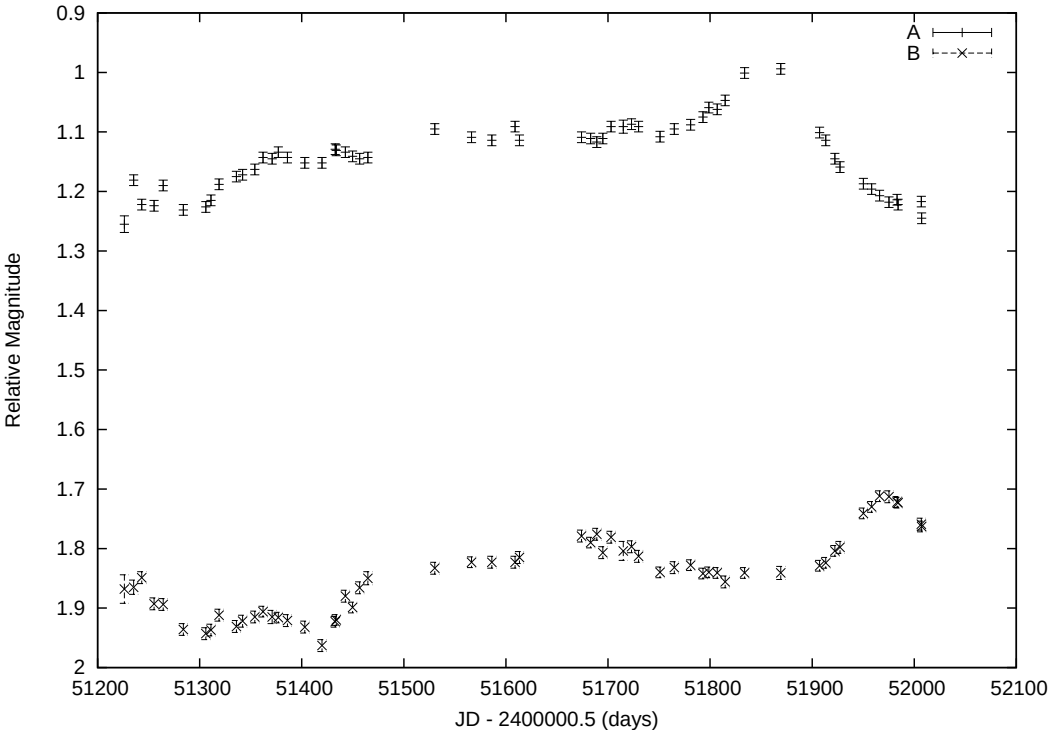

Figure 3.16: Light curves for SBS 1520+530 based on Burud et al. (2002b)'s data.

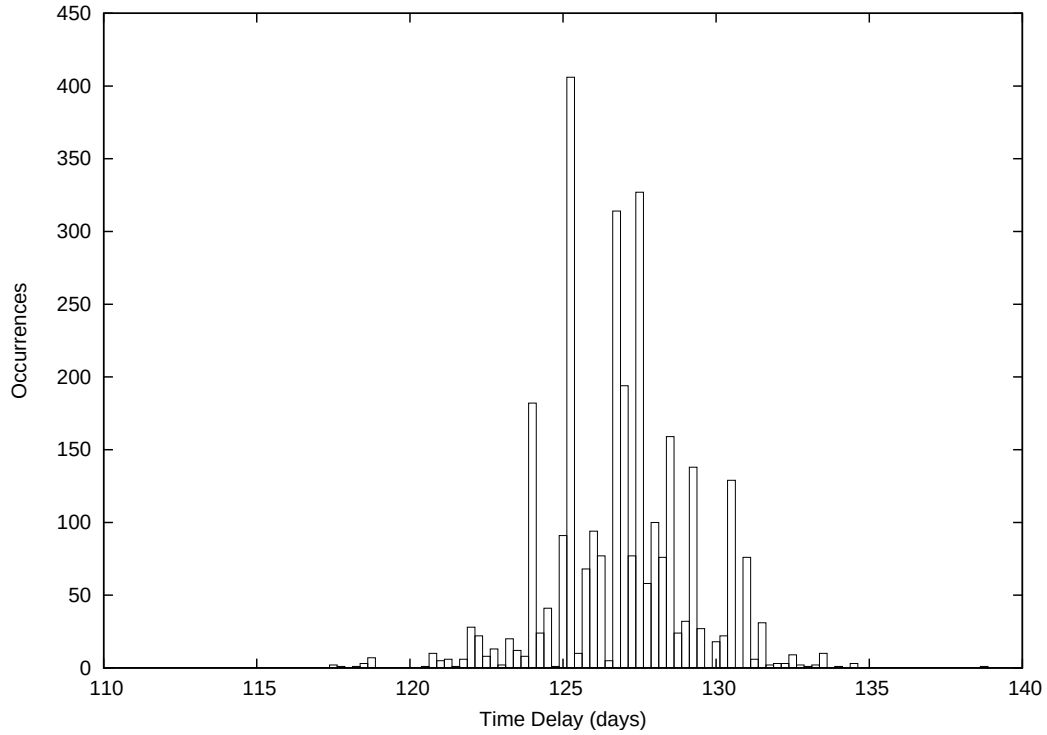

Figure 3.17: Sum of three histograms of 1000 runs each for SBS1520+530, using three different combinations of smoothing parameters.

The MD method yields a comparable time delay of $\Delta t_{AB} = 124.6 \pm 3.6$ days and confirms the shape of the histogram: the highest peak value at $\Delta t_{AB} \sim 125$ days and a clear secondary peak at $\Delta t_{AB} \sim 127.5$ days. Combining the values from both methods implies that $\Delta t_{AB} = 125.8 \pm 2.1$ days.

3.9 CLASS B1600+434

Jackson et al. (1995) argued that the probability that the double radio source CLASS B1600+434 was a gravitational lens was very high. Jaunsen & Hjorth (1997) detected the spiral lensing galaxy, and Fassnacht & Cohen (1998) estimated the lens and source redshift of the system at $z_l = 0.4144$, and $z_s = 1.589$ respectively.

Data, as shown in Fig. 3.18, were made available by Paraficz et al. (2006) but had been treated and analysed by Burud et al. (2000), who published a final time delay $\Delta t_{AB} = 51 \pm 4$ days, where A is the leading image, consistent with the time delay $\Delta t_{AB} = 47^{+12}_{-9}$ days from Koopmans et al. (2000) based on radio data.

The NMF method leads to a time delay $\Delta t_{AB} = 46.6 \pm 1.1$ days, but the histogram in Fig. 3.19 clearly shows that we cannot use the mean as the final value. The histogram has two distinct values of ~ 46 or ~ 48 days, so we prefer to speak of a delay of either $\Delta t_{AB} = 45.6^{+1.2}_{-0.4}$ days (68% error) or $\Delta t_{AB} = 45.6^{+2.8}_{-0.4}$ days (95% error).

These results are in marginal disagreement with the final delay proposed by Burud et al. (2000). However, Burud et al. (2000)'s final result is an average of four time delays, each of them calculated with a different method. Two of these methods also inferred a value of around ~ 48 days.

We could identify at least three explanations of our lower value and smaller error bars in comparison with Burud et al. (2000)'s time delay. The first one is the same again as for SBS 1520+530: our use of the reduced χ^2_{red} (see formula **??** in Chapter 2) instead of the χ^2, the latter introducing a bias towards

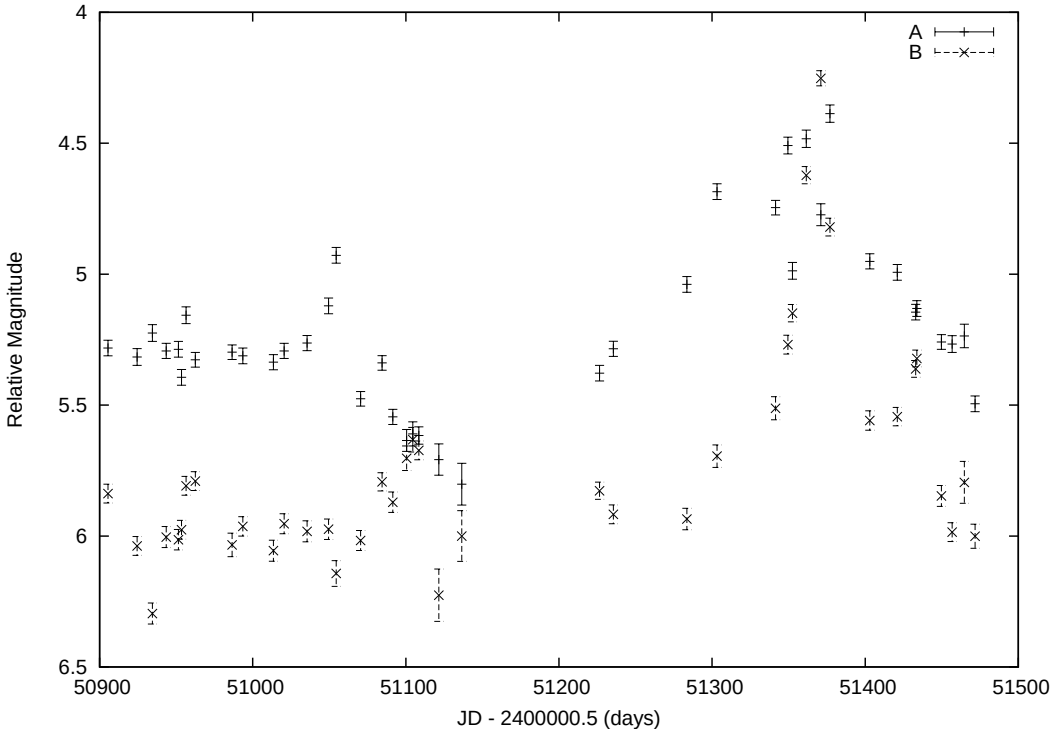

Figure 3.18: Light curves for CLASS B1600+434: 41 data points spread over nearly two years.

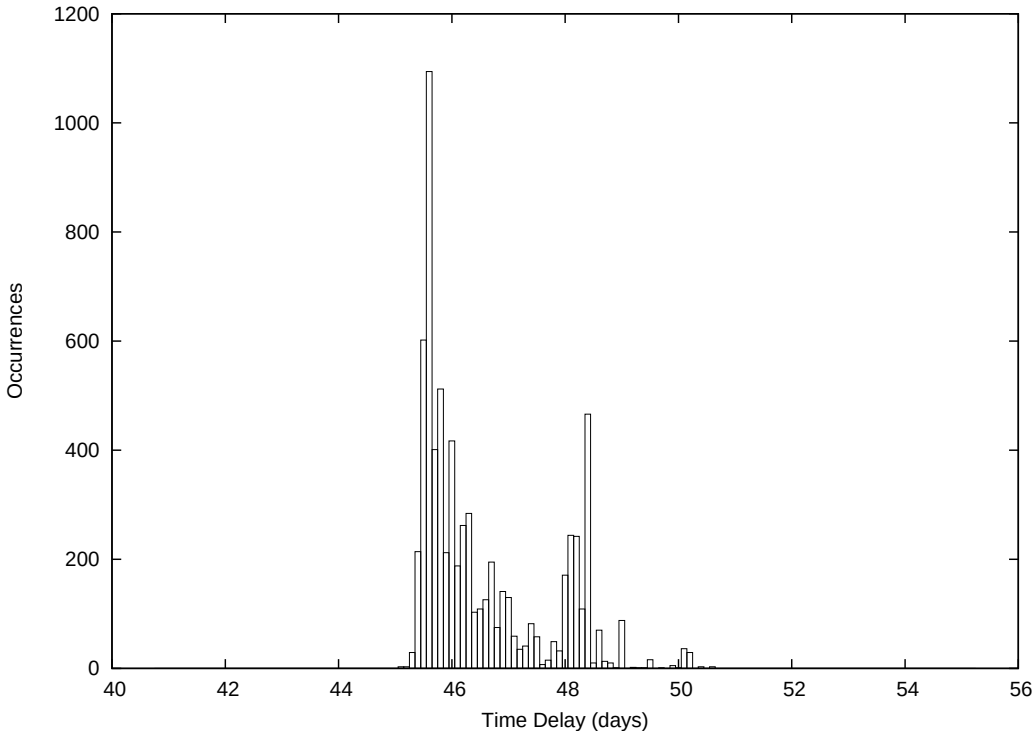

Figure 3.19: Sum of seven histograms of 1000 runs each for B1600+434, using seven different combinations of smoothing parameters.

longer delays. The second reason is the technical issue concerning the length of the model curve as explained in the same chapter, which was found to be crucial for the time delay of this system. Finally, we observed that higher values of the Lagrange multiplier weighting the smoothing term seemed to lead to longer time delay values, which disappeared with lower smoothing. Taking into account these three adjustments, nearly all values around ~ 51 days disappear from the histogram.

This is not the case for the MD method, which explains the slightly longer value of the time delay: $\Delta t_{AB} = 49.0 \pm 1.2$ days. Combining these results gives a delay of $\Delta t_{AB} = 47.8 \pm 1.2$ days. Even if these error bars imply that the time delay is very tightly constrained, we emphasize that the delay measurement is only based on 41 data points spread over nearly two years, which gives a relatively high weight to every single data point. When adding random errors, neither of the two methods leads to a histogram with a gaussian shape. A more finely sampled light curve might remedy this situation.

3.10 CLASS B1608+656

This quadruply imaged object was the first lens to be detected through the CLASS gravitational lens survey (Myers et al. 1995). Independently, Snellen et al. (1995) detected it as a 4 component radio source compatible with a gravitational lens.

Light curves for this quadruply lensed system were first analysed by Fassnacht et al. (1999) and subsequently improved in Fassnacht et al. (2002) by adding more data. Using three observing seasons, they published time delays of $\Delta t_{BA} = 31.5^{+2}_{-1}$, $\Delta t_{BC} = 36.0 \pm 1.5$, and $\Delta t_{BD} = 77.0^{+2}_{-1}$ days. Their analysis is based on a simultaneous fit to data from the three seasons but treats the curves only in pairs.

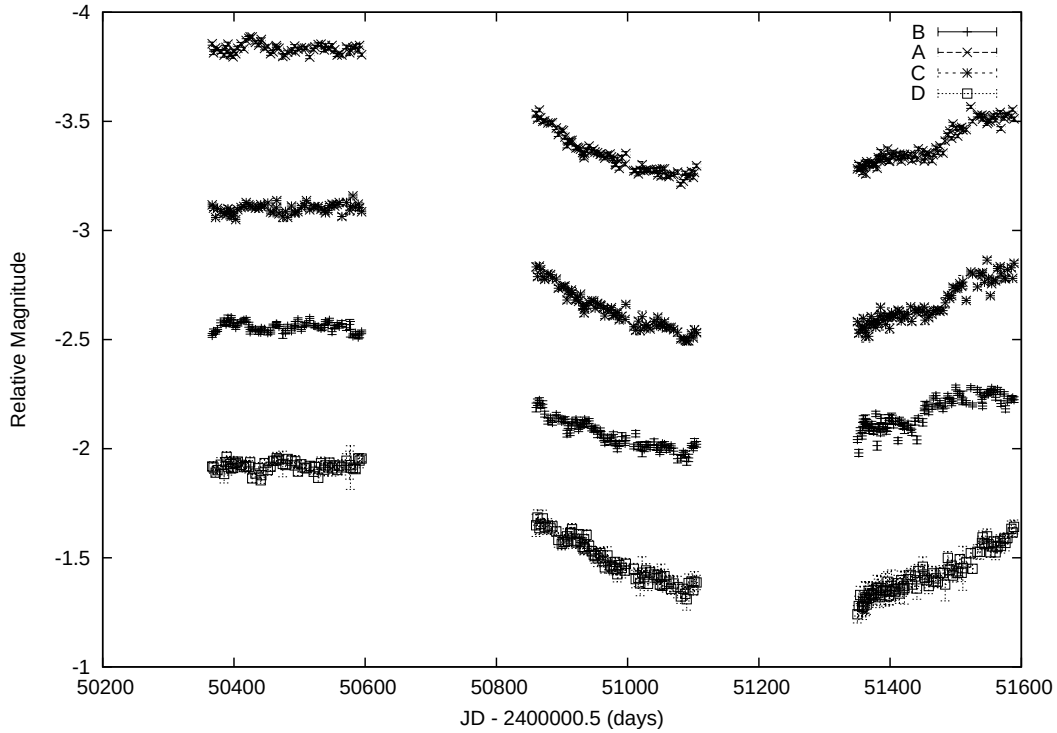

Figure 3.20: Light curves for CLASS B1608+656. The *B* curve has been shifted by half a magnitude for clarity.

We performed several tests on these light curves, which are shown in Fig. 3.20: first taking into account only the first and the third season separately (the second season not presenting useful structure),

then all data for the three seasons simultaneously, using the three and four curve version of our method as described in Chapter 2. This enables us to impose coherence between the pairs of time delays, which was not done by Fassnacht et al. (2002). The results, as illustrated in Fig. 3.21, confirm the previously published values, within the error bars, of $\Delta t_{BA} = 30.2 \pm 0.9$, $\Delta t_{BC} = 36.2 \pm 1.1$, and $\Delta t_{BD} = 76.9 \pm 2.3$ days.

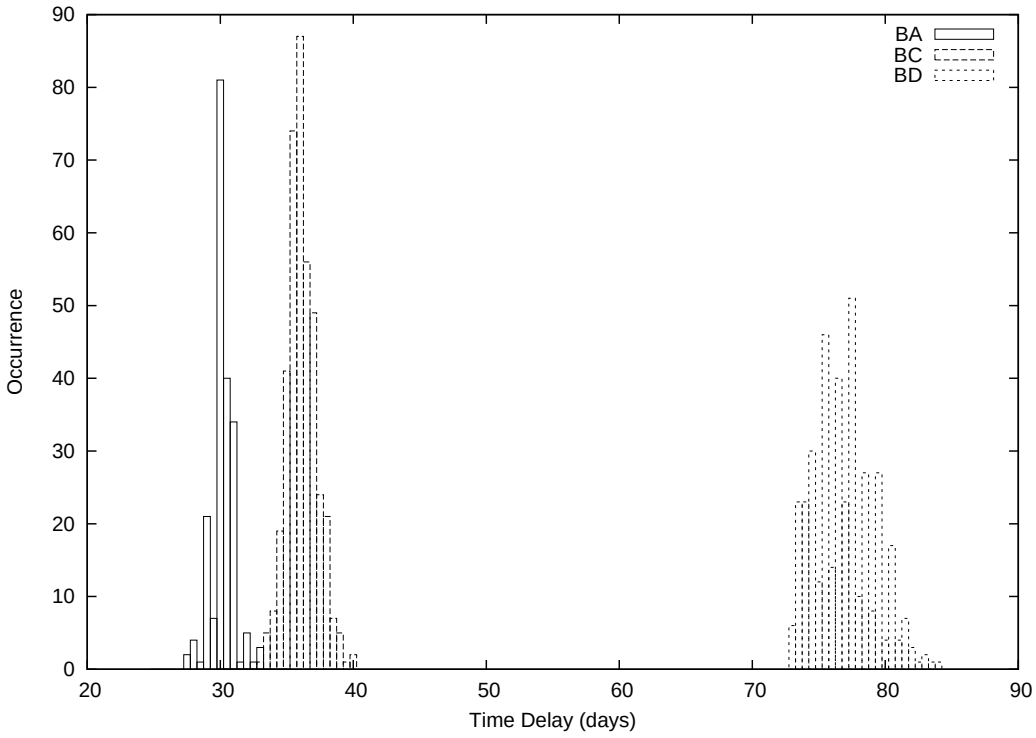

Figure 3.21: Histograms for the three time delays in CLASS B1608+656, using two different combinations of smoothing parameters for all seasons and three out of the four curves simultaneously.

One particularity deserves more attention: the value for Δt_{BA} changes slightly according to the seasons and the curves considered simultaneously. When leaving out the second season data (featureless), Δt_{BA} systematically converges towards $\Delta t_{BA} = 33.5 \pm 1.5$ days, as shown in Fig. 3.22. This is consistent with Fassnacht et al. (2002), who already mentioned a time delay of $\Delta t_{AC} \sim 2.5$ days. Even if this slight difference is probably due to microlensing and should be investigated in more detail, we chose to retain the final value, which is the one based on the use of all data.

The MD method entirely confirms these results of $\Delta t_{BA} = 32.9 \pm 2.9$, $\Delta t_{BC} = 35.2 \pm 2.5$, and $\Delta t_{BD} = 78.0 \pm 3.7$ days with another indication for $\Delta t_{AC} \sim 2.5$ days. Combining both methods results in the time delays of $\Delta t_{BA} = 31.6 \pm 1.5$, $\Delta t_{BC} = 35.7 \pm 1.4$, and $\Delta t_{BD} = 77.5 \pm 2.2$ days.

3.11 HE 2149-2745

This quasar was identified as a gravitational lens by Wisotzki et al. (1996). Two years later, Lopez et al. (1998) detected its lensing galaxy.

We reanalysed the data set made available by Burud et al. (2002b). These data consist of two light curves, one in the V-band and one in the I-band, as shown in Fig. 3.23. Burud et al. (2002a) published a time delay $\Delta t_{AB} = 103 \pm 12$ days where A is the leading image. This delay is based on the V-band data, but, according to Burud et al. (2002a), agrees with the I-band data.

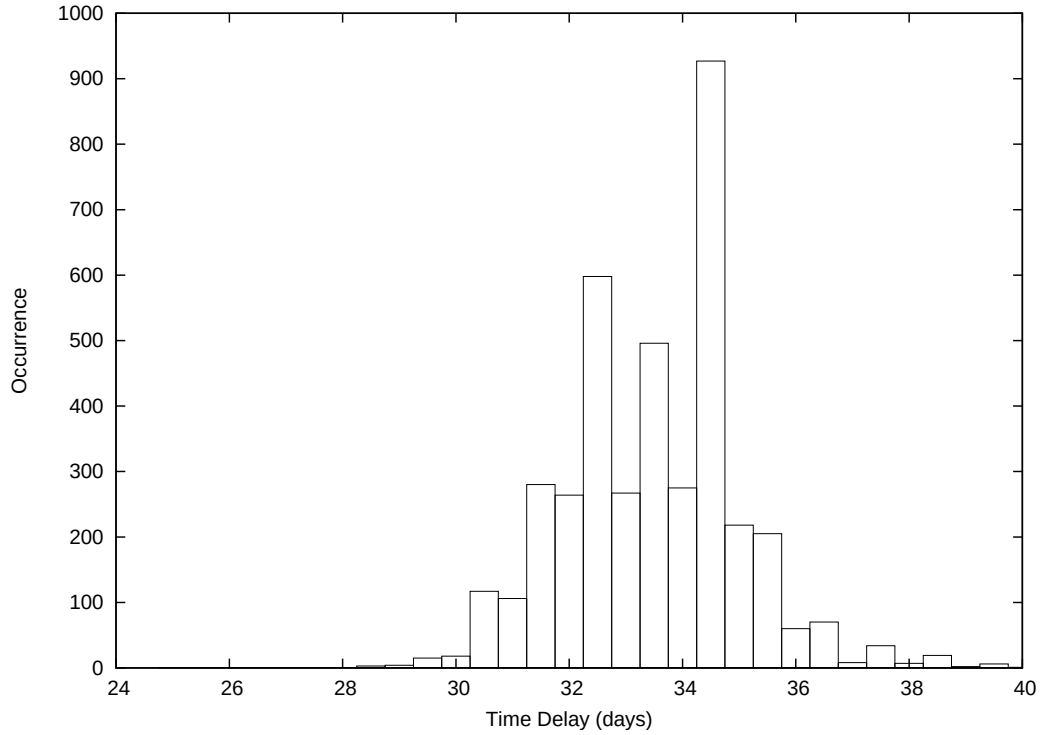

Figure 3.22: Sum of four histograms of 1000 runs each for Δt_{BA} in CLASS B1608+656, using two different combinations of smoothing parameters on the first and the third season.

Our tests, based on the light curves as such, and using both methods, clearly reveal two possible delays: one around $\sim 70 - 85$ days and one around $\sim 100 - 110$ days. Unfortunately, the light curves of images *A* and *B* show little structure and hardly overlap, except for some points in the second season, when shifting them for a delay of more than 100 days, especially in the *I*-band, which makes it very difficult to choose between the two possibilities. Moreover, once we add random errors to the model light curve and perform Monte Carlo simulations, we only obtain a forest of small peaks, spread over the entire tested range of $50 - 140$ days, instead of a gaussian distribution around one or two central peaks, demonstrating that these results are highly unstable. Leaving out two outlying data points in the B curve only slightly improves the situation: within the forest of peaks in Fig. 3.24, those in the range $75 - 85$ seem to be slightly more important than those over 100 days. Nevertheless, we cannot derive a reliable time delay from these data sets for this system.

3.12 Summary

We applied our NMF to 11 lensed quasar systems with known time delays. This allowed the validity of these time delay values to be evaluated in a coherent way. The use of a minimum dispersion method allowed us to check the independence of the results from the method. The results are summarized in Table 3.2.

We caution that some published time delay values should be interpreted with care: even if we have been able to confirm some values (time delays for JVAS B0218+357, HE 1104-1805, CLASS B1600+434, and for the three delays in the quadruply lensed quasar CLASS B1608+656) and give an improved value for one system, SBS 1520+530, many of the published time delays considered in our analysis have proven to be be unreliable for various reasons: the analysis is either too dependent on some data points, leads to multiple solutions, is sensitive to the addition of random errors, or is incoherent be-

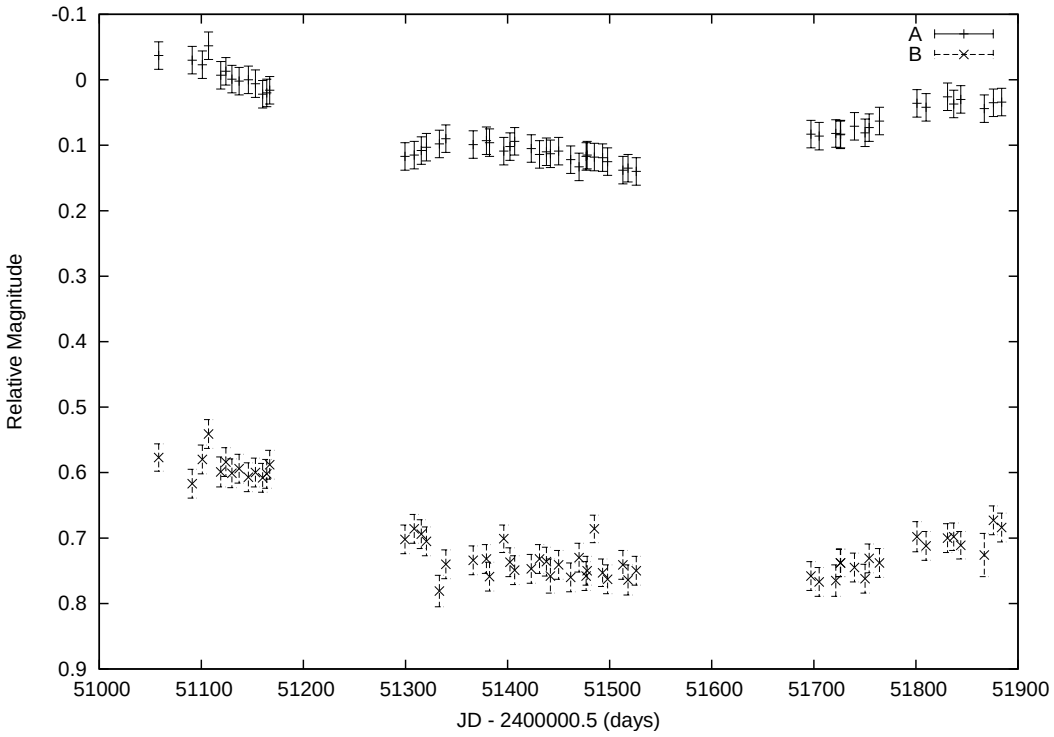

(a) V-band data

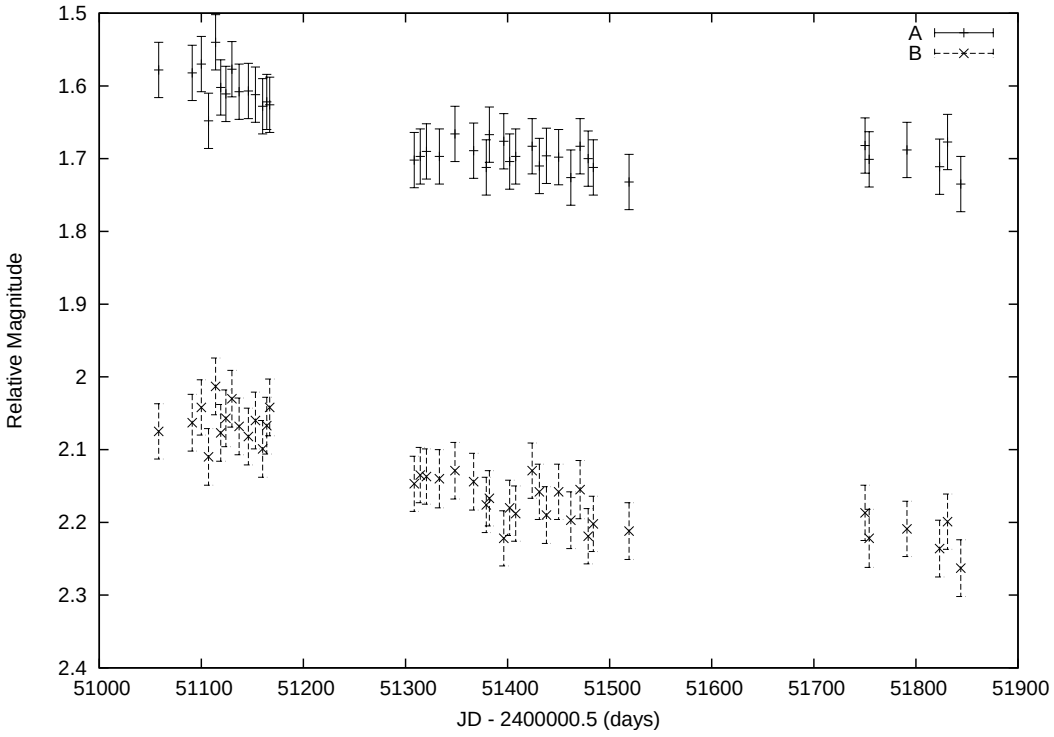

(b) I-band data

Figure 3.23: Light curves of HE 2149-2745 in the V-band and the I-band. The *B* curve has been shifted by one magnitude for clarity.

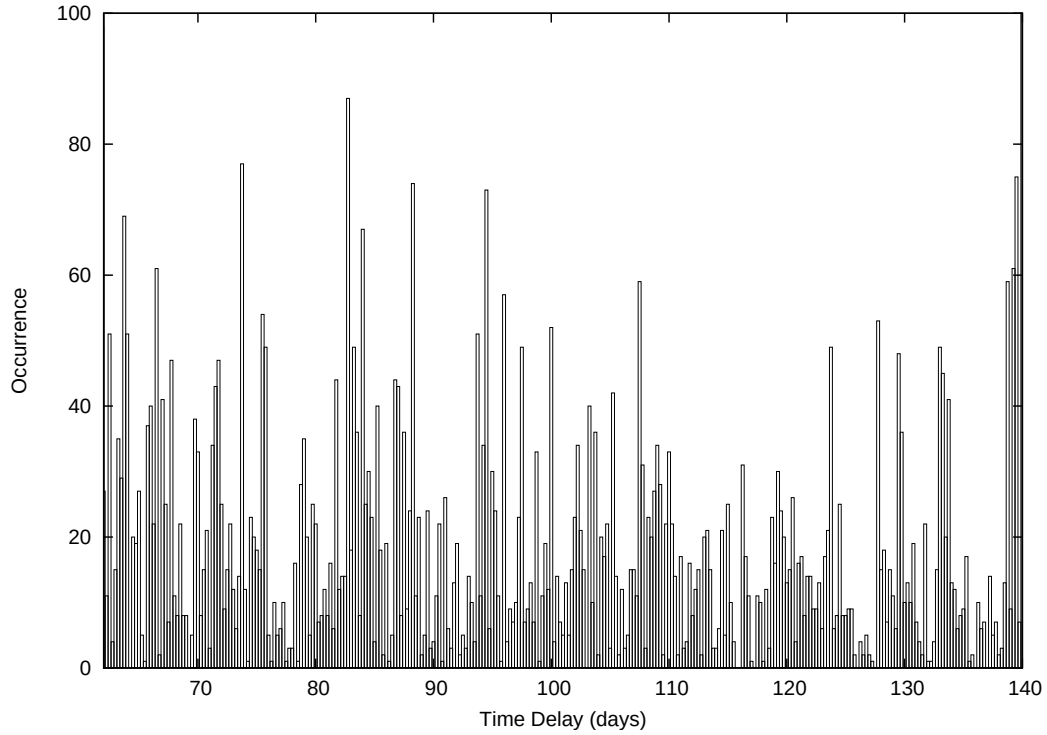

Figure 3.24: Sum of six histograms of 1000 iterations each for HE 2149-2745 leaving out two data points, using six different combinations of smoothing parameters.

tween the two different methods used.

Given the accuracy that is needed for time delays to be useful to further studies, we note that it will be necessary to perform long-term monitoring programs on dedicated telescopes to obtain high-quality light curves of lensed quasars, not only for new systems but also for the majority of the lenses in this sample, for which the time delay has been considered to be known. The COSMOGRAIL collaboration, which has been observing over 20 lensed systems for nearly a decade now, will soon be improving the time delay values for some of these systems for which the accuracy is unsatisfactory.

At the same time, it would be very useful and interesting to perform a similar study for every different method used to calculate time delays. In this way, the peculiarities of every method, and their influence on the published delays, can be evaluated more clearly, and at the same time it is an excellent test on the validity of a large sample of time delays.

System	Our Results	Published Values	Reference
JVAS B0218+357	$\Delta t_{AB} = 9.9^{+4.0}_{-0.9}$	$\Delta t_{AB} = 10.1^{+1.5}_{-1.6}$	Cohen et al. (2000)
	or	$\Delta t_{AB} = 12 \pm 3$	Corbett et al. (1996)
	$\Delta t_{AB} = 11.8 \pm 2.3$	$\Delta t_{AB} = 10.5 \pm 0.4$	Biggs et al. (1999)
SBS 0909+523	unreliable	$\Delta t_{BA} = 49 \pm 6$	Goicoechea et al. (2008)
		$\Delta t_{BA} = 45^{+11}_{-1}$	Ullán et al. (2006)
RX J0911+0551	2 solutions:	$\Delta t_{BA} = 150 \pm 6$	Burud (2001)
	$\Delta t_{BA} \sim 146$ or ~ 157	$\Delta t_{BA} = 146 \pm 4$	Hjorth et al. (2002)
FBQS J0951+2635	unreliable	$\Delta t_{AB} = 16 \pm 2$	Jakobsson et al. (2005)
HE 1104-1805		$\Delta t_{BA} = 152^{+2.8}_{-3.0}$	Poindexter et al. (2007)
	impossible to distinguish	$\Delta t_{BA} = 161 \pm 7$	Ofek & Maoz (2003)
	but identical	$\Delta t_{BA} = 157 \pm 10$	Wyrzykowski et al. (2003)
	within error bars	$\Delta t_{BA} = 162.2^{+6.3}_{-5.9}$	Morgan et al. (2008a)
PG 1115+080	dependent on method	$\Delta t_{CA} \sim 9.4$	Schechter et al. (1997)
		$\Delta t_{CB} = 23.7 \pm 3.4$	Schechter et al. (1997)
		$\Delta t_{CB} = 25.0^{+3.3}_{-3.8}$	Barkana (1997)
JVAS B1422+231	contradictory results	$\Delta t_{BA} = 1.5 \pm 1.4$	Patnaik & Narasimha (2001)
	between methods:	$\Delta t_{AC} = 7.6 \pm 2.5$	
	BAC or CAB?	$\Delta t_{BC} = 8.2 \pm 2.0$	
SBS 1520+530	$\Delta t_{AB} = 125.8 \pm 2.1$	$\Delta t_{AB} = 130 \pm 3$	Burud et al. (2002c)
		$\Delta t_{AB} = 130.5 \pm 2.9$	Gaynullina et al. (2005b)
CLASS B1600+434	$\Delta t_{AB} = 47.8 \pm 1.2$	$\Delta t_{AB} = 51 \pm 4$	Burud et al. (2000)
CLASS B1608+656	$\Delta t_{BA} = 31.6 \pm 1.5$	$\Delta t_{BA} = 31.5^{+2}_{-1}$	Fassnacht et al. (2002)
	$\Delta t_{BC} = 35.7 \pm 1.4$	$\Delta t_{BC} = 36.0 \pm 1.5$	
	$\Delta t_{BD} = 77.5 \pm 2.2$	$\Delta t_{BD} = 77.0^{+2}_{-1}$	
HE 2149-2745	unreliable	$\Delta t_{AB} = 103 \pm 12$	Burud et al. (2002a)

Table 3.2: Summary of time delays (in days) for 11 lensed systems.

Part II

COSMOGRAIL

1

The COSMOGRAIL Project

The COSMOGRAIL project, or the COSmological MOnitoring of GRAvItational Lenses, started in 2004 and was presented in Courbin et al. (2005). It aims at estimating the Hubble constant H_0 with a precision below 2% through the determination of time delays in gravitationally lensed quasars. It is an international collaboration involving research teams from five countries: Switzerland, Belgium, Uzbekistan, India, and the UK.

Using the time delay method to constrain the Hubble constant, as Refsdal (1964a) proposed it nearly 50 years ago, is only possible if we know - in addition to the time delay between the lensed quasar images - the redshift of the lens and the source, and if we have a model for the mass distribution of the lensing galaxy. The COSMOGRAIL project addresses all these issues, but mainly concentrates on the first aspect of the problem: the measurement of precise time delays, of which the uncertainty propagates linearly into the error on the final Hubble constant.

1.1 Telescopes

A long time program for the regular monitoring of more than 20 gravitational lenses requires a considerable amount of observing time. Here is an overview of the telescopes involved in COSMOGRAIL:

1.1.1 Mercator

The Belgian-Flemish Mercator telescope is a semi-robotic 1.2m telescope operated by the Institute for Astronomy of the Leuven University and located at the Observatorio del Roque de los Muchachos on La Palma, Canary Islands, Spain, at 2333m above sealevel. At the time of its participation in COSMOGRAIL, it was equipped with the MEROPE CCD camera having a field of view of 6.5' × 6.5' and a scale of 0.19 arcseconds per pixel.

Figure 1.1: The Mercator Telescope on La Palma, Canary Islands

The Mercator telescope observed 18 different gravitational lenses for the COSMOGRAIL project, some systematically and others sporadically, from 2004 until December 2008.

1.1.2 Maidanak

The Maidanak Observatory of the Ulugh Beg Astronomical Institute in Tashkent, Uzbekistan, is located at an altitude of 2593m above sealevel. The AZT-22 1.5m telescope at Maidanak is equipped with a SITE CCD 2048 × 800 array camera with a scale of 0.266 arcseconds per pixel and a field of view of 3.5' × 8.9'. During two seasons, a second camera (SI) was used having an array of 4096 × 4096 and a field of view of 18.1' by 18.1' with the same scale of 0.266 arcseconds per pixel.

From 2004 until 2008, 25 gravitational lenses have been observed for COSMOGRAIL with this telescope.

Figure 1.2: On the left the AZT-22 Telescope at Maidanak Observatory, Uzbekistan

1.1.3 Himalayan Chandra Telescope

Figure 1.3: The Himalayan Chandra Telescope in Hanle, India

The 2-m optical-infrared Himalayan Chandra Telescope (HCT) is located at the Indian Astronomical Observatory at 4500m altitude in Hanle to the north of the Western Himalaya, in India. It is remotely operated from CREST, near the village of Hosakote, India, via a dedicated satellite link. Both facilities are managed by the Indian Institute of Astrophysics in Bangalore. The telescope is equipped with the Hanle Faint Object Spectrograph Camera (HFOSC), a 2048 × 4096 pixels CCD camera with a field of view of 10' by 10' and a scale of 0.296 arcseconds per pixel.

The HCT telescope started observing a first lens for COSMOGRAIL at the end of 2005, and has increased its active participation from 2007 onwards until today, now monitoring 6 lenses.

1.1.4 Euler

The Swiss 1.2-m Euler telescope is operated by the Geneva Observatory of the University of Geneva and situated at the La Silla Observatory, Chile, at 2400m above sea level. Its C2 2048 × 2048 array CCD camera has a field of view of 11' by 11' and a scale of 0.344 arcseconds per pixel. This camera was replaced in September 2010 by EulerCAM, a CCD camera with a pixel scale of 0.215". In this work we only use C2 data, but not the more recent EulerCAM data. The bulk of the COSMOGRAIL data come from the Euler telescope, as it has been monitoring 25 lenses since

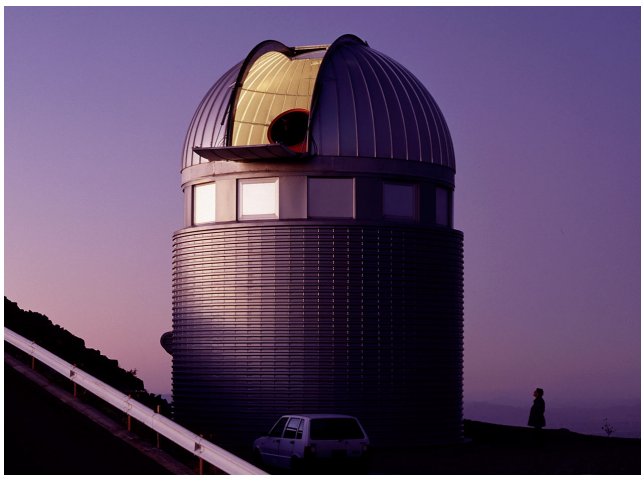

Figure 1.4: The Euler Telescope at La Silla, Chile

2004 up to now.

1.1.5 Liverpool Robotic Telescope

The Liverpool Robotic Telescope (LRT) is a 2.0-m fully robotic telescope at the Observatorio del Roque de Los Muchachos, La Palma, Canary Islands, Spain, and is owned and operated by the Astrophysics Research Institute of Liverpool. It observed 4 lensed quasars for COSMOGRAIL in 2007-2008, and one more in 2010, but we do not use these data in the present work.

Figure 1.5: The Liverpool Robotic Telescope on La Palma, Canary Islands, at sunrise

1.2 Publications

The COSMOGRAIL publications reflect the variety of aspects concerning the use of the time delay method to estimate the Hubble constant H_0. In Eigenbrod et al. (2005), the authors defined the best possible strategy, based on simulated light curves, to sample the observations of lensed quasars in such a way as to minimize the uncertainty on the deduced time delay, while taking into account the degree of variability of the quasar, the length of the time delay, and the presence of microlensing.

As the knowledge of the redshift of the lensing galaxy in a lensed quasar system is essential to its modelling, COSMOGRAIL measured these redshifts in VLT spectra of 15 multiply imaged quasars, and presented them in Eigenbrod et al. (2006a), Eigenbrod et al. (2006b), and Eigenbrod et al. (2007).

Uncertainties on the lens model generally make up for about half of the uncertainty on the Hubble constant. Different approaches for this modelling exist. In Saha et al. (2006b), pixelized lens models (Saha & Williams 2004) are used to predict time delays for a sample of gravitationally lensed quasars. Chantry et al. (2010) and Sluse et al. (2012) used precise astrometry from deconvolved Hubble Space Telescope images to better constrain the analytical lens models (Keeton 2001) of the lensed quasars for which these deep space based images were available.

The first time delays based on COSMOGRAIL data were published by Vuissoz et al. (2007) for the doubly lensed quasar SDSS J1650+4251 and one year later by Vuissoz et al. (2008) for the quadruply lensed quasar WFI J2033-4723. Time delays and a lens study of a second quadruply lensed quasar HE 0435-1223 were analysed in Courbin et al. (2011).

More recently, considerable effort has been put into a homogeneous way to treat COSMOGRAIL data, resulting in a standard COSMOGRAIL reduction procedure and the release of a software package PyCS (Python Curve Shifting) described in Tewes et al. (2012a).

The first results of this new approach is the precise time delay for the quadruply lensed quasar RX J1131-1231 in Tewes et al. (2012b). Time delays for 5 more doubly lensed quasars, mainly based on Mercator data, and analysed according to the new standards, will be presented in Eulaers et al. (2012b) and Eulaers et al. (2012a).

1.3 Personal contribution

I joined the COSMOGRAIL collaboration at the end of 2006. The light curves of WFI J2033-4723 served as a first test case for our time delay estimation method, the Numerical Model Fit. This method was further developed with the quadruply lensed quasar HE 0435-1223.

2

Data Reduction and Analysis

COSMOGRAIL data have been reduced in a homogeneous way using a set of Python scripts. This standard procedure is described in Tewes et al. (2012b) and summarized in this chapter.

2.1 Pre-reduction of Mercator Data

We used a semi-automated pipeline to carry out the pre-reduction of the Mercator CCD images, paying considerable attention to the visual inspection of the images. The bias, calculated as the median on the overscan zone, is subtracted from all frames. Then for every night, a masterflat combining ideally 8 twilight flats taken in a time span of maximum one week around the given night, is created. For the summer 2006 observations at the Mercator telescope, this time span has to be limited to one night due to the very rapidly changing aspect of the twilight flats during that summer. For some rare nights at the beginning of the observations, no twilight flats were available, so a flatfield based on all science frames taken during that night had to be created. In all cases, science frames are then divided by these masterflats or science flatfield. Using the SExtractor package (Bertin & Arnouts (1996)) we subtract the sky background and align the images on a chosen reference image. We then calculate a temporary normalization coefficient for each image, which is the median of the flux ratios of the reference image to the considered image for a chosen number of normalization stars.

2.2 Photometry

2.2.1 Deconvolution

The bottle-neck of the data reduction in terms of computation time is the construction of an individual Point Spread Function (PSF) per frame. Four stars are generally used to model this PSF. The pipeline allows us to compare different selections of PSF stars, which should ideally be well distributed around the lens and lie close to it. We can adapt the choice of PSF stars for individual images if necessary.

Photometry of the sources is obtained through simultaneous deconvolution of all frames using the MCS algorithm (Magain et al. (1998)), of which the main feature is the finite final resolution, which avoids artefacts. The deconvolved images have a pixel scale of half the telescope's pixel scale, and have a Gaussian PSF with a 2 pixels FWHM. The simultaneous deconvolution of all frames constrains very well the positions of the quasar images, even if not all data have been obtained under optimal seeing conditions. The flux of the point sources is allowed to vary from one frame to another, unlike the lensing galaxy, which is part of a numerical background that is held fixed for all the frames.

2.2.2 Renormalization

We then replace the temporary normalization coefficient that is based on SExtractor photometry by a more accurate coefficient that uses the photometry obtained after deconvolution of individual stars. For a given star we take the median value of its measured fluxes over all frames and divide this median flux by the star's flux measured on an individual image. This results in an individual coefficient for a given image and star. The new renormalization coefficient of one image is the median of these individual coefficients on one image, and its standard deviation divided by the number of renormalization stars is the renormalization error. Finally, a rescaling is applied so that the renormalization coefficient of the reference image equals one.

2.2.3 Error bars on the individual photometry

An estimation of the photometric shot noise σ_N, calculated for every quasar image and frame, is given by [1]:

$$\sigma_N = \sqrt{f_* + \frac{N_{sky} + R^2}{S}} \tag{2.1}$$

with f_* being the flux in the quasar image (expressed in number of photons), N_{sky} the sky level of the exposure, R the CCD read noise (both in photons per pixel), and S the PSF sharpness given by

$$S = \sum_{ij} (PS F_{ij})^2 \tag{2.2}$$

i.e. the sum over all pixels of the squared normalized fluxes of the PSF pixels.

2.3 Light Curves

2.3.1 Combining photometry per night

We now have the deconvolution photometry of the quasar images in every science frame and two associated errors, the shotnoise error and the renormalization error, which have to be combined into one measurement per night.

The data points in the light curves are the median photometry per night obtained by the simultaneous deconvolution of the images. Their error bars are the maximum of two kinds of error bars: an empirical error bar and an intrinsic one. Indeed, the total error on the night cannot be smaller than the one computed from the spread of the measurements in that night, nor can it be smaller than the error bar given by the photon noise combined with the renormalization error, so taking the maximum of both is justified. They are generally very close to one another.

The empirical error reflecting the spread of the measurements within one night is estimated by the standard deviation of the measurements in the night divided by the square root of the number of images in that night. As our photometry is a median value per night, the standard deviation is estimated via the Median Absolute Deviation (MAD) estimator (Hoaglin et al. (1983)) corrected by a scale factor for normal distributions. The MAD is defined as the median of the absolute values of the residuals from the data's median:

$$MAD = med_i\left(|X_i - med_j(X_j)|\right) \tag{2.3}$$

[1] Based upon Heyer, Biretta, 2005, WFPC2 Instrument Handbook, Version 9.1, Chapter 6

It is related to the standard deviation via $\sigma = K * MAD$. In case of a normal distribution, $K = \frac{1}{\phi^{-1}(0.75)} \approx 1.4862$, with ϕ^{-1} being the quantile function of the normal distribution.

On the other hand, the quadratic sum of the median shotnoise per night and the median renormalization error per night gives a theoretical estimate of the error on the combined data point. The fact that neither the empirical nor the theoretical error systematically dominates is a proof of the coherence of both approaches and justifies the idea of taking the maximum of both.

2.3.2 Combining telescopes

The final step is to put together the light curves of the same object coming from different telescopes. We choose the best light curve as the reference curve, and use the dispersion technique presented in Tewes et al. (2012a) to optimize the magnitude shifts between the curves of the *same* quasar image but from *different* telescopes. This can be a common magnitude shift per telescope or an individual shift per quasar image if we suspect differential reddening by absorption in the lensing galaxy. Small flux shifts can also be applied in order to correct for the colour difference between the lensing galaxy and the quasar images as observed by different R filters and CCD cameras on the telescopes.

2.4 Time Delay Analysis

For the time delay analysis of COSMOGRAIL light curves we use four different techniques in order to avoid a bias due to the method. Three of them, a spline fit, a dispersion minimization, and a method based on the variability of regression differences, are described and tested extensively in Tewes et al. (2012a) and have been released together as a free software package: Python Curve Shifting or PyCS. The fourth method is the Numerical Model Fit (NMF), as described in Chapter 2. We quickly summarize the main features of each of them:

1. **The dispersion-like technique** considers the time delay to be the shift between the light curves that minimizes the dispersion between these data. Microlensing is modelled by polynomials up to the third order, but no model light curve for the overall quasar variability is constructed here.

2. **The regression difference technique** calculates continuous regressions of the light curves, shifts them in time, makes the difference between them, and then searches for the time delay that minimizes the variability of these difference curves. Microlensing is not modelled here.

3. **The free knot spline technique** models the intrinsic quasar variability as well as the microlensing variations by fitting splines simultaneously to the light curves. The curves are shifted in time so as to optimize this fit.

4. **The Numerical Model Fit (NMF)** constructs a numerical model for the quasar variability together with a linear microlensing trend for a given time delay. The optimal time delay is the one that minimizes the difference between the data and this numerical model.

These four techniques are based on very different principles, so we expect them to be sensitive to different sources of error. By applying all of them to our light curves, we minimise the bias that might be due to the choice of the method.

We use a Monte Carlo approach for the error bar calculations. For the first three methods, these are based on perturbed simulated light curves with known time delays based on the spline fit as explained in Tewes et al. (2012a). For the last method, we use the numerical model light curve to which we add appropriate gaussian noise.

Epilogue

When I had been chosen in 2002 by the Euro Space Society, presided by Dirk Frimout, to participate as a language teacher in the International Space Camp at Huntsville, Alabama, USA, I could never have imagined how this experience would influence and change my life, and finally result in this PhD thesis. The prophecy of the words *"Sometimes, your second or third dream may lead you back to your first"*, spoken by the former NASA astronaut Mike Mullane, couldn't have become more true in my case: I returned to university, studied mathematics, arrived at the Institute of Astrophysics where I met Christophe, now my husband, started doing research on gravitationally lensed quasars, a subject I had written an essay on for school when I was 15, and even tried my luck in the ESA's astronauts selection in 2008.

A decade after this exciting week in Huntsville, I have now come to the end of my PhD, which unfortunately, but most probably, also rounds off this chapter in my life. Before saying farewell, it is time to express my gratitude.

- Thank you Prof. Pierre Magain, for having been my supervisor, and Dr. Frédéric Courbin, for the coordination of the COSMOGRAIL project, which was the framework of my PhD research topic.
- Thank you members of the jury, for the time you have taken to read and evaluate this manuscript.
- Thank you to all the collaborators in Liège, Geneva, Leuven and abroad, and especially to Malte, whose efficiency and ingenuity made it a great pleasure to work with him. Thank you for introducing me into the flexible world of Python, and for showing that code and scripts can be full of humour.
- Thank you Prof. Hans Van Winckel, for having given me the tremendous opportunity to do two observing runs, one at the Mercator Telescope in La Palma and one at the Euler Telescope in La Silla.
- Thank you to all my friends and family, who helped me relativise troubles, and focus on what is really important in life.
- Thank you Christophe, for all your help and support, and especially for being who you are to me.
- Thank you Elise, for having shown to me so many times that research is the most natural activity in the world. May those who can make their job out of this curiosity to explore realise how fortunate they are...

Eva Eulaers
Liège, October 2012

Bibliography

Bade, N., Siebert, J., Lopez, S. et al., 1997, RX J0911.4+0551: A new multiple QSO selected from the ROSAT All-Sky Survey., *Astron. & Astrophys.* **317**, L13–L16.

Barkana, R., 1997, Analysis of Time Delays in the Gravitational Lens PG 1115+080, *Astrophysical Journal* **489**, 21–+.

Bertin, E. & Arnouts, S., 1996, SExtractor: Software for source extraction., *Astron. & Astrophys., Suppl.* **117**, 393–404.

Biggs, A. D., Browne, I. W. A., Helbig, P. et al., 1999, Time delay for the gravitational lens system B0218+357, *Mon. Not. of the Royal Astron. Soc.* **304**, 349–358.

Bourassa, R. R., Kantowski, R. & Norton, T. D., 1973, The Spheroidal Gravitational Lens, *Astrophysical Journal* **185**, 747–756.

Browne, I. W. A., Wilkinson, P. N., Jackson, N. J. F. et al., 2003, The Cosmic Lens All-Sky Survey - II. Gravitational lens candidate selection and follow-up, *Mon. Not. of the Royal Astron. Soc.* **341**, 13–32.

Burud, I., 2001, *Gravitational lensing as a tool for determining the age of the Universe*, Ph.D. thesis, Institute of Astrophysics and Geophysics in Liege.

Burud, I., Courbin, F., Lidman, C. et al., 1998, High-Resolution Optical and Near-Infrared Imaging of the Quadruple Quasar RX J0911.4+0551, *Astrophysical Journal, Letters* **501**, L5+.

Burud, I., Courbin, F., Magain, P. et al., 2002a, An optical time-delay for the lensed BAL quasar HE 2149-2745, *Astron. & Astrophys.* **383**, 71–81.

Burud, I., Hjorth, J., Courbin, F. et al., 2002b, R-band photometry of SBS1520+530 (Burud+, 2002), *VizieR Online Data Catalog* **339**, 10481–+.

Burud, I., Hjorth, J., Courbin, F. et al., 2002c, Time delay and lens redshift for the doubly imaged BAL quasar SBS 1520+530, *Astron. & Astrophys.* **391**, 481–486.

Burud, I., Hjorth, J., Jaunsen, A. O. et al., 2000, An Optical Time Delay Estimate for the Double Gravitational Lens System B1600+434, *Astrophysical Journal* **544**, 117–122.

Burud, I., Magain, P., Sohy, S. & Hjorth, J., 2001, A novel approach for extracting time-delays from lightcurves of lensed quasar images, *Astron. & Astrophys.* **380**, 805–810.

Chantry, V., Sluse, D. & Magain, P., 2010, COSMOGRAIL: the COSmological MOnitoring of GRAvItational Lenses. VIII. Deconvolution of high resolution near-IR images and simple mass models for 7 gravitationally lensed quasars, *Astron. & Astrophys.* **522**, A95.

Chartas, G., Dai, X. & Garmire, G. P., 2004, Chandra and XMM-Newton Results on the Hubble Constant from Gravitational Lensing, *Measuring and Modeling the Universe* .

Chavushyan, V. H., Vlasyuk, V. V., Stepanian, J. A. & Erastova, L. K., 1997, SBS 1520+530: a new gravitationally lensed system at z=1.855., *Astron. & Astrophys.* **318**, L67–L70.

Christian, C. A., Crabtree, D. & Waddell, P., 1987, Detection of the lensing galaxy in PG 1115 + 080, *Astrophysical Journal* **312**, 45–49.

Chwolson, O., 1924, Über eine mögliche Form fiktiver Doppelsterne, *Astronomische Nachrichten* **221**, 329–+.

Claeskens, J.-F., 1998, *Aspects statistiques du phénomène de lentille gravitationnelle dans un échantillon de quasars très lumineux*, Ph.D. thesis, Université de Liège.

Claeskens, J.-F., Surdej, J. & Remy, M., 1996, J03.13 A and B: a new multiply imaged QSO candidate., *Astron. & Astrophys.* **305**, L9.

Cohen, A. S., Hewitt, J. N., Moore, C. B. & Haarsma, D. B., 2000, Further Investigation of the Time Delay, Magnification Ratios, and Variability in the Gravitational Lens 0218+357, *Astrophysical Journal* **545**, 578–590.

Coles, J., 2008, A New Estimate of the Hubble Time with Improved Modeling of Gravitational Lenses, *Astrophysical Journal* **679**, 17–24.

Cooke, J. H. & Kantowski, R., 1975, Time Delay for Multiply Imaged Quasars, *Astrophysical Journal, Letters* **195**, L11+.

Corbett, E. A., Browne, I. W. A., Wilkinson, P. N. & Patnaik, A., 1996, Radio Measurement of the Time Delay in 0218+357, in *Astrophysical Applications of Gravitational Lensing* (C. S. Kochanek & J. N. Hewitt, ed.), *IAU Symposium*, vol. 173, 37–+.

Courbin, F., Chantry, V., Revaz, Y. et al., 2011, COSMOGRAIL: the COSmological MOnitoring of GRAvItational Lenses. IX. Time delays, lens dynamics and baryonic fraction in HE 0435-1223, *Astron. & Astrophys.* **536**, A53.

Courbin, F., Eigenbrod, A., Vuissoz, C. et al., 2005, COSMOGRAIL: the COSmological MOnitoring of GRAvItational Lenses, in *Gravitational Lensing Impact on Cosmology* (Y. Mellier & G. Meylan, ed.), *IAU Symposium*, vol. 225, 297–303.

Courbin, F., Faure, C., Djorgovski, S. G. et al., 2012, Three quasi-stellar objects acting as strong gravitational lenses, *Astron. & Astrophys.* **540**, A36.

Courbin, F., Magain, P., Keeton, C. R. et al., 1997, The geometry of the quadruply imaged quasar PG 1115+080: implications for H_0_., *Astron. & Astrophys.* **324**, L1–L4.

Crampton, D., Schechter, P. L. & Beuzit, J.-L., 1998, Detection of the Galaxy Lensing the Doubly Imaged Quasar SBS 1520+530, *Astronomical Journal* **115**, 1383–1387.

Eddington, A. S., 1920, *Space, time and gravitation. an outline of the general relativity theory*.

Eigenbrod, A., Courbin, F., Dye, S. et al., 2006a, COSMOGRAIL: the COSmological MOnitoring of GRAvItational Lenses. II. SDSS J0924+0219: the redshift of the lensing galaxy, the quasar spectral variability and the Einstein rings, *Astron. & Astrophys.* **451**, 747–757.

Eigenbrod, A., Courbin, F. & Meylan, G., 2007, COSMOGRAIL: the COSmological MOnitoring of GRAvItational Lenses. VI. Redshift of the lensing galaxy in seven gravitationally lensed quasars, *Astron. & Astrophys.* **465**, 51–56.

Eigenbrod, A., Courbin, F., Meylan, G. et al., 2006b, COSMOGRAIL: the COSmological MOnitoring of GRAvItational Lenses. III. Redshift of the lensing galaxy in eight gravitationally lensed quasars, *Astron. & Astrophys.* **451**, 759–766.

Eigenbrod, A., Courbin, F., Vuissoz, C. et al., 2005, COSMOGRAIL: The COSmological MOnitoring of GRAvItational Lenses. I. How to sample the light curves of gravitationally lensed quasars to measure accurate time delays, *Astron. & Astrophys.* **436**, 25–35.

Einstein, A., 1936, Lens-Like Action of a Star by the Deviation of Light in the Gravitational Field, *Science* **84**, 506–507.

Etherington, I., 1933, On the definition of distance in general relativity, *Phil. Mag.* .

Eulaers, E. & Magain, P., 2011, Time delays for eleven gravitationally lensed quasars revisited, *Astron. & Astrophys.* **536**, A44.

Eulaers, E., Tewes, M., Asfandiyarov, I. et al., 2012a, COSMOGRAIL: the COSmological MOnitoring of GRAvItational Lenses. XIV: Time delays of the doubly lensed quasars SDSS J1650+4251, SDSS J0903+5028, and SDSS J1155+6346 .

Eulaers, E., Tewes, M., Magain, P. et al., 2012b, COSMOGRAIL: the COSmological MOnitoring of GRAvItational Lenses. XIII: Time delays of the doubly lensed quasars SDSS J1206+4332 and HS 2209+1914 .

Fassnacht, C. D. & Cohen, J. G., 1998, Keck spectroscopy of three gravitational lens systems discovered in the JVAS and CLASS surveys, *Astronomical Journal* **115**, 377.

Fassnacht, C. D., Pearson, T. J., Readhead, A. C. S. et al., 1999, A Determination of H_0 with the CLASS Gravitational Lens B1608+656. I. Time Delay Measurements with the VLA, *Astrophysical Journal* **527**, 498–512.

Fassnacht, C. D., Xanthopoulos, E., Koopmans, L. V. E. & Rusin, D., 2002, A Determination of H_0 with the CLASS Gravitational Lens B1608+656. III. A Significant Improvement in the Precision of the Time Delay Measurements, *Astrophysical Journal* **581**, 823–835.

Faure, C., Kneib, J.-P., Covone, G. et al., 2008, First Catalog of Strong Lens Candidates in the COSMOS Field, *Astrophysical Journal, Suppl.* **176**, 19–38.

Freedman, W. L., Madore, B. F., Gibson, B. K. et al., 2001, Final Results from the Hubble Space Telescope Key Project to Measure the Hubble Constant, *Astrophysical Journal* **553**, 47–72.

Freedman, W. L., Madore, B. F., Scowcroft, V. et al., 2012, Carnegie Hubble Program: A Mid-infrared Calibration of the Hubble Constant, *Astrophysical Journal* **758**, 24.

Gaynullina, E. R., Schmidt, R. W., Akhunov, O. T. B. et al., 2005a, VRc light curves of SBSG 1520+530 (Gaynullina+, 2005), *VizieR Online Data Catalog* **344**, 53–+.

Gaynullina, E. R., Schmidt, R. W., Akhunov, T. et al., 2005b, Microlensing in the double quasar SBS 1520+530, *Astron. & Astrophys.* **440**, 53–58.

Gil-Merino, R., Wisotzki, L. & Wambsganss, J., 2002, The Double Quasar HE 1104-1805: A case study for time delay determination with poorly sampled lightcurves, *Astron. & Astrophys.* **381**, 428–439.

Goicoechea, L. J., Shalyapin, V. N., Koptelova, E. et al., 2008, First robotic monitoring of a lensed quasar: Intrinsic variability of SBS 0909+532, *New A* **13**, 182–193.

Hagen, H.-J., Engels, D. & Reimers, D., 1999, The Hamburg Quasar Survey. III. Further new bright quasars, *Astron. & Astrophys., Suppl.* **134**, 483–487.

Hege, E. K., Hubbard, E. N., Strittmatter, P. A. & Worden, S. P., 1981, Speckle interferometry observations of the triple QSO PG 1115 + 08, *Astrophysical Journal, Letters* **248**, L1–L3.

Henry, J. P. & Heasley, J. N., 1986, High-resolution imaging from Mauna Kea - The triple quasar in 0.3-arc S seeing, *Nature* **321**, 139–142.

Hinshaw, G., Weiland, J. L., Hill, R. S. et al., 2009, Five-Year Wilkinson Microwave Anisotropy Probe Observations: Data Processing, Sky Maps, and Basic Results, *Astrophysical Journal, Suppl.* **180**, 225–245.

Hirv, A., Olspert, N. & Pelt, J., 2011, Towards the Automatic Estimation of Time Delays of Gravitational Lenses, *Baltic Astronomy* **20**, 125–144.

Hjorth, J., Burud, I., Jaunsen, A. O. et al., 2002, The Time Delay of the Quadruple Quasar RX J0911.4+0551, *Astrophysical Journal, Letters* **572**, L11–L14.

Hoaglin, D. C., Mosteller, F. & Tukey, J. W., 1983, *Understanding robust and exploratory data anlysis*.

Impey, C. D., Falco, E. E., Kochanek, C. S. et al., 1998, An Infrared Einstein Ring in the Gravitational Lens PG 1115+080, *Astrophysical Journal* **509**, 551–560.

Jackson, N., de Bruyn, A. G., Myers, S. et al., 1995, 1600+434: a new gravitational lens system, *Mon. Not. of the Royal Astron. Soc.* **274**, L25–L29.

Jakobsson, P., Hjorth, J., Burud, I. et al., 2005, An optical time delay for the double gravitational lens system FBQ 0951+2635, *Astron. & Astrophys.* **431**, 103–109.

Jarosik, N., Bennett, C. L., Dunkley, J. et al., 2011, Seven-year Wilkinson Microwave Anisotropy Probe (WMAP) Observations: Sky Maps, Systematic Errors, and Basic Results, *Astrophysical Journal, Suppl.* **192**, 14.

Jaunsen, A. O. & Hjorth, J., 1997, Detection of a spiral lens galaxy and optical variability in the gravitational lens system B1600+434., *Astron. & Astrophys.* **317**, L39–L42.

Johnston, D. E., Richards, G. T., Frieman, J. A. et al., 2003, SDSS J090334.92+502819.2: A New Gravitational Lens, *Astronomical Journal* **126**, 2281–2290.

Jones, M. E., Edge, A. C., Grainge, K. et al., 2005, H_0 from an orientation-unbiased sample of Sunyaev-Zel'dovich and X-ray clusters, *Mon. Not. of the Royal Astron. Soc.* **357**, 518–526.

Kayo, I., Inada, N., Oguri, M. et al., 2010, Eight New Quasar Lenses from the Sloan Digital Sky Survey Quasar Lens Search, *Astronomical Journal* **139**, 1614–1621.

Keeton, C. R., 2001, Computational Methods for Gravitational Lensing, *ArXiv Astrophysics e-prints* .

Keeton, C. R. & Kochanek, C. S., 1997, Determining the Hubble Constant from the Gravitational Lens PG 1115+080, *Astrophysical Journal* **487**, 42.

Keeton, C. R. & Moustakas, L. A., 2009, A New Channel for Detecting Dark Matter Substructure in Galaxies: Gravitational Lens Time Delays, *Astrophysical Journal* **699**, 1720–1731.

Klimov, Y. G., 1963, The Deflection of Light Rays in the Gravitational Fields of Galaxies, *Soviet Physics Doklady* **8**, 119–+.

Kochanek, C. S., Falco, E. E., Schild, R. et al., 1997, SBS 0909+532: A New Double Gravitational Lens or Binary Quasar?, *Astrophysical Journal* **479**, 678–+.

Kochanek, C. S., Morgan, N. D., Falco, E. E. et al., 2006, The Time Delays of Gravitational Lens HE 0435-1223: An Early-Type Galaxy with a Rising Rotation Curve, *Astrophysical Journal* **640**, 47–61.

Koopmans, L. V. E., de Bruyn, A. G., Xanthopoulos, E. & Fassnacht, C. D., 2000, A time-delay determination from VLA light curves of the CLASS gravitational lens B1600+434, *Astron. & Astrophys.* **356**, 391–402.

Kristian, J., Groth, E. J., Shaya, E. J. et al., 1993, Imaging of the gravitational lens system PG 1115+080 with the Hubble Space Telescope, *Astronomical Journal* **106**, 1330–1336.

Kundic, T., Cohen, J. G., Blandford, R. D. & Lubin, L. M., 1997a, Keck Spectroscopy of the Gravitational Lens System PG 1115+080: Redshifts of the Lensing Galaxies., *Astronomical Journal* **114**, 507–510.

Kundic, T., Turner, E. L., Colley, W. N. et al., 1997b, A Robust Determination of the Time Delay in 0957+561A, B and a Measurement of the Global Value of Hubble's Constant, *Astrophysical Journal* **482**, 75.

Lawrence, C. R., Neugebauer, G., Weir, N. et al., 1992, Infrared observations of the gravitational lens system B1422+231, *Mon. Not. of the Royal Astron. Soc.* **259**, 5P–7P.

Liebes, S., 1964, Gravitational Lenses, *Physical Review* **133**, B835–B844.

Linder, E. V., 2011, Lensing time delays and cosmological complementarity, *Phys. Rev. D* **84**(12), 123529.

Lopez, S., Wucknitz, O. & Wisotzki, L., 1998, Detection of the lensing galaxy in HE 2149-2745, *Astron. & Astrophys.* **339**, L13–L16.

Magain, P., Courbin, F. & Sohy, S., 1998, Deconvolution with Correct Sampling, *Astrophysical Journal* **494**, 472–+.

Magain, P., Surdej, J., Swings, J.-P. et al., 1988, Discovery of a quadruply lensed quasar - The 'clover leaf' H1413 + 117, *Nature* **334**, 325–327.

Magain, P., Surdej, J., Vanderriest, C. et al., 1992, Q 1208 + 1011 - The most distant imaged quasar, or a binary?, *Astron. & Astrophys.* **253**, L13–L16.

Michell, J., 1784, On the Means of Discovering the Distance, Magnitude, &c. of the Fixed Stars, in Consequence of the Diminution of the Velocity of Their Light, in Case Such a Diminution Should be Found to Take Place in any of Them, and Such Other Data Should be Procured from Observations, as Would be Farther Necessary for That Purpose. by the Rev. John Michell, B. D. F. R. S. I a Letter to

Henry Cavendish, Esq. F. R. S. and a. S., *Royal Society of London Philosophical Transactions Series I* **74**, 35–57.

Morgan, C. W., Eyler, M. E., Kochanek, C. S. et al., 2008a, Simultaneous Estimation of Time Delays and Quasar Structure, *Astrophysical Journal* **676**, 80–86.

Morgan, C. W., Kochanek, C. S., Dai, X. et al., 2008b, X-Ray and Optical Microlensing in the Lensed Quasar PG 1115+080, *Astrophysical Journal* **689**, 755–761.

Morgan, N. D., Snyder, J. A. & Reens, L. H., 2003, SDSS J1650+4251: A New Gravitational Lens, *Astronomical Journal* **126**, 2145–2151.

Mosquera, A. M. & Kochanek, C. S., 2011, The Microlensing Properties of a Sample of 87 Lensed Quasars, *Astrophysical Journal* **738**, 96.

Myers, S. T., Fassnacht, C. D., Djorgovski, S. G. et al., 1995, 1608+656: A Quadruple-Lens System Found in the CLASS Gravitational Lens Survey, *Astrophysical Journal, Letters* **447**, L5.

Myers, S. T., Jackson, N. J., Browne, I. W. A. et al., 2003, The Cosmic Lens All-Sky Survey - I. Source selection and observations, *Mon. Not. of the Royal Astron. Soc.* **341**, 1–12.

Ofek, E. O. & Maoz, D., 2003, Time-Delay Measurement of the Lensed Quasar HE 1104-1805, *Astrophysical Journal* **594**, 101–106.

Oguri, M., 2007, Gravitational Lens Time Delays: A Statistical Assessment of Lens Model Dependences and Implications for the Global Hubble Constant, *Astrophysical Journal* **660**, 1–15.

Oguri, M., Inada, N., Hennawi, J. F. et al., 2005, Discovery of Two Gravitationally Lensed Quasars with Image Separations of 3" from the Sloan Digital Sky Survey, *Astrophysical Journal* **622**, 106–115.

Oscoz, A., Serra-Ricart, M., Mediavilla, E. et al., 1997, Support for the Gravitational Lens Interpretation of SBS 0909+532, *Astrophysical Journal, Letters* **491**, L7+.

Paraficz, D., Hjorth, J., Burud, I. et al., 2006, Variability of 5 gravitationally lensed QSOs (Paraficz+, 2006), *VizieR Online Data Catalog* **345**, 59001–+.

Paraficz, D., Hjorth, J. & Elíasdóttir, Á., 2009, Results of optical monitoring of 5 SDSS double QSOs with the Nordic Optical Telescope, *Astron. & Astrophys.* **499**, 395–408.

Patnaik, A. R., Browne, I. W. A., King, L. J. et al., 1993, B0218+35.7 - A gravitationally lensed system with the smallest separation, *Mon. Not. of the Royal Astron. Soc.* **261**, 435–444.

Patnaik, A. R., Browne, I. W. A., Walsh, D. et al., 1992, B1422+231 - A new gravitationally lensed system at Z = 3.62, *Mon. Not. of the Royal Astron. Soc.* **259**, 1P–4P.

Patnaik, A. R. & Narasimha, D., 2001, Determination of time delay from the gravitational lens B1422+231, *Mon. Not. of the Royal Astron. Soc.* **326**, 1403–1411.

Pelt, J., Hjorth, J., Refsdal, S. et al., 1998, Estimation of multiple time delays in complex gravitational lens systems, *Astron. & Astrophys.* **337**, 681–684.

Pelt, J., Kayser, R., Refsdal, S. & Schramm, T., 1996, The light curve and the time delay of QSO 0957+561., *Astron. & Astrophys.* **305**, 97–+.

Pelt, J., Refsdal, S. & Stabell, R., 2002, Bias and consistency in time delay estimation methods: Case of the double quasar HE 1104-1805, *Astron. & Astrophys.* **389**, L57–L60.

Pindor, B., Eisenstein, D. J., Inada, N. et al., 2004, SDSS J115517.35+634622.0: A Newly Discovered Gravitationally Lensed Quasar, *Astronomical Journal* **127**, 1318–1324.

Poindexter, S., Morgan, N., Kochanek, C. S. & Falco, E. E., 2007, Mid-IR Observations and a Revised Time Delay for the Gravitational Lens System Quasar HE 1104-1805, *Astrophysical Journal* **660**, 146–151.

Press, W. H., Rybicki, G. B. & Hewitt, J. N., 1992a, The time delay of gravitational lens 0957 + 561. I - Methodology and analysis of optical photometric data. II - Analysis of radio data and combined optical-radio analysis, *Astrophysical Journal* **385**, 404–420.

Press, W. H., Rybicki, G. B. & Hewitt, J. N., 1992b, The Time Delay of Gravitational Lens 0957+561. II. Analysis of Radio Data and Combined Optical-Radio Analysis, *Astrophysical Journal* **385**, 416.

Refsdal, S., 1964a, On the possibility of determining Hubble's parameter and the masses of galaxies from the gravitational lens effect, *Mon. Not. of the Royal Astron. Soc.* **128**, 307–+.

Refsdal, S., 1964b, The gravitational lens effect, *Mon. Not. of the Royal Astron. Soc.* **128**, 295–+.

Refsdal, S. & Surdej, J., 1994, Gravitational Lenses, *Reports of Progress in Physics* **57**, 117–185.

Remy, M., Surdej, J., Smette, A. & Claeskens, J.-F., 1993, Optical imaging of the gravitational lens system B 1422+231, *Astron. & Astrophys.* **278**, L19–L22.

Riess, A. G., Li, W., Stetson, P. B. et al., 2005, Cepheid Calibrations from the Hubble Space Telescope of the Luminosity of Two Recent Type Ia Supernovae and a Redetermination of the Hubble Constant, *Astrophysical Journal* **627**, 579–607.

Russell, H. N., 1937, A relativistic eclipse, *Scientific American* **156**, 76.

Saha, P., 2000, Lensing Degeneracies Revisited, *Astronomical Journal* **120**, 1654–1659.

Saha, P., Coles, J., Macciò, A. V. & Williams, L. L. R., 2006a, The Hubble Time Inferred from 10 Time Delay Lenses, *Astrophysical Journal, Letters* **650**, L17–L20.

Saha, P., Courbin, F., Sluse, D. et al., 2006b, COSMOGRAIL: the COSmological MOnitoring of GRAv-Itational Lenses. IV. Models of prospective time-delay lenses, *Astron. & Astrophys.* **450**, 461–469.

Saha, P. & Williams, L. L. R., 1997, Non-parametric reconstruction of the galaxy lens in PG 1115+080, *Mon. Not. of the Royal Astron. Soc.* **292**, 148.

Saha, P. & Williams, L. L. R., 2004, A Portable Modeler of Lensed Quasars, *Astronomical Journal* **127**, 2604–2616.

Saha, P. & Williams, L. L. R., 2006, Gravitational Lensing Model Degeneracies: Is Steepness All-Important?, *Astrophysical Journal* **653**, 936–941.

Saha, P. & Williams, L. L. R., 2011, PixeLens: A Portable Modeler of Lensed Quasars, *Astrophysics Source Code Library* 2007.

Sandage, A., Tammann, G. A., Saha, A. et al., 2006, The Hubble Constant: A Summary of the Hubble Space Telescope Program for the Luminosity Calibration of Type Ia Supernovae by Means of Cepheids, *Astrophysical Journal* **653**, 843–860.

Sanitt, N., 1971, Quasi-stellar Objects and Gravitational Lenses, *Nature* **234**, 199–203.

Schechter, P. L., Bailyn, C. D., Barr, R. et al., 1997, The Quadruple Gravitational Lens PG 1115+080: Time Delays and Models, *Astrophysical Journal, Letters* **475**, L85+.

Schechter, P. L., Gregg, M. D., Becker, R. H. et al., 1998, The First FIRST Gravitationally Lensed Quasar: FBQ 0951+2635, *Astronomical Journal* **115**, 1371–1376.

Schechter, P. L., Udalski, A., Szymański, M. et al., 2003, Microlensing of Relativistic Knots in the Quasar HE 1104-1805 AB, *Astrophysical Journal* **584**, 657–663.

Schmidt, M., 1963, 3C 273 : A Star-Like Object with Large Red-Shift, *Nature* **197**, 1040–+.

Schneider, P., 1985, A new formulation of gravitational lens theory, time-delay, and Fermat's principle, *Astron. & Astrophys.* **143**, 413–420.

Schneider, P., 2006, *Extragalactic Astronomy and Cosmology*.

Schneider, P., Ehlers, J. & Falco, E. E., 1992, *Gravitational Lenses*, Springer-Verlag.

Sluse, D., Chantry, V., Magain, P. et al., 2012, COSMOGRAIL: the COSmological MOnitoring of GRAvItational Lenses. X. Modeling based on high-precision astrometry of a sample of 25 lensed quasars: consequences for ellipticity, shear, and astrometric anomalies, *Astron. & Astrophys.* **538**, A99.

Snellen, I. A. G., de Bruyn, A. G., Schilizzi, R. T. et al., 1995, Radio Observations of the Quadruple Lens 1608+656, *Astrophysical Journal, Letters* **447**, L9.

Spergel, D. N., Bean, R., Doré, O. et al., 2007, Three-Year Wilkinson Microwave Anisotropy Probe (WMAP) Observations: Implications for Cosmology, *Astrophysical Journal, Suppl.* **170**, 377–408.

Surdej, J., Magain, P., Swings, J.-P. et al., 1987, A new case of gravitational lensing, *Nature* **329**, 695.

Surdej, J., Remy, M., Smette, A. et al., 1993, Two new very close pairs of quasars with discordant redshifts and a gravitational lens candidate, in *Liege International Astrophysical Colloquia* (J. Surdej, D. Fraipont-Caro, E. Gosset, S. Refsdal & M. Remy, eds.), *Liege International Astrophysical Colloquia*, vol. 31, 153.

Suyu, S. H., Treu, T., Blandford, R. D. et al., 2012, The Hubble constant and new discoveries in cosmology, *ArXiv e-prints* .

Tewes, M., Courbin, F. & Meylan, G., 2012a, COSMOGRAIL XI: Techniques for time delay measurement in presence of microlensing, *ArXiv e-prints* .

Tewes, M., Courbin, F., Meylan, G. et al., 2012b, COSMOGRAIL XII: Time delays and 9-yr optical monitoring of the lensed quasar RX J1131-1231, *ArXiv e-prints* .

Tikhov, G. A., 1938, Sur la déviation des rayons lumineux dans le champ de gravitation des é toiles, *Izvestiya Glavnoj Astronomicheskoj Observatorii v Pulkove* **16**.

Tsvetkova, V. S., Vakulik, V. G., Shulga, V. M. et al., 2010, PG1115+080: variations of the A2/A1 flux ratio and new values of the time delays, *Mon. Not. of the Royal Astron. Soc.* **406**, 2764–2776.

Ullán, A., Goicoechea, L. J., Zheleznyak, A. P. et al., 2006, Time delay of SBS 0909+532, *Astron. & Astrophys.* **452**, 25–35.

Vakulik, V. G., Shulga, V. M., Schild, R. E. et al., 2009, Time delays in PG 1115+080: new estimates, *Mon. Not. of the Royal Astron. Soc.* **400**, L90–L93.

Vanderriest, C., Wlerick, G., Lelievre, G. et al., 1986, Variability of the gravitational mirage P.G. 1115+080, *Astron. & Astrophys.* **158**, L5–L8.

Vanderriest, C., Wlerick, G., Tartag, A. et al., 1983, Structure and photometry of the gravitational mirage PG 1115 + 080, in *Liege International Astrophysical Colloquia* (J.-P. Swings, ed.), *Liege International Astrophysical Colloquia*, vol. 24, 182–191.

von Soldner, J. G., 1804, Ueber die ablenkung eines lichtstrals von seiner geradlinigen bewegung, *Berliner Astronomisches Jahrbuch* 161–172.

Vuissoz, C., Courbin, F., Sluse, D. et al., 2007, COSMOGRAIL: the COSmological MOnitoring of GRAvItational Lenses. V. The time delay in SDSS J1650+4251, *Astron. & Astrophys.* **464**, 845–851.

Vuissoz, C., Courbin, F., Sluse, D. et al., 2008, COSMOGRAIL: the COSmological MOnitoring of GRAvItational Lenses. VII. Time delays and the Hubble constant from WFI J2033-4723, *Astron. & Astrophys.* **488**, 481–490.

Walsh, D., 1989, 0957 + 561: The Unpublished Story, in *Gravitational Lenses* (J. M. Moran, J. N. Hewitt, & K.-Y. Lo, ed.), *Lecture Notes in Physics, Berlin Springer Verlag*, vol. 330, 11–+.

Walsh, D., Carswell, R. F. & Weymann, R. J., 1979, 0957 + 561 A, B - Twin quasistellar objects or gravitational lens, *Nature* **279**, 381–384.

Weymann, R. J., Latham, D., Roger, J. et al., 1980, The triple QSO PG1115+08 - Another probable gravitational lens, *Nature* **285**, 641–643.

Wisotzki, L., Koehler, T., Kayser, R. & Reimers, D., 1993, The new double QSO HE 1104-1805: Gravitational lens with microlensing or binary quasar?, *Astron. & Astrophys.* **278**, L15–L18.

Wisotzki, L., Koehler, T., Lopez, S. & Reimers, D., 1996, Discovery of a new gravitationally lensed QSO with broad absorption lines., *Astron. & Astrophys.* **315**, L405.

Wisotzki, L., Wucknitz, O., Lopez, S. & Sorensen, A. N., 1998, First estimate of the time delay in HE 1104-1805, *Astron. & Astrophys.* **339**, L73–L76.

Wyrzykowski, L., Udalski, A., Schechter, P. L. et al., 2003, The Optical Gravitational Lensing Experiment. Optical Monitoring of the Gravitationally Lensed Quasar HE1104–1805 in 1997–2002, *Acta Astron.* **53**, 229–240.

York, T., Jackson, N., Browne, I. W. A. et al., 2005, CLASS B0631+519: last of the Cosmic Lens All-Sky Survey lenses, *Mon. Not. of the Royal Astron. Soc.* **361**, 259–271.

Young, P., Deverill, R. S., Gunn, J. E. et al., 1981, The triple quasar Q1115+080A, B, C - A quintuple gravitational lens image, *Astrophysical Journal* **244**, 723–735.

Zwicky, F., 1937a, Nebulae as Gravitational Lenses, *Physical Review* **51**, 290–290.

Zwicky, F., 1937b, On the Probability of Detecting Nebulae Which Act as Gravitational Lenses, *Physical Review* **51**, 679–679.